6-30-2011 12:00 AM

The Complex Paragenetic History of Basal Negaunee Iron Formation Iron Ores, Tilden Mine, Marquette District, Upper Michigan

Natalie J. Pietrzak, *The University of Western Ontario*

Supervisor: Dr. Norm Duke, *The University of Western Ontario*

A thesis submitted in partial fulfillment of the requirements for the Doctor of Philosophy degree in Geology

The Complex Paragenetic History of Basal Negaunee Iron Formation Iron Ores,Tilden Mine, Marquette District, Upper Michigan

by

Natalie Pietrzak

Graduate Program in Geology

A thesis submitted in partial fulfillment
of the requirements for the degree of
Doctor of Philosophy

The School of Graduate and Postdoctoral Studies
The University of Western Ontario
London, Ontario, Canada

THE UNIVERSITY OF WESTERN ONTARIO
School of Graduate and Postdoctoral Studies

CERTIFICATE OF EXAMINATION

Supervisor

_____
Dr. Norm Duke

Supervisory Committee

_____
Dr. Robert Hodder

_____
Dr. Gordon Southam

Examiners

_____
Dr. Robert Hodder

_____
Dr. Gordon Southam

_____
Dr. Ron Martin

_____
Dr. Bill Cambray

The thesis by

Natalie Jane Pietrzak

entitled:

The Complex Paragenetic History of Basal Negaunee Iron Formation Iron Ores,Tilden Mine, Marquette District, Upper Michigan

is accepted in partial fulfillment of the
requirements for the degree of
Doctor of Philosophy

_____ _____
Date Chair of the Thesis Examination Board

Abstract

Variable mineral chemistry and textures of basal Negaunee iron ores mined in the Main Tilden Pit have led to metallurgical difficulties. Core-logging and detailed petrography supported by microprobe investigations, identify three upward fining lithofacies within the Main Pit Carbonate and overlying Martite ore domains: 1) Basal Clastics; 2) Medial BIF; and 3) Granular Iron Formation. Growth fault related subsidence controlled deposition of the Basal Clastics, comprised of detrital quartz dispersed in a matrix of chlorite, cemented by ferri-hydrite, chert and Mg-siderite. Subsequent starvation of any clastic input led to cyclic iron-silica precipitation throughout the deposition of Medial BIF. Increasing wave action accompanied marine transgression caused deposition of granular rip-up clasts to form the Upper Granular Iron Formation. These domains are cross-cut by numerous chloritized feeder dykes and are capped by a greenstone Pillar, indicating overlapping mafic magmatism.

Low grade regional metamorphism attending the 1850 Ma Penokean arc-continent collision led to magnetite growth, carbonate grain coarsening and chlorite crystallization. Metamorphic fluids facilitated martite replacement of magnetite and deformation led to developing local platy specularite schists. A late retrograde hydrothermal overprint post-dates peak thermal conditions that accompanied the development of the 1750 Ma Republic Metamorphic Node. This is expressed by high-Fe chlorite, Fe-dolomite/ankerite, zoned Mn-rich siderite with associated trace Cu-Fe sulphide and REE bearing fluro-apatite and monazite, diagnostic of an “IOCG” type signature.

This complex paragenetic history accounts for the unpredictable geometallurgical response of the basal Negaunee iron ores. Treatment difficulties relate to: 1) variable silica-iron separation occurs due to liberation from detrital quartz versus massive mosaic and granular textured chert; 2) the bulk iron content is expressed not only in iron oxide but in iron carbonate and iron chlorite; and 3) the intense late IOCG overprint proximal to the Southern Shear Zone.

Keywords: Negaunee, Iron Formation, Tilden Mine, Iron Ore Paragenesis, Menominee Group, Marquette Range Supergroup, Iron Formation Paleoenvironment, Penokean Orogeny.

Acknowledgements

This thesis was proposed by Cliffs Natural Resources Ltd. to address metallurgical issues pertaining to the Tilden Pit. The research was funded in part by Cliffs Natural Resources Ltd. and an NSERC-IPS scholarship. I would like to thank the main supervisors: Dr. Norm Duke, Glenn Scott, Helene Lukey and Dr. Bob Hodder. Thank you Norm for all the tireless discussions, edits and ideas to help coalesce my thoughts to their fruitful conclusions. Thank you to Glenn and Helene for all of your generosity in terms of time, support, technical data and funding, and use of the Cliffs Cottage. Working with you has been a pleasure and made this thesis very easy and a joy to research. Thank you to Bob Hodder for bringing this thesis to my attention in the first place and always being there for helpful advice and comments.

I would also like to acknowledge Dr. Gord Southam for the opportunity of conducting iron formation experiments and all the information and ideas pertaining to early oceans and microbes; and to Bob Barnett for help with petrographic investigations and the lengthy thought provoking discussions. I would like to give a special thank you to Jim, my husband for all of your technical skills with the microprobe analyses and filtering of the data. Thank you Jim for all of your patience, help and support right to the finish line. To my mom, dad, sisters and grandparents, thank you for your support and encouragement to fulfill this special goal and reach my potential.

Table of Contents

List of Tables

List of Figures

List of Plates

List of Appendices

Appendix A: Informal Use of Terms

Appendix B: Sample List including the drill holes, sample locations, domain assigned and lithofacies for each sample. This list is to be used in conjunction with the Appendix B2 map.

Appendix B2: Cross-section map. Sample Locations of the drill holes investigated in this these. Elevations relative To sea level are marked by the blue numbers on the left side of the diagram. The X,Y and Z co-ordinates are listed in the Sample List of Appendix B.

Appendix C: Microprobe Analyses including carbonate, chlorite, iron oxides and apatite.

Appendix C material is available as a digital copy.

Chapter 1: Introduction

1.1 Opening Statement

Pricing of iron ore is measured by US cents per dry metric tonne per iron unit which is equivalent to US cents per 1000 kilograms. Iron unit prices have increased from 0.279 $US /dry metric tonne in 2001 to 2.10 $US/dry metric tonne in 2010 (Figure 1.0). This rise in price is largely due to the increased demand by the industrial development of Asia, most notably China (Reuters, 2010). The jump in demand and price of iron ore has rejuvenated exploration programs throughout North America, South America as well as Australia. It has sparked numerous mergers and takeover attempts, including Cliff's recent 4.9 billion dollar acquisition of the Consolidated Thompson Bloom Lake Mine, Quebec and the recent ArcelorMittal takeover of Baffinland Iron Mine Corp. which holds the Mary River iron deposits situated on northern Baffin Island.

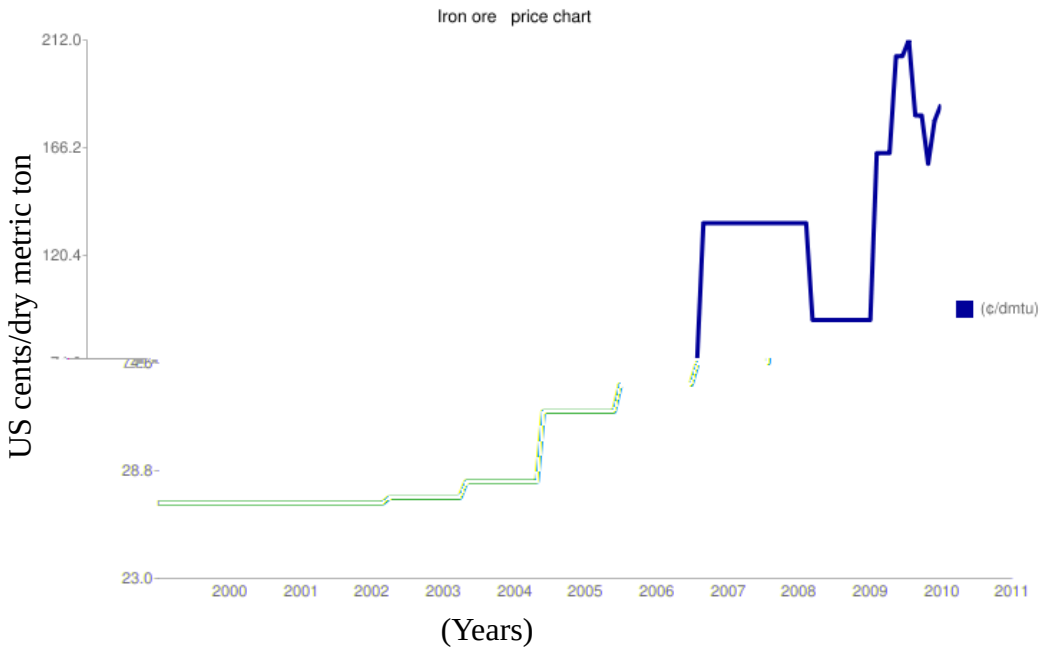

Figure 1.0: A graph depicting the change in iron ore prices from 2000 to 2011 (Mongabay, 2011).

The three largest global iron ore producing companies include Vale, Rio Tinto and BHP Billiton. The increased demand for iron has also prolonged the life of many producing iron ore deposits, such as Cliffs Natural Resources Ltd. Empire and Tilden iron ore operations at Ishpeming, Michigan (Figure 1.1). Current open pit mining of the Empire and Tilden pits are among the largest producing iron mines in North America, supplying iron ore pellets to North American customers. The operating Tilden pit extracts iron ore from the Negaunee Iron Formation and is the subject of this thesis. Cliffs Natural Resources Ltd. is the oldest operating iron ore company in North America and has shaped the historical development of northern Michigan and the Great Lakes region.

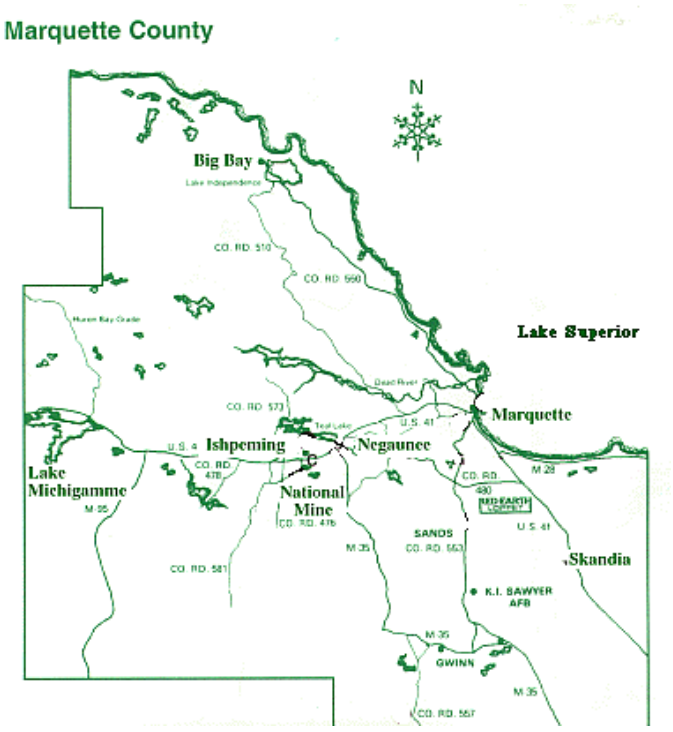

Figure 1.1: Map of the Lake Superior Region including the villages of Negaunee and Ishpeming (Exploring the North, 2011).

1.2 Mining History of the Region and Cliffs Natural Resources Ltd.

The first notable iron ore discovery in the Lake Superior Region was reported from the Marquette Mineral District in 1844 (Boyum, 1975). The town of Negaunee 23 kilometers east of Marquette is the site of the Jackson Mine, the first iron ore mine brought into production in the United States in 1845. Formed initially as the Cleveland Iron Mining Company in 1847, the current Cliffs Natural Resources Ltd. still has its head office in Cleveland, Ohio. It now has diversified holdings that include iron ore, coal and chromite. The operations located at Ishpeming made its first substantial shipment (1,479 tonnes) in 1855. The first Soo Lock was opened in 1855 in Sault Ste. Marie, Michigan to facilitate production and shipping (Boyum, 1975). Initial mining efforts such as those at the Jackson Mine and at Carp River focused on producing ore from charcoal furnaces to make pig iron. Until the 1950's production included both open pit and underground methods to recover high grade direct-shipping iron ore. Since the 1950's there has been mining of lower grade taconite followed by pelletization, as from Cliffs' Eagle Mills, Humboldt, Republic and Empire mines (Boyum, 1975).

A joint program with the U.S. Bureau of Mines at Minneapolis led to the successful development of selective flocculation-flotation process, a procedure used today in the pellitization process (Boyum, 1975). The Tilden Mine came on stream in 1974, mining the basal oxidized portion of the Negaunee Iron Formation. Although other minor iron formations of the Marquette Range Supergroup contributed to iron ore production within the Marquette Mineral District, the Negaunee Iron Formation remains the principal producer. As of 2011, the Empire, Tilden and CDIII open pit mines at Ishpeming are all currently active.

1.3 Definitions: Banded Iron Formations and Iron Ores

Iron ores in the Tilden Pit are not high-grade direct shipping but low grade taconite ores processed to form iron pellets. The pelletization process enriches the iron grade from less than 40% Fe in banded iron formation extracted from the pit up to 60% Fe in the final

pellet product. Classically, banded iron-formations are considered a sedimentary rock type that is typically Archean or Paleoproterozoic in age. A banded iron formation is a chemical precipitate characterized by alternating amorphous silica-rich and iron-rich layers. James (1955) initially defined an iron formation as a "chemical sediment typically thin-bedded or laminated, containing 15% or more Fe of sedimentary origin, commonly but not necessarily containing layers of chert". Trendall (1983) revised the definition to "anomalously high Fe content" and removed the minimum 15% lower limit. It is the large quantity of iron that makes these rocks particularly economic.

James (1954) identified four main iron-formation facies comprising all iron formations including: 1) oxide; 2) carbonate; 3) silicate; and 4) sulphide. Oxide facies are considered the most economic, typically containing 30-35% Fe. This can be further subdivided into magnetite and hematite according to the dominant oxide. The Main Tilden Pit was originally considered an example of an oxide facies iron formation that is dominantly comprised of hematite. However, portions of the pit may in fact represent oxide-carbonate facies iron formation. There is a transition in oxide species from stratigraphically lower magnetite, to martite, to stratigraphically higher hematite ores.

Both existing mining terminology and lithofacies division developed herein are employed in defining ore domains in this thesis. Informal use of several common terms can be found in Appendix A. The metallurgical Main Pit Carbonate and Martite Domains, delineated through mine development, are defined in the following chapter 2. A lithofacies classification was applied to these same metallurgical domains over the course of the current research. Lithofacies descriptions including textural and mineral chemical variations are addressed in chapters 3 and 4.

1.4 Location and Access

The Marquette Range Supergroup is a thick Paleoproterozoic metasedimentary succession that contains multiple banded iron formations, including the Negaunee Iron Formation. It forms the bedrock geology of the Marquette Mineral District of Michigan, which incorporates the towns of Negaunee, Marquette and Ishpeming. The Negaunee Iron Formation typically forms topographic highs such as Jasper Knob at Ishpeming and

the ridges where the Empire, CDIII and Tilden mines are sited. Outcrop exposure beyond the mine property boundaries is quite limited as the area is generally covered by deciduous forests. Where exposed, iron formation outcrops are moderately oxidized. Iron formation exposed in the mine workings is fresh but typically covered in brown oxidized iron dust due to ongoing blasting and mining, making it difficult to identify lithofacies. The best way to investigate the Negaunee Iron Formation is within non-active historic mine pits and in drill core.

Cliffs Natural Resources Ltd. operations are located in Ishpeming, approximately 23 km east of the shore of Lake Superior and the city of Marquette (Figure 1.1). The southern most Tilden Pit straddles the faulted contact between the Negaunee Iron Formation and the Archean-aged Southern Gneiss Complex. As of 2010, the Tilden Pit dimensions measure 707 meters at its widest point at the surface, 1,593 meters long and approximately 350 meters deep (Figure 1.2). Tapering downward to the base, the current bottom of the pit is 152 meters wide, and 721 meters long. Access to the mine is controlled by security entrances as pit operations involve continual year round ore removal and periodic blasting. Current mining is focused on the basal Main Pit Carbonate Domain, and this is the specific focus of this thesis.

Plate 1.0: Tilden Pit dimensions as of 2007. At the surface it is 1,593 meters long, 707 meters wide and 350 meters deep. At its base it is 721 meters long and 152 wide.

The Tilden deposit is unique in the Lake Superior region in that the principle production (over 75%) is from hematite flotation ore. All other mining operations in the region are based on mining magnetite ore or high-grade hematite direct shipping ore.

1.5 Statement of the Problem

Mining of Tilden's Main Pit Carbonate Domain has presented Cliff's staff with metallurgical challenges. The Main Pit Carbonate Domain represents an oxidized portion of the Negaunee Iron Formation that is comprised of complex iron ore mineralogy. The variability in mineral textures and chemistry has led to difficulties during separation and concentration processes that ultimately affect pellet quality. Standard operation procedure is to sample every second drill hole (~12 meters apart) and analyze for bulk major element geochemistry. Utilizing the bulk chemistry, including total head iron, phosphorous and silica, ore mixing ratios are calculated to ensure the desired proportions of element abundances for consistent mill feed. Historically, bulk geochemical analyses have been accurate enough in predicting ore-processing response however in current mining of the Main Pit Carbonate Domain these practices have been less successful. The bench tests that are used to predict plant response have also been unreliable.

The definition of ore zones has been based on the metallurgical process response of differing ore types. The differing ore zones have been assigned a "Domain" designation for mine planning purposes. Definitions and the characteristic bulk geochemistry of each domain are addressed in Chapter 2. Metallurgical definitions of domains are applied in the absence of any geological data for the explanation of deviations in ore-processing response.

1.6 Objectives

The primary objective of this thesis is to define the ore zones on the basis of detailed paragenetic relationships of the differing iron ore mineral assemblages. The secondary objectives for this thesis are threefold:

1) To delineate lithofacies within the metallurgically defined Main Pit Carbonate and Martite domains by utilizing textural and mineral chemical mapping.

2) Develop a metallogenic model for the iron ore that accounts for the detailed paragenetic relationships demonstrated by the various ore types.

3) Apply the metallogenic model to predict the metallurgical response to complex ores within the Main Pit Carbonate Domain.

Mineral textural and mineral chemical variations are used to subdivide the Main Pit Carbonate and Martite domains into differing lithofacies. Characterization of each of the lithofacies was determined by core-logging, petrographic investigations and detailed microprobe analyses. The apparent change in lithological facies both laterally and vertically provided evidence not only for a change in depositional environment over time, but variations in subsequent diagenetic, metamorphic and late hydrothermal overprints. A paleoenvironment interpretation and paragenetic sequence of the subsequent overprints are described. The lithofacies of the Main Pit Carbonate and Martite domains are linked to the bulk head chemistry recorded in exploration drill holes. The comparison of mineral textures and mineral chemistry to whole rock analyses clearly demonstrates both textures and mineral chemistry affect liberation, ore-mixing ratio calculations and ultimately the pellet quality. Combining all data, a metallogenic model is proposed that accounts for the complex paragenetic evolution and metallurgical response of iron ores in the Carbonate and Martite domains of the Tilden Pit.

Chapter 2: Penokean Geotectonic Framework

2.1 Introduction

The Tilden Mine is situated in the Upper Michigan Peninsula on the south shore of Lake Superior. The region is central to the Penokean role in the amalgamation of Laurentia between 2.4 and 1.7 Ga (Sims et al., 1980). This region has experienced a protracted Penokean orogenic history that included rifting of the Neoarchean shield, island arc accretion, foreland basin development and late thermal doming. The Penokean orogen (1875-1750 Ma) was subsequently reactivated during the 1.1 Ga Keweenawan rifting event that resulted in widespread mafic dyke swarms and regional flood basalt volcanism (Hoffman, 1987). This chapter outlines the Penokean orogenic cycle from the 2.4 Ga rifting on the south margin of the Superior Province, development of juvenile 1.9 Ga island arcs, 1850 Ma arc accretion and foreland basin development, and terminal thermal doming at 1750 Ma. It then considers the depositional history of the Marquette Range Supergroup and concludes with a discussion on the tectonic setting of the Negaunee Iron Formation.

2.2 The Penokean Orogenic Cycle

Although Archean events are not the focus of this thesis, a 2.7 Ga regional deformation zone juxtaposes the Neoarchean Superior craton against an older Mesoarchean gneiss terrane to the south and this boundary plays a large role in subsequent Paleoproterozoic history. The Great Lakes Tectonic Zone extends 1200 kilometers from Minnesota, USA into Ontario, Canada (Figure 2.0). Although not well defined in Ontario, the northern limit is the Murray fault system (Sims et al., 1980). Subsequent Paleoproterozoic depositional history in the Lake Superior and Lake Huron regions relates to reactivating the Great Lakes Tectonic Zone.

As early as 2.4 Ga, diachronous crustal foundering accommodated by high angle normal faulting resulted in the formation of structural basins parallel to the Great Lakes

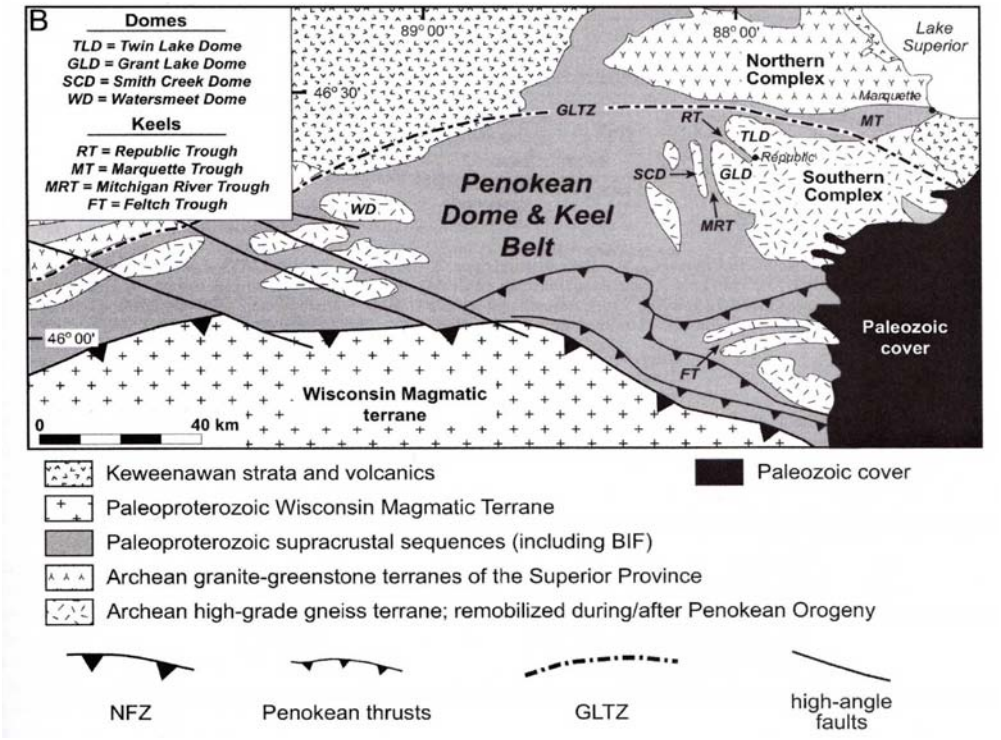

Figure 2.0: The Marquette Range Supergroup bounded by the Archean Superior Province (north) and the Wisconsin Magmatic Terrane (south). Note the Marquette Range Supergroup has a parallel trend to the Great Lakes Tectonic Zone (GLTZ) (Tinkham and Marshak, 2004).

Tectonic Zone (Sims et al., 1980). Three depositional prisms formed along this structural zone, consisting of the Huronian Supergroup on the north shore of Lake Huron, the Marquette Range Supergroup in Michigan, and the Animikie Supergroup in Minnesota (Figure 2.1). Young (1983) suggests that the Huronian Supergroup and the Marquette Range Supergroup represent the early ~2.4 Ga rifting phase of the Penokean cycle. This same author correlates the basal Chocolay Group of the Marquette Range Supergroup to the upper Cobalt Group of the Huronian Supergroup. Basal Chocolay Group equivalents are missing in the Mesabi and Gunflint ranges of the Animikie Supergroup suggesting rifting propagated westward. Both the Huronian and Marquette Range form depositional prisms that thickened to the south. The northern portions of these basins are typified by thin sequences of sediments whereas southern more mobile segments have thicker sequences of sediments interbedded with volcanics (Sims et al., 1980). Deformation

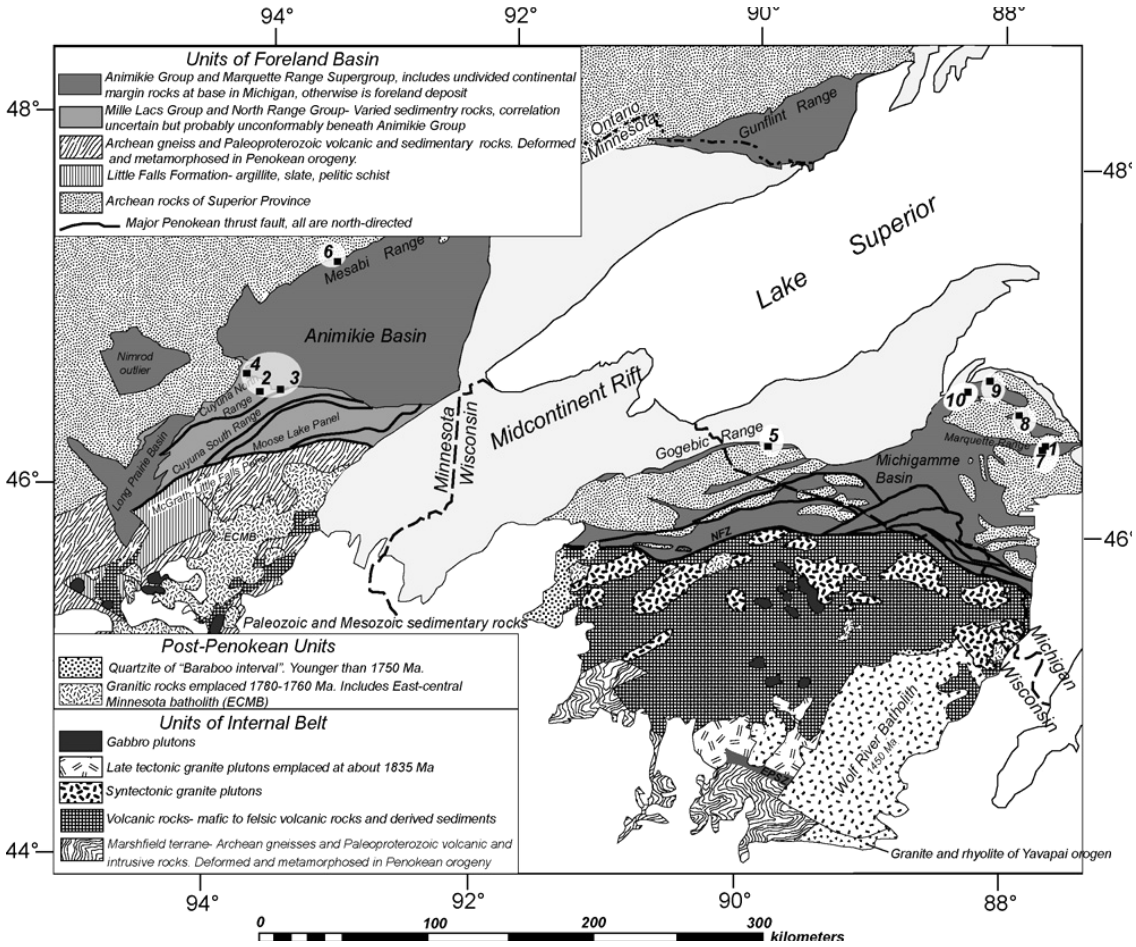

Figure 2.1: A map depicting the regional geology of the western Superior Lake region, USA. Note that the Animikie and Marquette Range Supergroup are considered partly contemporaneous. The Niagara Fault Zone represents the faulted boundary between the Marquette Range Supergroup and the Wisconsin Magmatic Terrane (Vallini et al., 2007)

intensity is lower in the north and more intense to the south, reflecting increasing crustal instability.

Sims et al., (1980) support the interpretation that the lower Chocolay and Menominee groups of the Marquette Range Supergroup represent early rifting and passive margin sedimentation prior to Penokean collision (Figure 2.2). Chocolay Group sediments represent early rift facies clastics. The Menominee Group sediments however represent deposition on a stable shelf (Young, 1983). The Menominee dolomite, argillite and iron formation succession is attributed to stable passive margin sedimentation.

Ojankangas et al, (2001) proposes intracratonic sedimentation that progressed to an Atlantic-style passive margin setting.

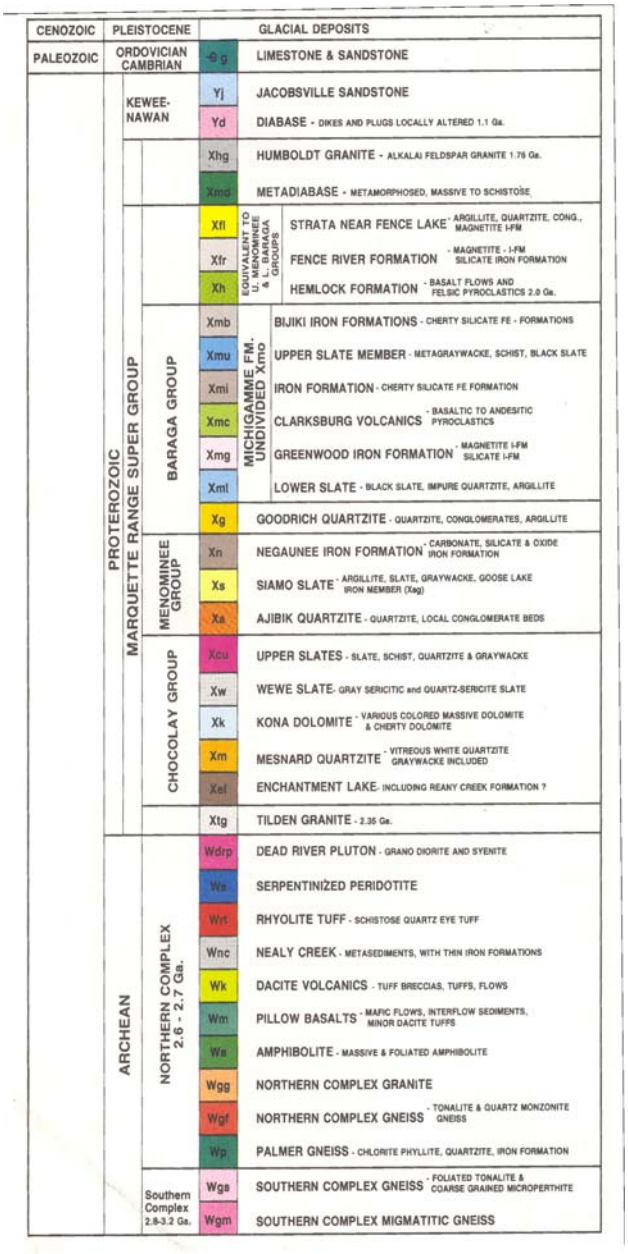

Figure 2.2: A stratigraphic section representing the Marquette Range Supergroup (compiled from publications of USGS, Michigan Department of Natural Resources, Michigan Technology University, Cleveland-Cliffs Iron Company and Callahan Mining Corporation 2007).

Intrusion of the 2.2 Ga Nippissing diabase sills within the Huronian Supergroup indicates early rift magmatism accompanied sedimentation (Corfu and Andrews, 1986). Geochemical signatures of the metadiabase sills in the Menominee and volcanics within the Baraga Groups, also supports a continental rift setting (Sims et al., 1980). Sm-Nd dating of megascopic eukaryotic algae sampled within the Negaunee Iron Formation has yielded dates of 2110 +/- 52 Ma, suggesting that the iron formation deposition that caps the Menominee Group occurred by ~ 2.1 Ga (Hans and Runnegar, 1992). Nd-isotopic signatures have also shown there is no change in provenance between the Chocolay and the Menominee Groups as both groups are sourced from the northern Superior Craton (Sims et al., 1980).

Rifting between 2.4 and 2.1 Ga was followed by south-directed subduction that formed the 1.9 Ma juvenile-arc comprising the Wisconsin Magmatic Terrane (Schultz and Cannon, 2007). Absence of arc-type igneous rocks in the north prior to 1875 Ma supports initial south-dipping subduction. This resulted in decrease in age and increase in abundance of Penokean-aged plutons from north to south across the Wisconsin Magmatic Terrane (Hoffman, 1988; Van Schmus et al., 1987). When the Superior craton could no longer subduct beneath the southern island arc terranes, subduction polarity switched to north-directed (Schneider et al., 2002). Accretion of the Wisconsin Magamatic Terrane to the Superior craton, initiated the deposition of the turbiditic sediments of the Baraga Group onto the foreland (Van Schmus, 1976; Barovich et al., 1989).

A major erosonal unconformity at the base of the Goodrich Quartzite separates the Menominee and the Baraga groups (Figure 2.2). Vallini et al., (2007) propose that this represents uplift and erosion ca. 1860 Ma. A reversal in sediment provenance is marked by this unconformity as the Menominee Group is sourced from the northern Superior craton while the Baraga Group is sourced from the southern terranes (Sims et al., 1980). Identification of 1850 Ma Sudbury Event impactites have been recently documented across the Marquette Range and Animikie supergroups (Cannon et al., 2010). Spherulitic units mark the stratigraphic tops of the Mesabi and Gunflint iron ranges of the Animikie Group (Figure 2.3). In the Marquette Range Supergroup, however, the Sudbury impact occurs below the Bijiki, but well above the basal Goodrich Quartzite of the Baraga Group (Cannon et al., 2010). This recent stratigraphic correlation

indicates that the Negaunee Iron Formation is likely much older than the proposed 1874 Ma date of Schneider et al., (2002). By 1835 Ma the continued northward directed compression developed the 1200 km long Penokean fold and thrust belt parallel to the Great Lakes Tectonic Zone (Van Schmus, 1976; Schneider et al., 2002).

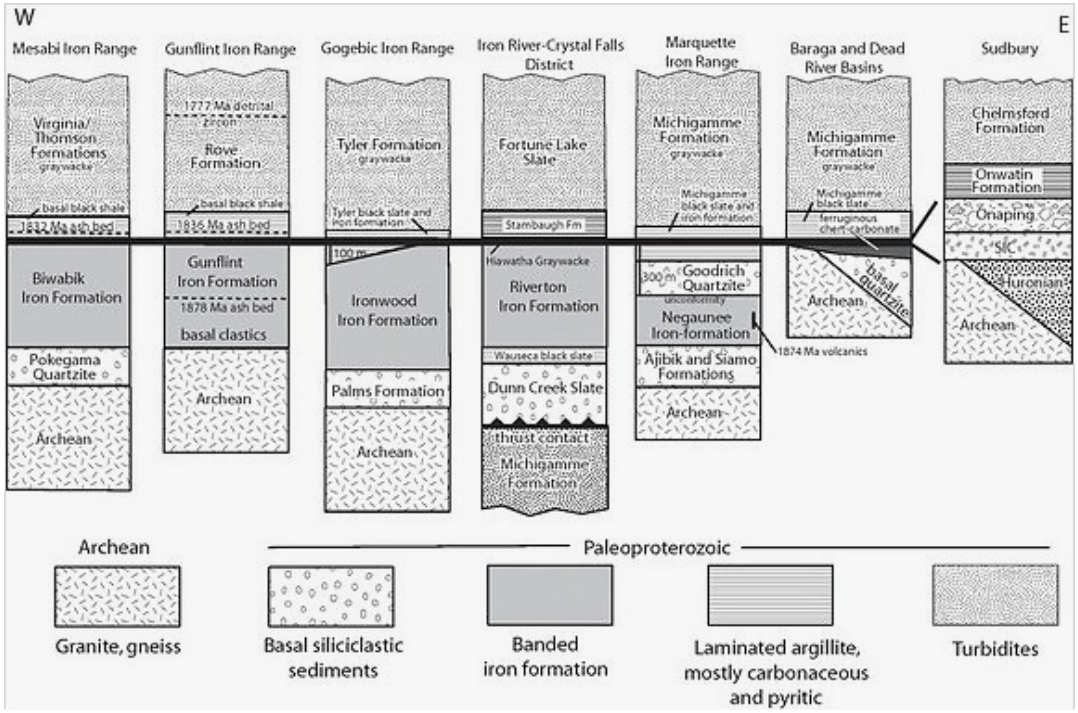

Figure 2.3: Cross section correlation by Cannon et al., (2010) illustrating the stratigraphic position of the Sudbury Impact Event layer across the Great Lakes region. Note how the spherulitic layer terminates most iron formation deposition with the exception of the Negaunee.

2.3 Penokean Deformation of the Marquette Range Supergroup

The Penokean fold and thrust belt parallels the Great Lakes Tectonic Zone. Mesoarchean basement outliers are exposed in the cores of domes within this belt (Sims et al., 1980). Regional folds are typically open, inclined to the northwest, and characterized by a steep SE-dipping penetrative cleavage (Sims et al., 1980). Penokean tectonic fabrics developed between 1870 to 1830 Ma (Sims and Peterman, 1983). Original growth fault extension

accommodating passive margin rifting focused reverse faulting during Penokean transpressional collision and resulted in basin inversions (Lukey et al., 2007). Second-order structures within the Marquette Range Supergroup consist of local upright to steeply inclined anticlines and synclines with low angle northwest or southeast plunges (Cambray, 2002).

Peak thermal metamorphism post dates regional compression and is attributed to such anorogenic plutonism as the 1760 Ma Humbolt granite. Tinkham and Marshak (2004) show that metamorphic isograde outline gneiss domes (Figure 2.4A). These same authors interpret the regional dome and keel structural patterns to signify the collapse of the Penokean orogen. The supracrustal keels of the Marquette Range Supergroup are bounded by shear zones and displaced downward relative to the interior of gneiss domes. The dome and keel structural development at 1760 Ma occurred 70 million years after the Penokean arc-craton collision (Tinkham and Marshak, 2004).

Development of the post-orogenic Republic Metamorphic Node resulted in the thermal metamorphism that overprinted the Marquette region (James, 1955). Schneider et al., (1996) report $^{40}Ar/^{39}Ar$ ages between 1720 and 1680 Ma for developing the Republic Metamorphic Node. Metamorphic grade in the Marquette District increases from chlorite grade, in the east near Negaunee, to sillimanite grade near the village of Republic (Figure 2.4B). The Tilden Pit lies just outboard of the biotite isograde (James, 1955). Haase (1979) identified three metamorphic zones within the Negaunee on the basis of specific iron-rich mineral assemblages. These zones of increasing metamorphic grade from east to west include: Zone 1, defined by the occurrence of stilpnomelane or minnesotaite or both co-existing with quartz and siderite; Zone 2, defined by ubiquitous grunerite-bearing assemblages co-existing with quartz and siderite; and Zone 3, defined by the appearance of garnet or Ca-amphibole or both and further subdivided into garnet and Ca-amphibole co-existing with grunerite and garnet, and Ca-amphibole coexists with clinopyroxene, olivine and grunerite. According to Haase (1979) the Tilden mine occurs in Zone 1 and lies between chlorite grade to the east and biotite grade to the west. Notably, neither stilpnomelane nor minnesotaite were identified in the current investigation at the Tilden Pit.

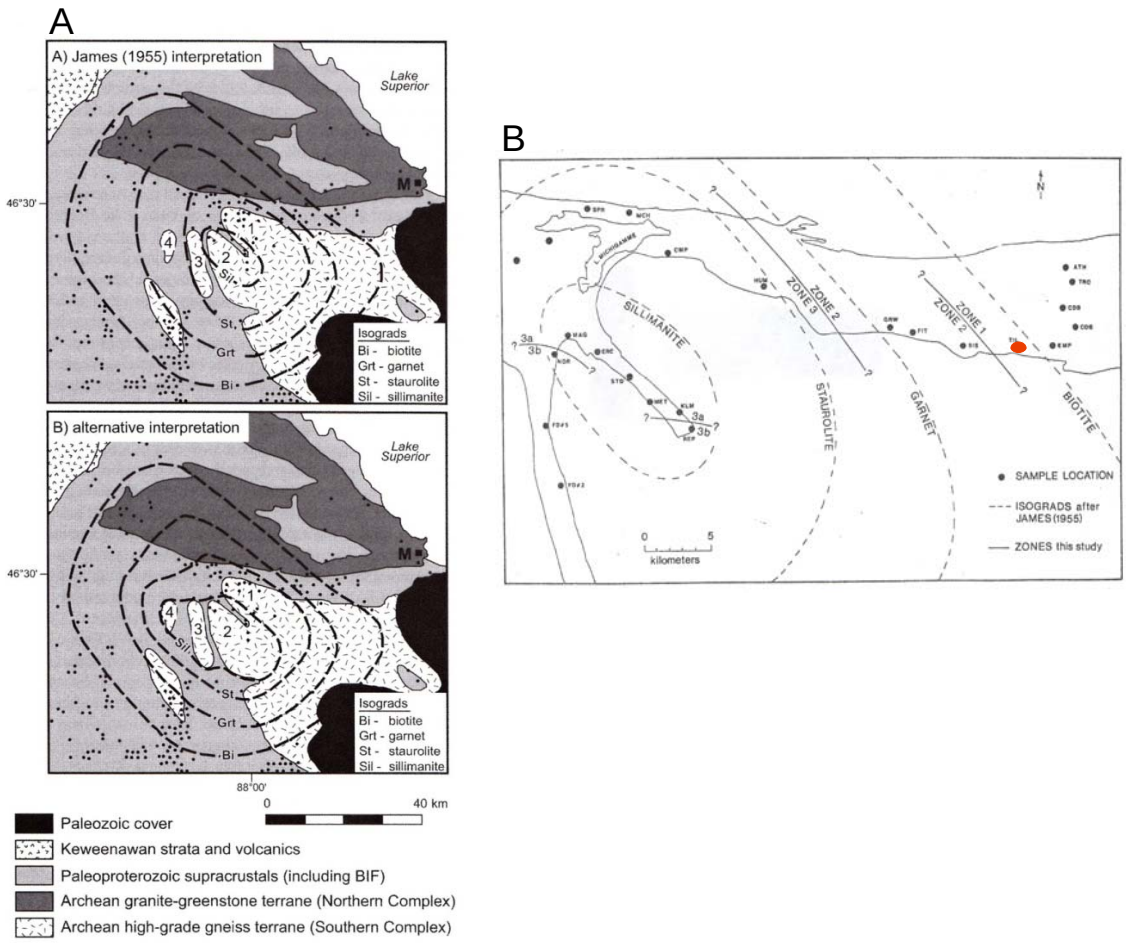

Figure 2.4: The isograd boundaries according to (a) Tinkham and Marshak (2004) and (B) by Haase (1979) showing the increasing metamorphic grade to the west. Note the approximate location of the Tilden Mine (red dot) close to the Biotite-Chlorite isograd boundary.

Schultz and Cannon (2007) have recently proposed that the thermal metamorphic overprint of the Marquette Range Supergroup may relate to the far field accretion of the younger Yavapai arc system. These authors and Karlstron et al. (2001) note that the domal uplift in central Wisconsin coincides with the compressive deformation of the ~ 1760 Ma Yavapai orogen, approximately 200 km south of the Penokean orogen. They suggest the post-Penokean anorogenic plutonism was driven in part by compression due to continent-arc accretion to the south. Schultz and Cannon (2007) also propose that a late hydrothermal overprint of the Great Lakes Tectonic Zone may be related to accretion of the Mazatal arc system. These authors observed that in Wisconsin and part of

Michigan basement rocks beneath deformed quartzites yield 1630 Ma cooling ages that temporally link this late hydrothermal overprint to docking of the Mazatal arc.

Late shear zone reactivation accounts for the late hydrothermal overprint of the Negaunee Iron Formation proximal to the Southern Shear Zone. At the Champion mine molybdenite, copper and gold mineralization is attributed to a late hydrothermal fluid influx accompanying shearing that post dates the thermal peak (Babcock, 1966). Both the Tilden and Champion mines occur on the same northern structural boundary of the Republic Metamorphic Node and recent Os-Re dating of the molybdenite and Mn-bearing magnetites at Champion has yielded ages ranging from 1672 to 1570 Ma (Waggoner, 2010).

2.4 Sedimentary History of the Marquette Range Supergroup

The Marquette Range Supergroup is a Paleoproterozoic continental margin sedimentary succession that lies unconformably on the southern margin of the Archean Superior craton (Schneider et al., 2002). It forms an east-west basin, which is 24-100 km wide and 310 km long (Figure 2.5), striking across the Upper Peninsula of Michigan (Van Schmus and Hinze, 1985). The thickness of the Marquette Range Supergroup varies from 2000 meters in the north to 7500 meters in the south (James et al., 1968). Sims et al., (1980) proposes that similar to the Huronian, southward sediment thickening is a result of dip-slip downthrown fault movement on the southern Superior margin. Differential subsidence occurred throughout the depositional history. Larue and Sloss (1980) also propose Marquette basin sedimentation is related to passive margin rifting prior to Penokean collision. Foundering of the underlying Archean basement reactivated Archean faults across the passive margin (Schultz, 1990; Sims et al., 1980). Cliffs' Tilden Pit is located on the southeastern margin of the Marquette Iron Range where it is in fault contact with the Mesoarchean 3.2 - 2.8 Ga Southern Gneiss Complex (Figure 2.1).

The siliciclastic and chemical sedimentary rock cycles of the Marquette Range Supergroup comprises the lower Chocolay, medial Menominee and upper Baraga/Paint River groups. All three groups represent upward fining sequences (Figure 2.2). The

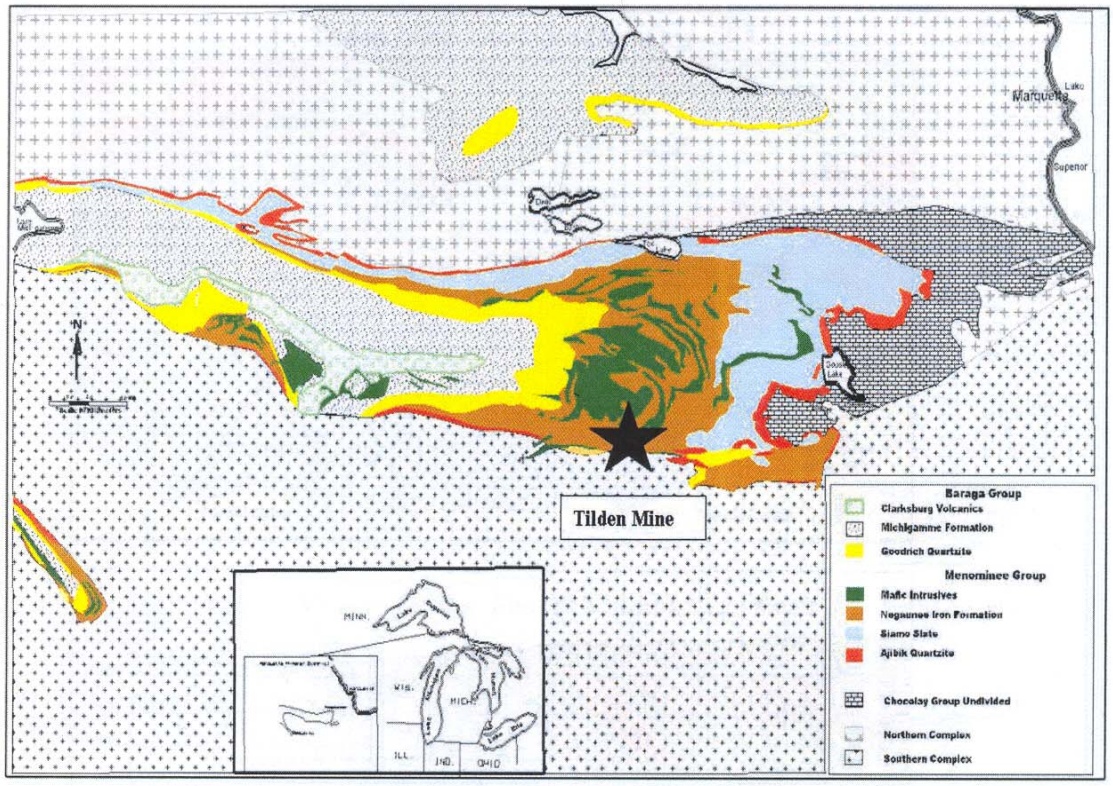

Figure 2.5: A generalized geology map of the Marquette Range Supergroup in contact with the Southern Complex. The Tilden Mine is located on the contact between the Negaunee Iron Formtation (brown) and the Southern Complex (cross-pattern) (Lukey et al., 2007).

lower Chocolay Group is dominated by shelf facies quartzites and dolomites. From bottom to top it is comprised of the Enchantment Lake Conglomerate, Mesnard Quartzite, Kona Dolomite and Wewe Slate (Gair, 1970). The Chocolay is unconformably overlain by the argillitic Menominee Group that includes from bottom to top the Ajibik Quartzite, Siamo Slate and Negaunee Iron Formation (Cannon and Gair, 1970). The Negaunee Iron Formation represents the upper member of the Menominee Group and is the dominant supplier of iron ore in the Marquette District. Both the Chocolay and Menominee groups represent shallow water facies deposited in local fault-bounded troughs (Larue and Sloss, 1980).

The Baraga and locally occurring Paint River groups unconformably overlie the Menominee Group (Gair, 1970). From bottom to top the Baraga Group includes the Goodrich Quartzite, Michigamme Slate, Clarksburg Volcanics and Bijiki Iron Formation (Larue and Sloss, 1980). The overlying Baraga and Paint River groups are turbiditic sequences deposited during widespread, rapid subsidence caused by northward migration of a foredeep on the leading edge of the overthrust Wisconsin Magmatic Terrane (Sims et al., 1980; Hoffman 1988). Young (1983) supports this interpretation and further suggests that the thick overlying Baraga Group represents arc derived turbiditic rocks deposited in an extensive foreland basin that developed during crustal downwarping. The Baraga overstepped the underlying platformal Chocolay and Menominee groups northwards (Young, 1983). The reversal in sedimentary provenance is recorded by a marked erosional unconformity between the basal Baraga Group Goodrich Quartzite and underlying Negaunee Iron Formation capping the Menominee Group.

2.5 Tectonic Setting of the Negaunee Iron Formation

Most of the iron ore mined in Michigan has been extracted from the Superior-type Negaunee Iron Formation of the Marquette Range. Lesser production has also come from the younger Riverton Iron Formation of the Menominee Range and Ironwood Iron Formation of the Gogebic Range (North, 1993). The Negaunee reaches a thickness of 1300 meters within the Marquette trough and changes from dominantly siderite-chert mineral assemblages in the north to magnetite-hematite-chert assemblages in the south (Lukey et al., 2007). The majority of the Negaunee Iron Formation consists of carbonate, carbonate-silicate or carbonate-oxide facies (James, 1954; Gair, 1975). The Negaunee contact with the underlying Siamo Slate is transitional and includes Fe-silicate, Fe-carbonate, and Fe-oxide facies of iron formation. The middle Negaunee is dominated by Fe-carbonate and Fe-carbonate-oxide facies iron formation and the upper Negaunee is dominated by hematite-jasper facies iron formation (Cannon, 1975). This general pattern of hematite facies at the stratigraphic top, medial carbonate and basal mixed facies iron formation holds throughout the Marquette District (James, 1955; Haase, 1979).

Although the depositional history of the Menominee Group has been well established, the tectonic setting and date of the Menominee remains controversial. Much of the controversy polarizes over the age and significance of metadiabase units interlayered within the Negaunee and whether these units correlate to the Hemlock Volcanics. Gair (1956) placed the Hemlock Formation within the upper Baraga Group and considered the chloritized metadiabases within the Negaunee to be much older. Van Schmus and Bickford (1981) dated the Hemlock volcanics to be ~1910 Ma and supported the interpretation that the Hemlock volcanics are younger than the 2.2 Ga Negaunee Iron Formation. Cannon (1986) and Schneider et al., (2002) interpret the Hemlock volcanics to lie unconformably on the lower Chocolay Group and suggest the Hemlock volcanics correlate to the Menominee Group. These authors report dates of 1874 Ma for the Hemlock and suggest a regional correlation for the Negaunee.

Direct dating of the altered metadiabase units that interfinger with the Negaunee have been unsuccessful and therefore correlations remain speculative. Schneider et al., (2002) reinterpret the Hemlock Formation to be contemporaneous with the metadiabase units within the Negaunee Iron Formation and suggest foredeep deposition overlapped with arc magmatism to give rise to the Negaunee metadiabases as well as the Hemlock and Clarksburg Volcanic formations. These authors propose the Menominee was deposited in a back arc basin as opposed to a foreland basin.

However, on the basis of present data it seems likely that the Hemlock on Chocolay unconformity correlates with the Goodrich on Negaunee unconformity, and that this unconformity marks a substantial time gap between passive margin and foreland deposition. The metadiabase units within the Negaunee may indicate that passive margin deposition terminated with active rifting at the outer margin of the shelf, signifying the rift-drift transition around 2.1 Ga. The young 1874 Ma Negaunee age proposed by Schneider et al., (2002) is not consistent with the 2.1 Ga Sm-Nd date reported by Hans and Runnegar (1992). Nor is it stratigraphically supported by the 1850 Ma impactite marker of the Sudbury Event that occurs well above the unconformity separating the Negaunee Iron Formation and overlying Baraga Group.

Chapter 3: Stratigraphy and Petrography

3.1 Introduction

Iron ore of the Tilden Pit has been historically subdivided into metallurgical domains based on bulk geochemical signatures and other metallurgical characteristics. This chapter will first review pit geology and present the definitions and ore characteristics of the metallurgical domains. Much of the information is courtesy of the Cliffs technical staff. Detailed petrographic descriptions of the lithofacies constituting the Main Pit Carbonate and Martite domains are then presented. The metadiabase capping the Martite Domain as well as the effects of the late hydrothermal overprint are also described.

3.2 Geology of the Tilden Mine

The Tilden Mine occurs at the southern boundary of the Paleoproterozoic Marquette Range Trough (Figure 3.0) where it is in fault contact with the Mesoarchean Southern Gneiss Complex or locally the Palmer Gneiss (Webster, 1999; Cambray, 2002). The Southern Shear Zone likely originated as a basin margin normal fault accommodating basin subsidence along the Great Lakes Tectonic Zone. It was reactivated during the transpressional Penokean collision and now is a reverse fault that dips about 65^{o} north (Cambray, 2002). The fault is highly chloritized and contains sheared remnants of metadiabase (Lukey et al., 2007). The dominating structure in the pit is a 100 meter scale asymmetric anticline with its axial plane dipping subparallel to the Palmer Gneiss and which plunges 30^{o} northwest (Figure 3.0). The steeper southern limb is truncated by the Southern Gneiss Complex.

Two ages of mafic rocks occur in the mine: old syn-sedimentary metadiabases and young 1.1 Ga Keweenawan dykes related to the Mid-continent rift. The older series have relict fine porphyritic to diabasic/ophitic texture but are strongly overprinted by chlorite-carbonate alteration assemblages, particularly in deformation zones (Scott and

Lukey, 1999). The younger Keweenawan dykes are of fresh diabase (Lukey et al., 2007). Due to rapid facies changes and the lack of clear marker horizons, the older metadiabase

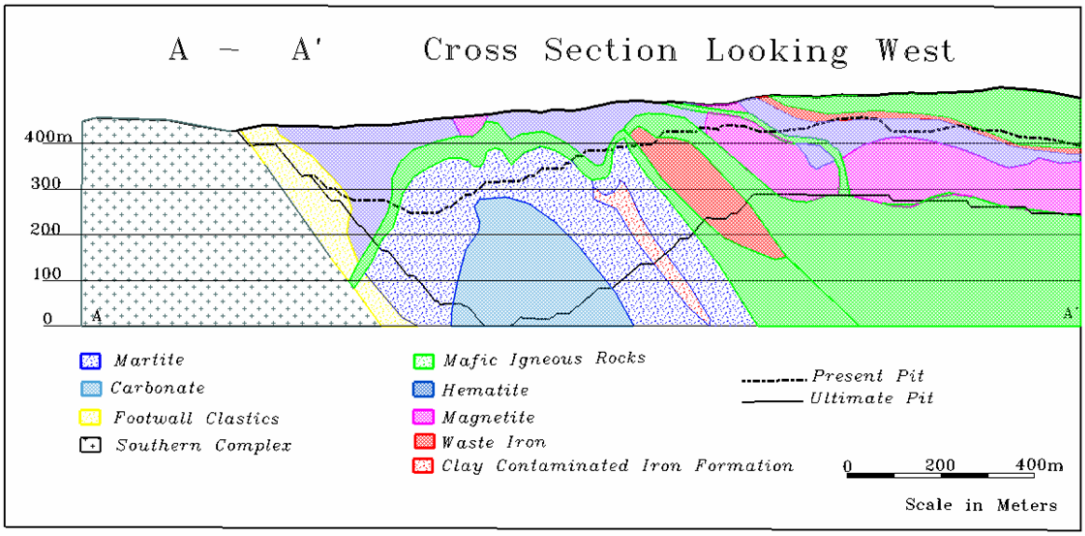

Figure 3.0: A stratigraphic cross-section (A-A' of figure 2.6) that illustrates the anticline as defined by mapping of the igneous "Pillar" marker. The southern limb of the anticline has a steeper dip than the northern limb and is truncated by the sheared contact with the Southern Complex. The Main Pit Carbonate and Martite Domains are located beneath the igneous Pillar (Scott and Lukey, 1999).

units have been used as marker horizons for stratigraphic and structural correlation. The basal metadiabase unit, termed the Pillar, is folded and thins over the crest of the anticline. Numerous chloritized dykes cross-cut the stratigraphy beneath the Pillar and are identified as feeder dykes.

3.2.1 Ore Domains

Mining of the deposit by 14 meter high benches accommodates the size of operating equipment, and geotechnical logistics. Mine plans and grade control are based on geochemical data on 8 x 8 x 14 meter blocks. Differing ore types showing metallurgical consistency forms the basis of resource modeling (Scott and Lukey, 1999). Metallurgical variations defined at blast pattern scale have led to subdivision of the Tilden Pit flotation ores into differing ore domains (Lukey et al., 2007). These domains usually correspond to stratigraphic intervals but may be fault bounded or defined by non-conformable alteration/oxidation fronts (Lukey et al., 2007). Importantly, the domains are

characterized by metallurgical response and not by texture. The primary flotation ore domains are shown in Figure 3.1 and their mineralogy, bulk geochemistry and metallurgical characteristics are summarized in Table 3.0. Metallurgical variations, important in mine planning and ore blending, reflect the variation in such processes as primary deposition, diagenesis, metamorphic and hydrothermal overprinting. There is an overall change upward from dominantly ferrous to ferric iron mineralogy. In all domains, chert is a dominant constituent (Scott and Lukey, 1999).

Domain	Lithofacies	Textures	Mineralogy	Geochemistry
310	Clastics	- detrital quartz - fractures and brecciation	quartz + chlorite + magnetite + magnesite-siderite	High Al, Mg, Ca, Mn, Fe and low P
340	Clastics	- detrital quart - fracture and brecciation	quartz + chlorite + magnetite + magnesite-siderite	High Al, Mg, Ca, Mn, Fe and low P
340	Medial BIF	- chert bands, detrital quartz and granular textures	quartz + magnetite + mart/hem + chlorite+ mag-sid + Fe-dol-ank	High Al, Mg, Ca, Mn, Fe and low P
340	Granular bands	- Gramular texture with rare chert bands	quartz + mart/hem + magnetite +/- chlorite +/- Fe-dol-ank +/- apatite +/- monazite	High Al, Mg, Ca, Mn, Fe and low P
350	Granular Iron Formation	- granular texture with rare chert bands	quartz + mart/hem + magnetite +/- chlorite +/- Fe-dol-ank +/- apatite +/- monazite	Low Al, Mg, Ca, Mn, Fe and High P

Table 3.0: A table summarizing the characteristics of the Clastic (310), Main Pit Carbonate (340) and Martite (350) Domains.

In computer modeling, the domains are designated by a three digit numerical code. The Main Pit Carbonate (340) Domain is the primary focus of this thesis (Figure 3.1). However, the investigation continues into the overlying Martite (350) Domain up to the base of the Pillar. On the basis of the whole rock geochemistry supplied by the mine, the Main Pit Carbonate Domain is higher in Al, Ca and Mg but lower in P compared to the Martite Domain (Figure 3.2). The contact of the Main Pit Carbonate Domain with the

Martite Domain (Figure 3.3) is marked by a dramatic decrease in magnetic iron (magnetite) content (Figure 3.4). Based on satmagan readings the Carbonate Domain is typically in sharp contact with the Martite Domain (Figure 3.5). However locally the boundary is transitional over 10 to 20 meters (Lukey et al., 2007). Thin (10 meter) magnetite-bearing interbeds are locally present above the contact but the upward trend is to increasing martite (Scott and Lukey, 1999).

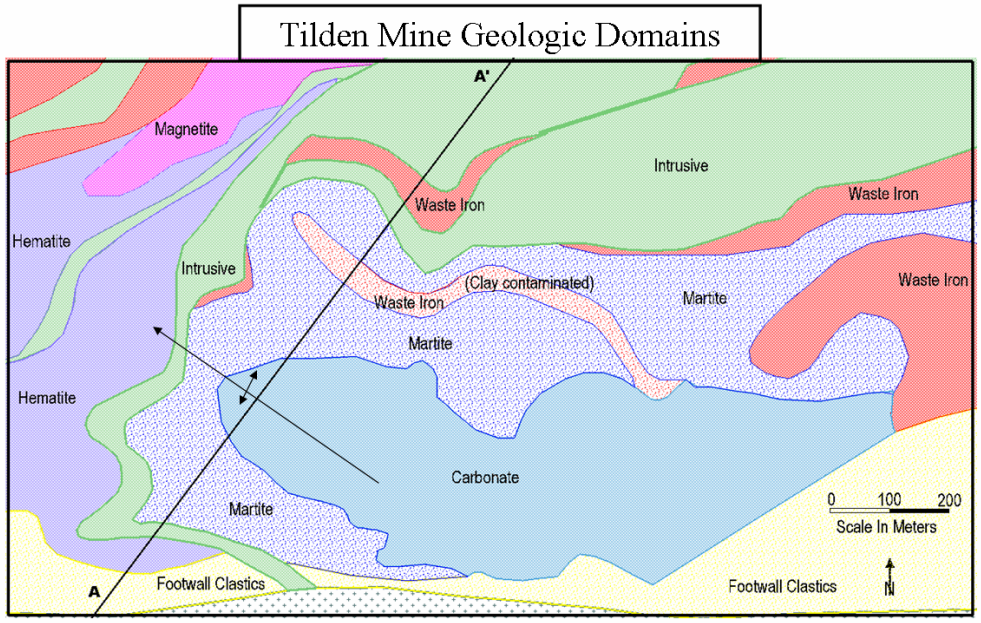

Figure 3.1: A generalized geology map of the domains defined by the Tilden technical staff. The Main Pit Carbonate and Martite Domains are the focus of the thesis. Note the shallowly plunging northwest anticline delineated by the igneous Pillar horizon (Scott and Lukey, 1999).

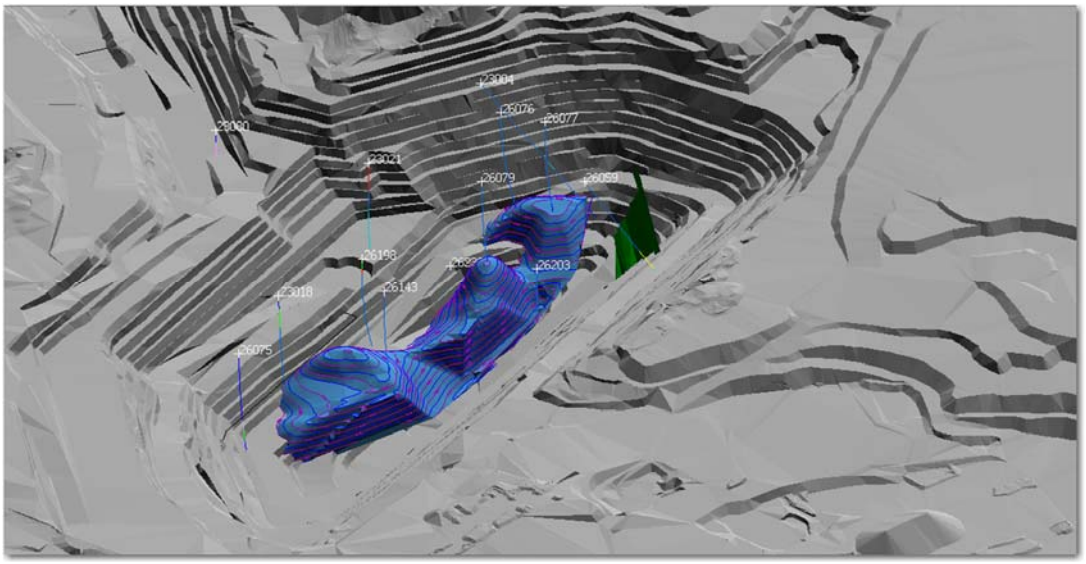

Figure 3.2: A contour map delineating the top of the Main Pit Carbonate (340) Domain as it is identified in the pit in contact with the overlying Martite Domain. Drill holes used in the current research are labelled with white numbers. The green plane represents the location of the Tower Fault. Map courtesy of Cliffs Technical Staff.

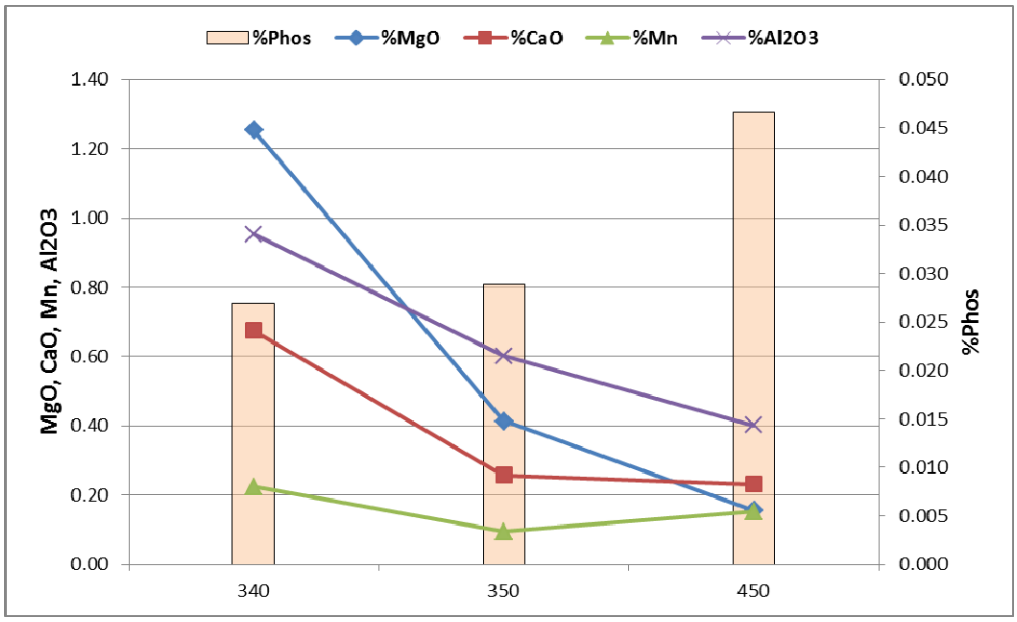

Figure 3.3: A graph showing the bulk geochemistry of the Main Pit Carbonate (340), Martite (350) and Hematite (450) domains respectively.

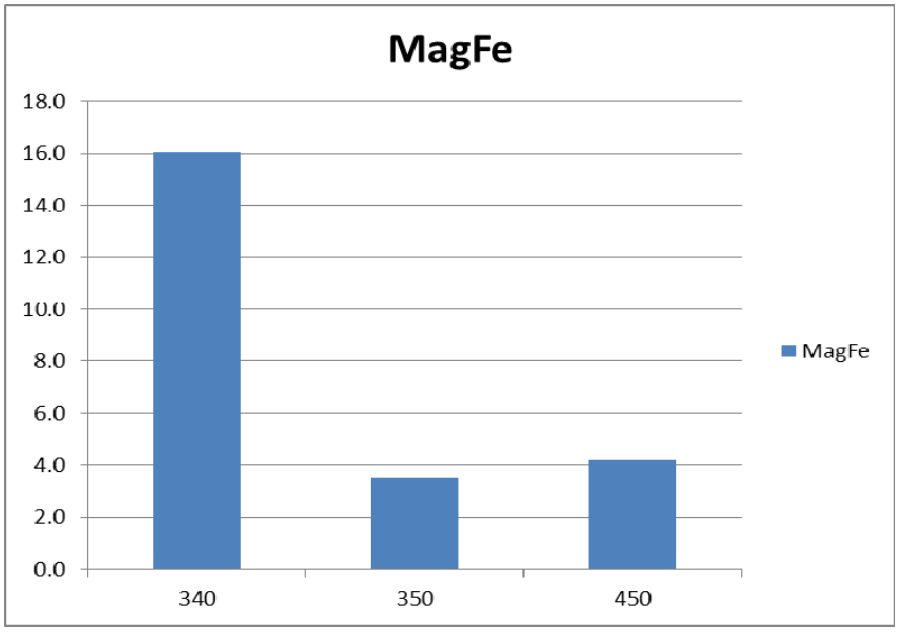

Figure 3.4: A graph showing magnetic iron content of the Main Pit Carbonate (340) Domain, Martite (350) Domain and Hematite Domain (450).

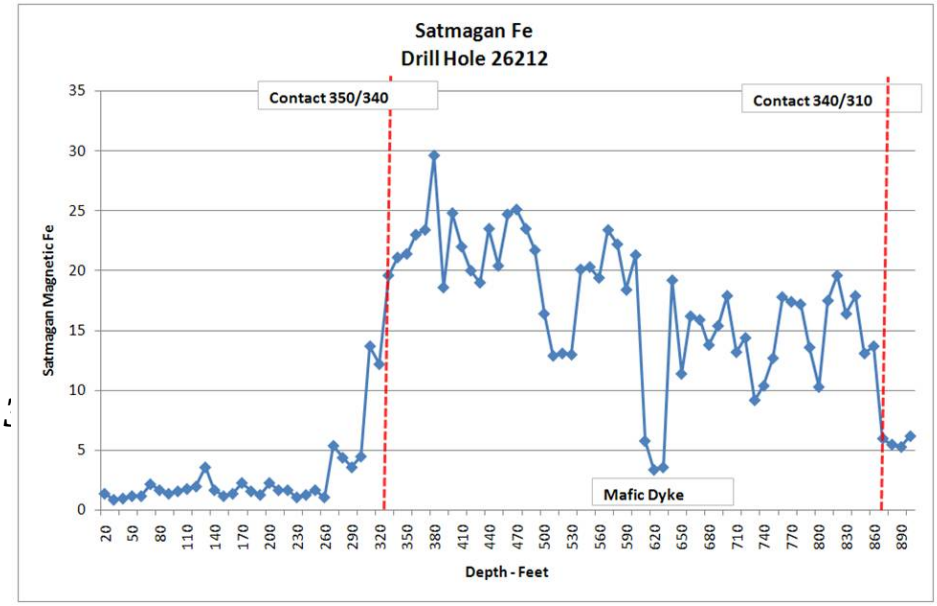

Figure 3.5: Example of a Satmagan reading down drill hole 26-212 delineating the contact between the Main Pit Carbonate (340) and Martite (350), the Main Pit Carbonate (340) and lower Clastic (310) domains.

The lower Clastic (310) Domain grades upward into the Main Pit Carbonate (340) Domain. There is a generally sharp contact against the overlying Martite (350) Domain, and it is capped by the Pillar (230) Domain. The Pillar separates the Martite Domain from the upper Hematite (450) Domain. The lower Clastic Domain (Figure 3.1) comprises the southern margin, and thin clastic units are interstratified within the iron formation of the Main Pit Carbonate Domain (Scott and Lukey, 1999). The Clastic Facies of both the Clastic Domain and the Main Pit Carbonate Domain is coarsest and thickest proximal to the Southern Gneiss Complex. Several deep holes have intersected Clastics Facies below the Main Pit Carbonate Domain well north of the fault, but it is unclear if these deep holes have intersected the Clastic Domain proper (Scott and Lukey, 1999).

The flotation ores within the Tilden Pit are constrained within the Main Pit Anticline (Figure 3.0). The greatest diversity of ore types occurs along the axis of the fold (Lukey et al., 2007). As defined by blast patterns and development drilling, the Main Pit Carbonate Domain cores the axis of the Main Pit Anticline. It has unusual and variable bulk geochemistry and complex mineral textures. The domain designation was originally based on the carbonate content, primarily siderite, and dominant iron oxide

minerals of magnetite and martite (Scott and Lukey, 1999). Designation for the Martite Domain is based on the dominant iron oxide minerals being martite and hematite and the absence of magnetite and carbonate (Scott and Lukey, 1999). The general upward mineralogical variation centered along the axis of the Main Pit Anticline is from ferrous iron dominant magnetite-carbonate-chlorite of the Main Pit Carbonate Domain to ferric martite of the Martite Domain to microplaty hematite-goethite of the Hematite Domain (Scott and Lukey, 1999). The Waste (330) Domain represents iron formation below concentrate grade targets for economic pellet recovery. The Hematite (450) and Waste (330) domains are not investigated in this thesis.

3.3 Detailed Petrography

A location map of strategically selected drill holes and listing of the core sample suite chosen for detailed petrographic study are provided in Appendix A. The primary compositions and texture of the chemical sediments that comprise an iron formation are controversial topics. Furthermore, Archean and Paleoproterozoic iron formations have been subjected to multiple overprints that have modified primary features. Within the Tilden Pit the primary mineralogy of the Negaunee Iron Formation has been masked by regional metamorphism accompanying the 1850 Penokean regional deformation as well as late retrograde hydrothermal conditions accompanying the 1750 Ma thermal overprint. On the basis of detailed petrographic examination, the variety of textures and the mineral assemblages exhibited by the flotation ores at the Tilden mine can be separated paragenetically into initial primary, complex early diagenetic, medial metamorphic and late hydrothermal stages of mineral growth. This and the following chapter document this complex paragenetic history in terms of mineral texture and mineral chemistry. Although subject to metamorphic and hydrothermal overprints, lithofacies correlations based on relict primary and diagenetic textures and mineral compositions may be cautiously employed.

Primary textures such as granules, including peloids and ooids, have been preserved through replacement by diagenetic, metamorphic and hydrothermal mineral assemblages. The term “primary” in this chapter refers to relict original textures that

have been preserved by secondary replacement. Based on relict primary textures, three distinct lithofacies comprise both the Main Pit Carbonate and Martite domains including: 1) Basal Clastics; 2) Medial Banded Iron Formation (BIF); and 3) Granular Iron Formation (GIF) (Figure 3.6). The unique, diagnostic macro- and microscopic textures of these three basal Negaunee lithofacies are described below.

To aid Cliffs Natural Resources in mine planning, these three lithofacies constitute distinct *textural subdomains* for metallurgical purposes. Each lithofacies represents a unique depositional process that has been subsequently modified by diagenetic, metamorphic and hydrothermal overprinting. Description of the three lithofacies will be in ascending stratigraphic order from Basal Clastics, to Medial Banded Iron Formation, to Upper Granular Iron Formation. A metadiabase "Pillar" (or 330 Domain) overlies the Upper GIF unit and caps the Martite Domain. As emplacement of the Pillar may have played a role in the diagenetic overprint of the underlying Carbonate and Martite domains it is also described.

3.4 Basal Clastic Facies

The Basal Clastic Facies is the lowermost rock type exposed in the Tilden Pit (Plate 3.0). It comprises the entire basal Clastic (310) Domain and the lower portion of the overlying Main Pit Carbonate Domain. This clastic lithology may represent a transitional stratigraphic contact between the Negaunee Iron Formation and the underlying Siamo Slate. However, the basal contact has not been intersected in drill core and therefore the total thickness of clastic sediments is currently undefined. Bulk rock geochemistry shows crude iron for the basal Clastic Domain is ~35% weight Fe prior to pelletization (Table 3.0). Due to its relatively low iron content, Cliffs generally considers the Clastic Domain to be the non-economic base of the Negaunee Iron Formation.

The Basal Clastic Facies is thickest proximal to the intersection of the Palmer Gneiss and Tower faults (Figure 3.1). The lateral extent of this unit is undetermined but it likely pinches out at depth to the north. It is speculated that the clastics are related to growth fault movement on the Southern Shear.

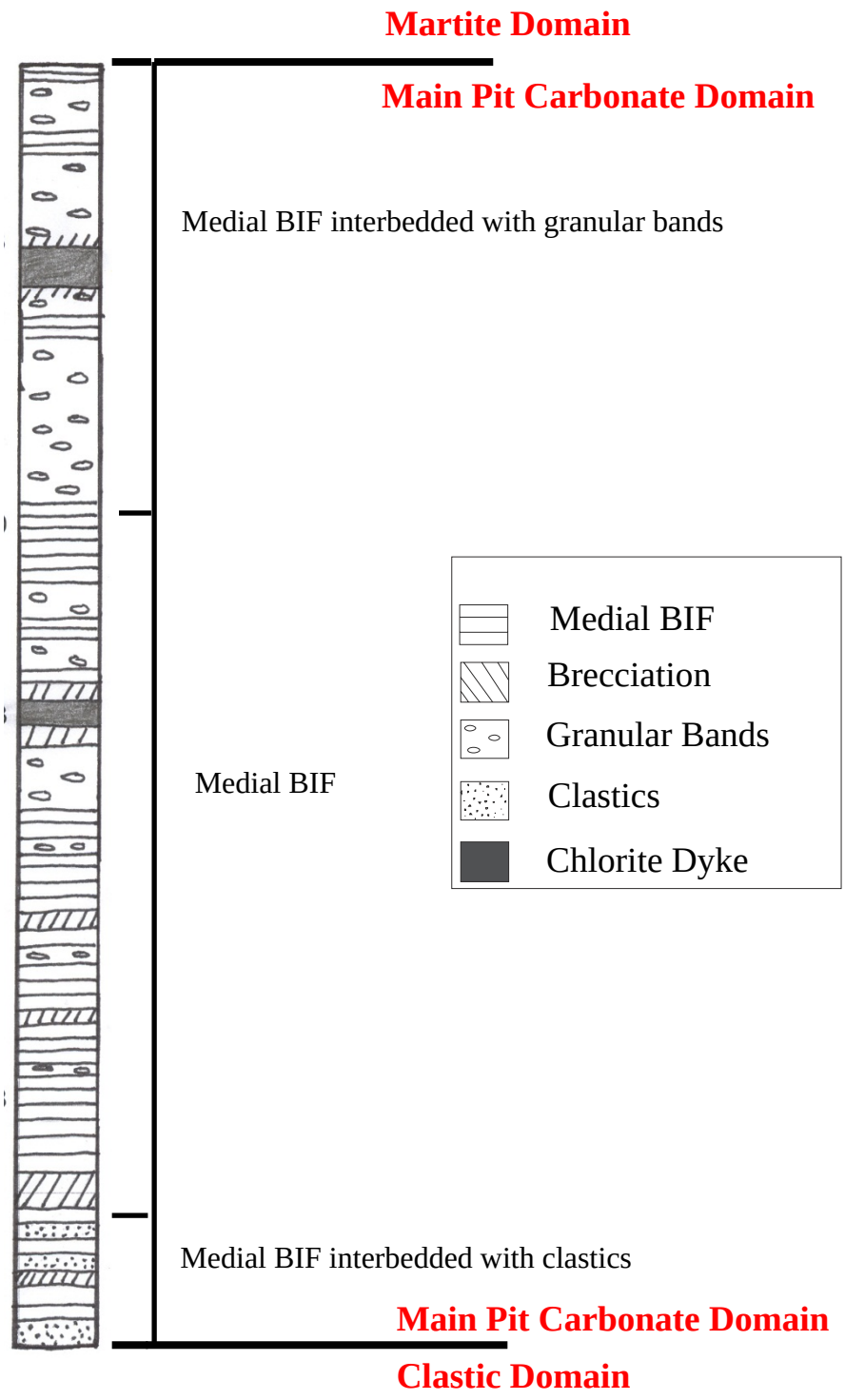

Figure 3.6: An idealized cross-section of the Medial BIF textures of the Main Pit Carbonate Domain. Section is approximately 60 meters.

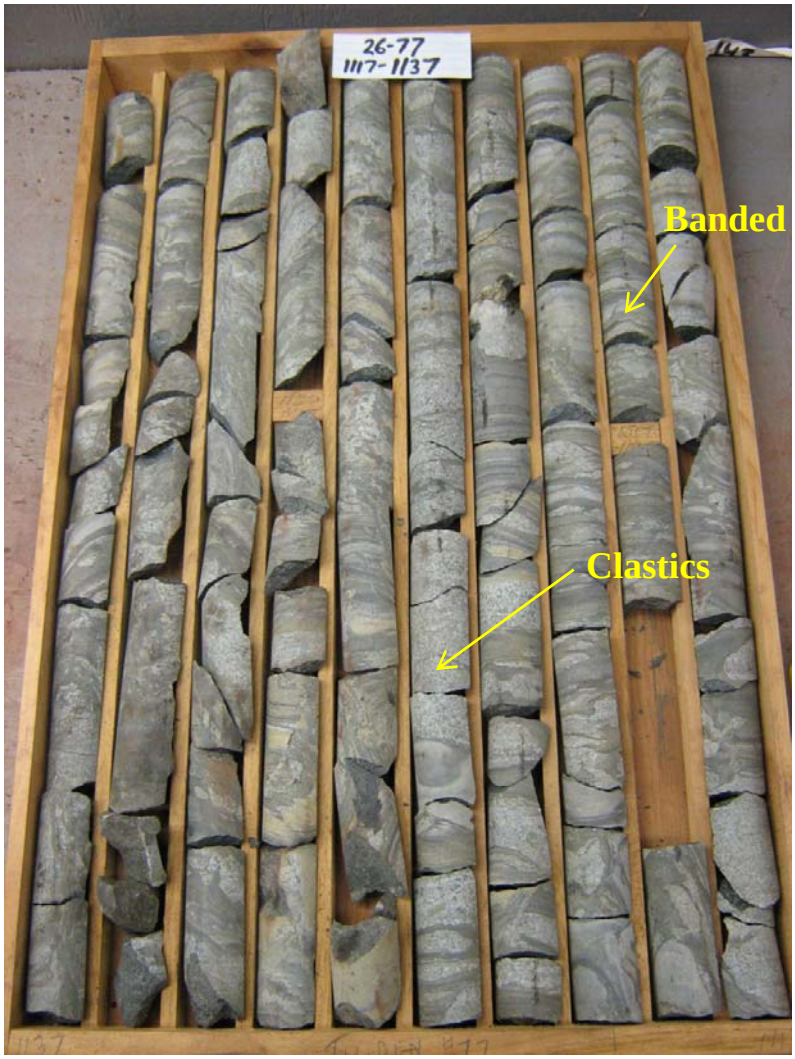

Plate 3.0: Drill core of hole 26-77- (1117-1137) depicting coarse clastics interbedded with Medial BIF at the base of the Main Pit Carbonate Domain.

This unit can be subdivided into coarse-grained and fine-grained layers. A coarse clastic lithology dominates throughout the entire Basal Clastic Facies. Fine grained and coarse grained clastics comprise bands well into the overlying Main Pit Carbonate Domain (Plate 3.0). The detrital textures of the coarse Basal Clastics indicate little transport, suggesting rapid basin subsidence accommodated marine transgression. In core, coarse-grained clastics are dominantly green in colour and contain dispersed coarse (1-4 mm) detrital quartz grains in a dominantly chlorite matrix (Plate 3.1a). The high chlorite content gives rise to a diagnostic green colour that makes this unit distinctive in

drill core and outcrop. In core, fine-grained clastics are dark grey in colour, may or may not contain minor amounts of detrital quartz and have lesser matrix chlorite (Plate 3.1b). In general, there is a subtle decrease in the grain size of the detrital quartz within coarse clastics upsection.

A

B

Plate 3.1: Clastic lithofacies: (a) coarse clastics (sample 23-70-1113); and (b) fine grained variety (sample 26-70-1236).

Monocrystalline quartz grains are the dominant mineral occurring in thin sections of the coarse clastics, with modal percentages estimated between 40-60% (Plate 3.2a). The matrix mineral assemblage is chlorite-magnetite-siderite. The precursor rock is

interpreted to be an immature, poorly sorted quartz-wacke sandstone. In thin section, the matrix of the fine grained clastics is comprised of mud-sized chlorite, carbonate, magnetite and minor illite/sericite (Plate 3.2b). The precursor rock was likely an iron-rich mudstone.

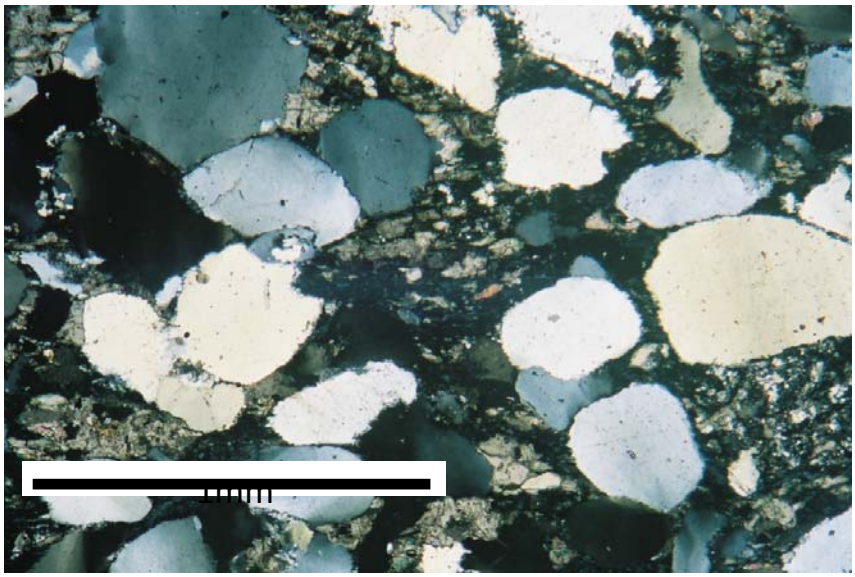

Plate 3.2a: Photomicrograph in cross polarized light of coarse grained clastic texture in sample 26-077-1119. Detrital quartz grains display strained extinction. Late carbonate, chlorite and magnetite are interstitial to the quartz grains.

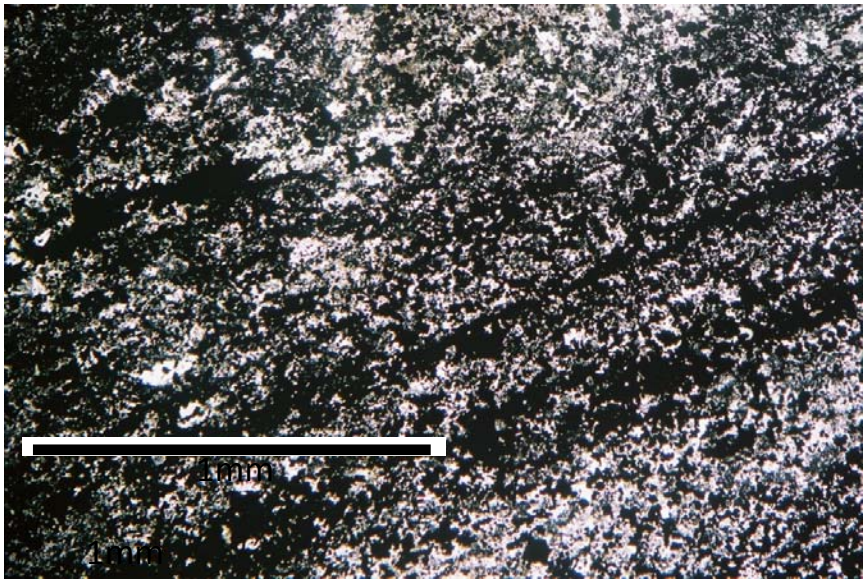

Plate 3.2b: Photomicrograph of fine grained clastic texture in sample 26-075-1296. Note the mud matrix and lack of detrital quartz grains (plane polarized light).

Detrital quartz in the coarse grained clastics ranges between < 1 mm and 4 mm and are sub-rounded to angular. These grains occasionally have margins of silica cement in uniform extinction with the primary grain. The uniform extinction suggests diagenetic cementation involving pore water that was similar in composition to the depositional basin waters and in equilibrium with the detrital quartz grains (Deer et al., 1966). The monocrystalline detrital quartz grains commonly exhibit strained extinction indicating deformation. As strain directions are random and not oriented the deformation occurred prior to transport and deposition. The detrital grains may have been sourced in the deformed basement gneiss to the south. The lack of rounding suggests a short transport distance (Kuenen, 1958; Boggs, 1969). Detrital quartz is commonly absent in the fine grained clastic and where present, is generally less than 1 mm in diameter. Quartz is also a cement component of the chlorite-carbonate-illite/sericite mud matrix.

Lath shaped to fibrous chlorite typically comprises up to 25% of the coarse clastic lithofacies. Grain size ranges from < 1mm to 2 mm. The chlorite is interstitial and secondary, growing around the detrital quartz grains. In the fine grained clastics, the chlorite is very fine grained (<0.1 mm) and occurs as a minor component in the mud matrix of the rock. It is unlikely that chlorite occurred as primary detritus but forms secondary metamorphic overgrowths on precursor matrix minerals.

The carbonate component of the clastics varies in species and grain size. In coarse clastics, anhedral Mg-siderite is blocky and occurs interstitial to detrital quartz intergrown with chlorite and iron oxides, suggesting it originated as a matrix constituent. Coarse grain sizes range up to 1-2 mm. Less than 0.1 mm anhedral to fibrous Mg-siderite is intergrown with quartz, chlorite and illite/sericite in the fine grained matrix. Mg-siderite in the fine grained clastics likely originates as primary or diagenetic carbonate that has been subsequently recrystallized (Boggs, 1995). The coarse interstitial Mg-siderite may represent diagenetic precipitation and cementing related to basinal fluid circulation and chemical precipitation out of a formational brine during diagenesis (Chang et al., 1998). All primary or diagenetic carbonates were subjected to metamorphism and show subsequent grain coarsening.

The characteristic iron oxide occurring in the Clastic Facies is essentially magnetite whereas martite and/or hematite are rare to absent. The majority of the

magnetite forms large blocky grains ranging in size from 0.5 to 2 mm. The coarse idioblastic textures indicate metamorphic growth (Plate 3.3a). Occasionally these magnetite grains contain cores of ferri-hydrite. This suggests primary/diagenetic precipitation of ferri-hydrite such as goethite. Ferri-hydrite acted as a nucleation for the late growth of magnetite and subsequent grain coarsening to produce porphyroblastic textures. The clastics show the greatest variation in iron oxide species proximal to the Tower Fault. At deepest levels intersected in drilling the iron oxide is dominantly magnetite, however, at shallower levels the magnetite is increasingly replaced by martite or hematite (Plate 3.3b). In shallow level replacement of magnetite by martite/hematite, the oxidation product still retains the original blocky texture of magnetite. Martite replacement of magnetite and growth of specularite is linked to late metamorphic conditions.

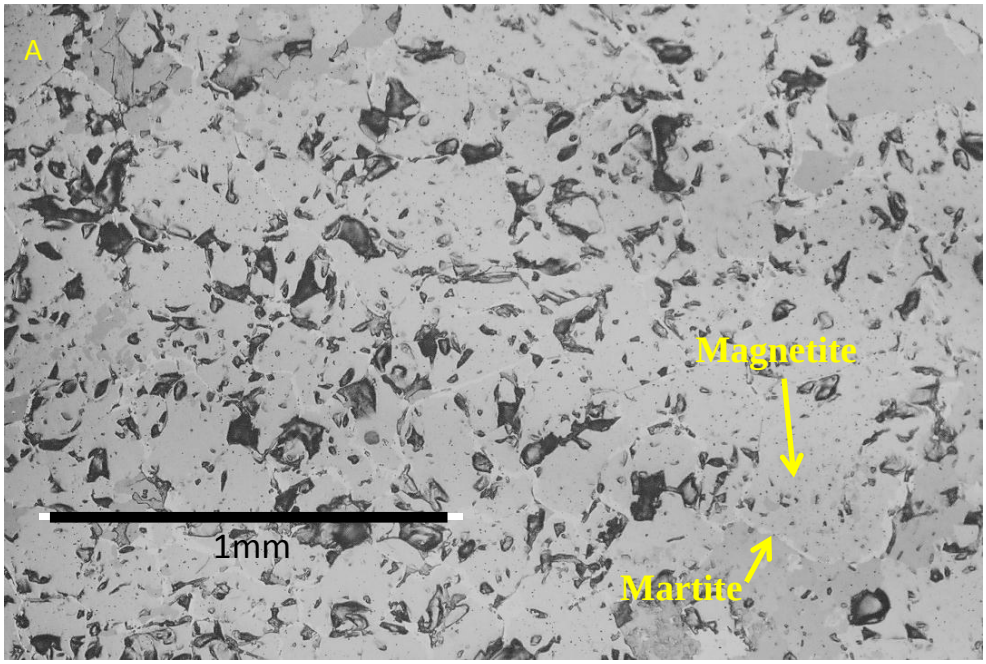

Figure 3.3a: Coarse grained texture of metamorphic magnetite with minor martite replacement in sample 26-075-1234 (reflected light).

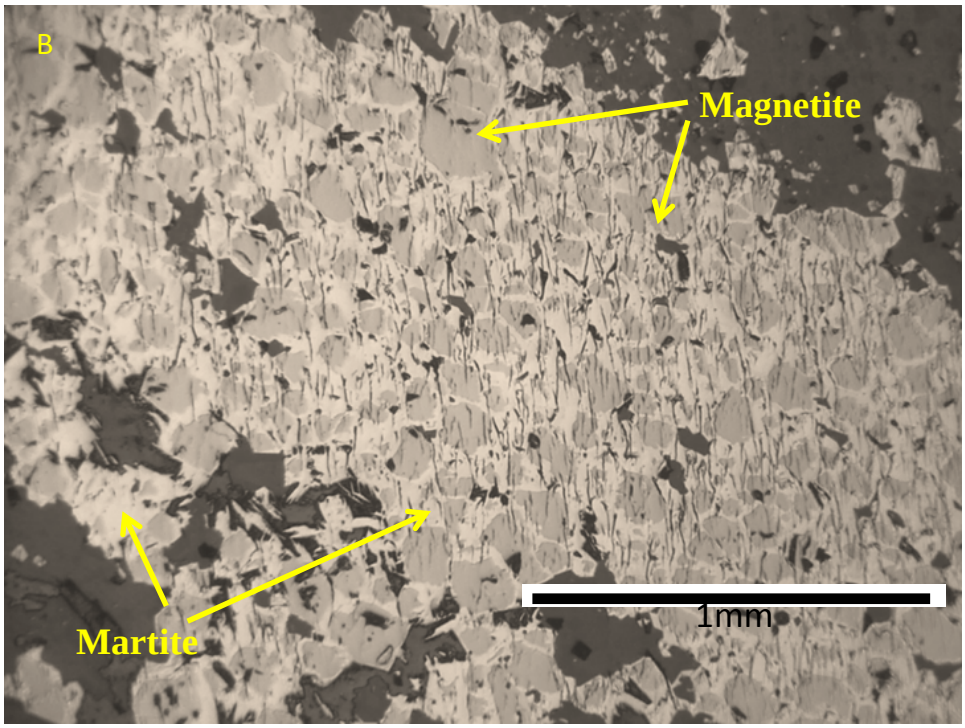

Figure 3.3b: Coarse grained texture of metamorphic magnetite with increased martite replacement at a shallower elevation in sample 26-198-768 (reflected light).

3.5 Medial Banded Iron Formation Facies

The Medial Banded Iron Formation (BIF) Facies comprises the bulk of the Main Pit Carbonate Domain. This thin (1-3 cm) banded unit is up to 60 meters thick and tracks across the entire Tilden Pit. It has a general iron recovery of ~42 weight% Fe. Bands of the Basal Clastics are interbedded with the Medial BIF, indicating overlapping sedimentation (Plate 3.0). The clastic bands decrease in thickness and frequency upward and ultimately disappear within a few tens of meters. Green chloritic clastics forming some of the bands suggest silicate facies BIF in this transition.

Medial BIF bands do not contain primary depositional features such as cross-beds, wave or current ripples. As clastics disappear the Medial BIF Facies becomes interbedded with the overlying GIF (Plate 3.4). The contact between the Medial BIF and overlying GIF approximates the boundary between the Main Pit Carbonate and Martite domains (Figure 3.0). This boundary has been observed to be sharp but is locally gradational.

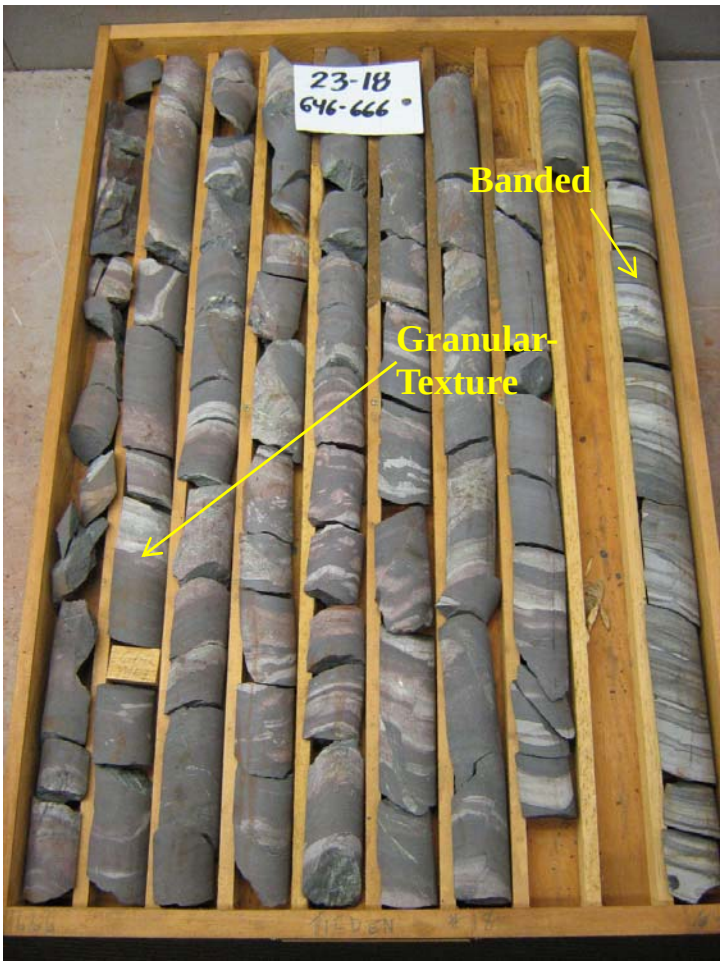

Plate 3.4: Drill core from hole 23-18-(646-666) depicting granular-textured bands interbeds within the Medial BIF Facies.

The defining feature of the Medial BIF Facies is alternating 1-3 cm bands. It is laminated to thinly bedded, displaying dark grey iron oxides, white to grey chert, reddish jasper, cream carbonate and pinkish to reddish grey granular textured layers (Plate 3.5). The mineral assemblage for each band type is unique. Grey-black bands are dominantly iron oxide with minor chlorite and carbonate. Chert bands are monomineralic cryptocrystalline quartz containing only trace amounts of chlorite and carbonate (Plate 3.6). The carbonate bands have mixed fine grained carbonate and chert with minor chlorite. The granular textured bands show cryptocrystalline quartz cementing primary ferri-hydrite granules and contain minor chlorite with rare apatite.

Plate 3.5: Representative samples of the Medial BIF facies. Band lithologies are: white cryptocrystalline chert, yellow carbonate, black oxides, pinkish granular-chert and speckled clastics. Note that there are multiple fractures and offsets that cross-cut banding.

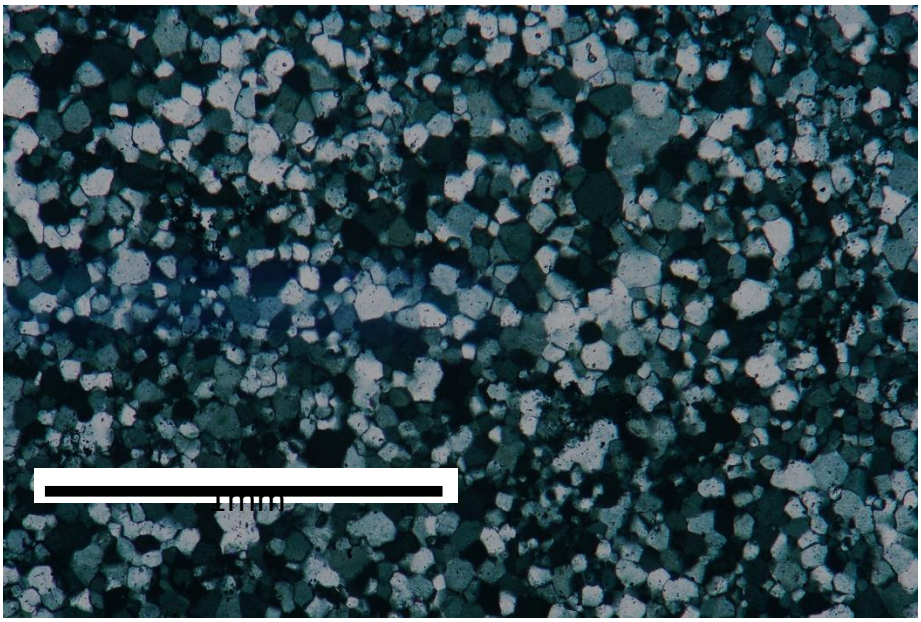

Plate 3.6: A photomicrograph of grey-white chert band comprised of cryptocrystalline chert and lacking iron oxides in sample 26-198-762 (plane polarized light).

Detrital quartz grains occur in clastic bands and as discontinuous fine lags within the bands of chert, carbonate and oxides (Plate 3.7). Detrital quartz laminae signify the "last gasp" of clastic sedimentation in a starved environment - perhaps sand laminae deposited in deeper or quiet water due to storm waves (Trendall, 2002). If so, this suggests the BIF deposition occurred below storm wave base with a diminishing influx of clastics. Possibly the detrital laminations could also represent aeolian recycling from a subaerial environment (Boggs, 1969).

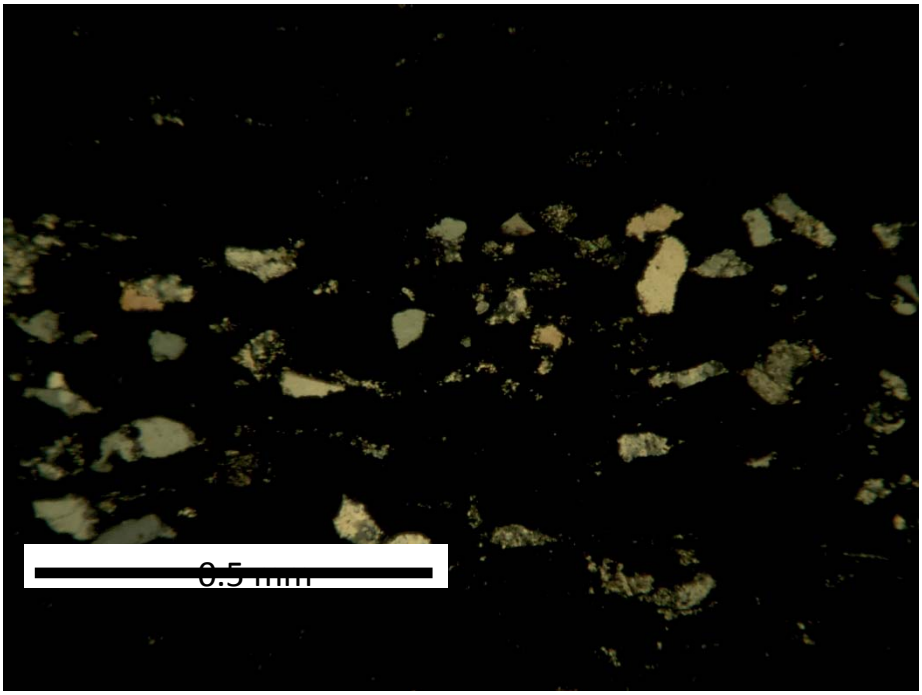

Plate 3.7: Photomicrograph of detrital quartz laminae within an oxide band of sample 26-075-1089 (cross polarized light).

Chert bands are comprised of monomineralic quartz derived by recrystallization of primary chemically precipitated siliceous ooze or through complete secondary replacement. The monomineralic chert bands lack evidence for replacement so more likely represent primary silica precipitation. Jasper bands contain micromillimeter "dust particles" of ferri-hydrite that were trapped within the precipitating silica (Plate 3.8). In granular bands, cryptocrystalline quartz is the dominant mineral surrounding and infilling ferri-hydrite granules, indicating diagenetic silica cementation (Maliva and Siever, 1989).

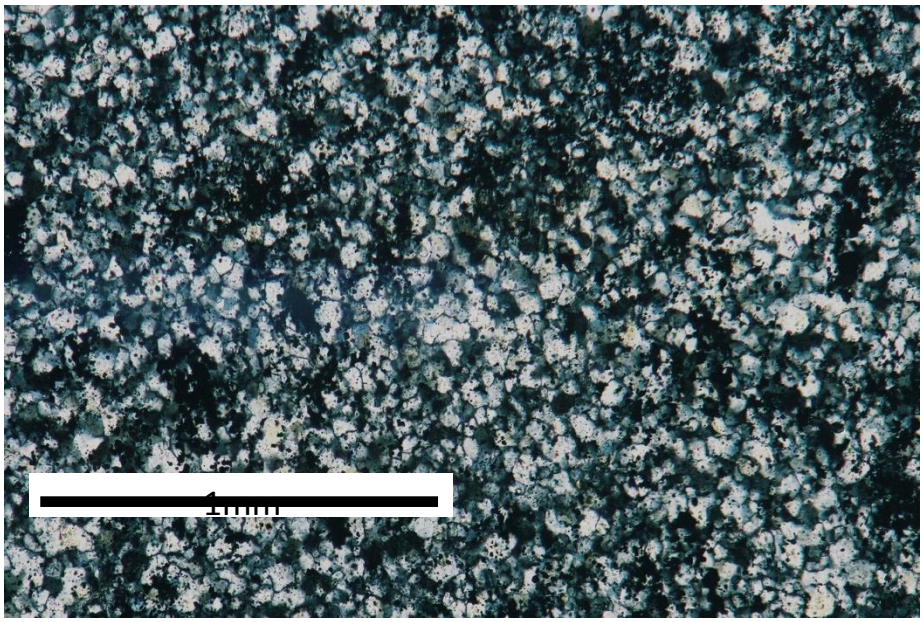

Plate 3.8: Photomicrograph of jasper bands containing impurities of ferri-hydrite and iron oxides scattered throughout in sample 26-143-1018 (plane polarized light).

Chlorite is a minor constituent in the Medial BIF Facies. However, fine grained, feathery to lath shaped chlorite is common within some oxide, carbonate and chert cemented granular bands. Two varieties of chlorite are in evidence. Dispersed chlorite within the chert and granule structures are metamorphic products replacing a minor clay component. Late hydrothermal chlorite is restricted to fractures and crosscutting veinlets.

Carbonate in the Medial BIF Facies can also be subdivided into two stages of mineral growth, a primary/diagenetic variety and a late hydrothermal species. Both species exhibit unique mineral chemistry. Minor Mg-siderite occurring as isolated grains within some chert and within specific clastic bands appears to be a primary or diagenetic product. These carbonates are fine grained (0.2 to 0.5 mm), anhedral and overgrow chert. The majority of carbonate in the Medial BIF is hydrothermal and is restricted to late fractures.

Four iron oxide and hydroxide species occur within all band types and include ferri-hydrite, magnetite, martite and hematite. The size and distribution of iron species is greatly influenced by the specific lithology. Barren cryptocrystalline chert bands do not contain iron oxides or hydroxides. The ferri-hydrite and hematite (up to 30%) constituent

of the granular-textured bands typically rinds the granules (Plate 3.9). The ferri-hydrite is commonly overgrown by blocky magnetite porphyroblasts. Ferri-hydrite and hematite are disseminated throughout the jasper bands, and again are commonly overgrown by fine magnetite. Magnetite is the dominant mineral (up to 90%) in the oxide bands, occurring as coarse blocky aggregates. Blocky magnetite is relatively minor (up to 10%) and is up to 1 mm in the carbonate bands. Minor magnetite disseminated within the granular bands is very fine grained (<0.1 mm).

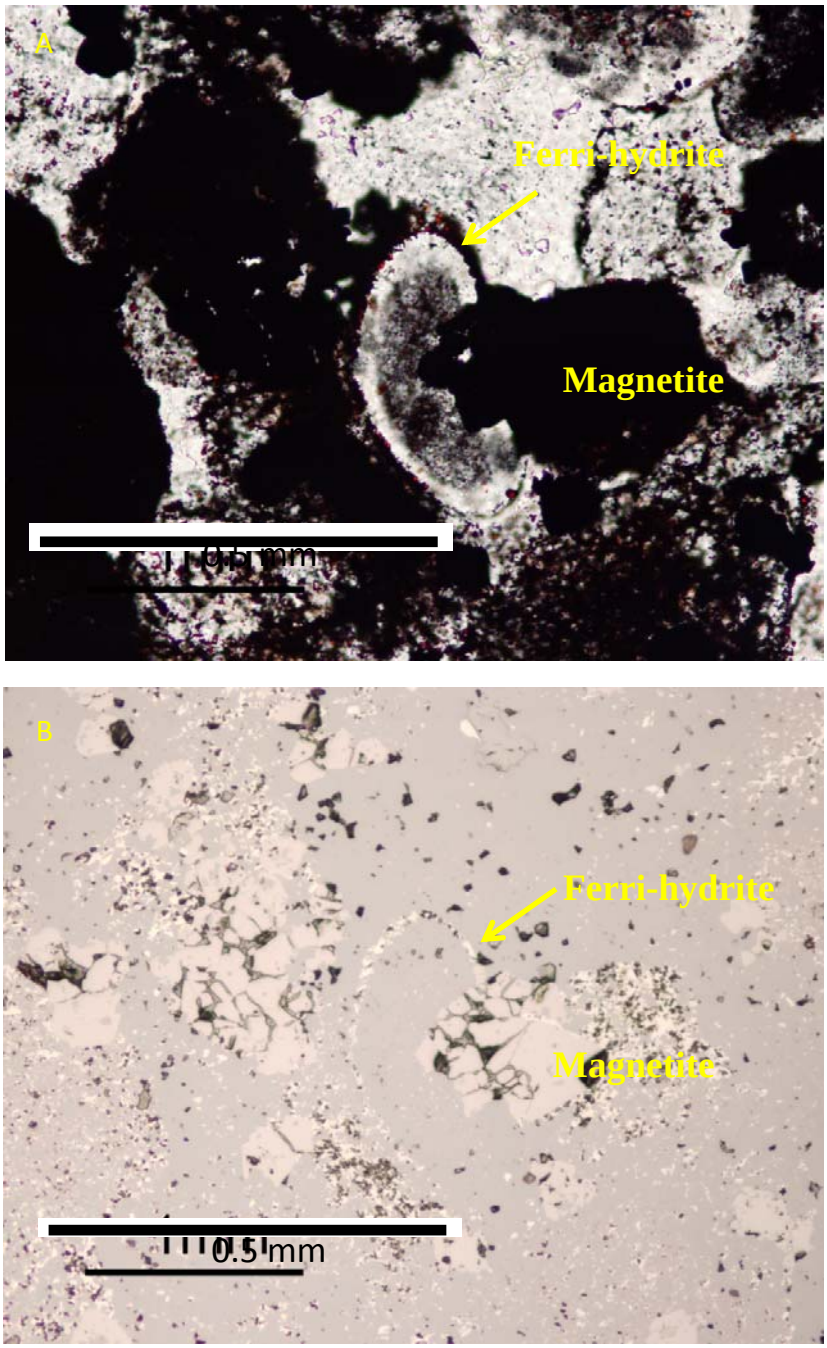

Plate 3.9: Photomicrograph of a granule rinded by ferri-hydrites in a granular-textured band of sample 26-075-1136 overgrown by blocky magnetite. (A) is in plane polarized light and; (B) is in reflected light.

Increasing martite or hematite rinds develop on euhedral magnetite upsection (Plate 3.10). The secondary martite and hematite are crystalline and not earthy, indicating higher temperature replacement as opposed to meteoric weathering (Lascelles, 2006). The degree of martite replacement varies with respect to the co-existing minerals. A high degree of martite replacing magnetite is associated with the occurrence of low Fe-dolomite/ankerite species or near absence of siderite. Conversely, low degrees of martite replacement are related to the presence of Mg-siderite species. Specular hematite dominates the granular bands upsection. Specularite occurs as laths that grow around and between the martite-replaced magnetite grains indicating metamorphic growth (Plate 3.11). Locally specular hematite laths define a subtle foliation.

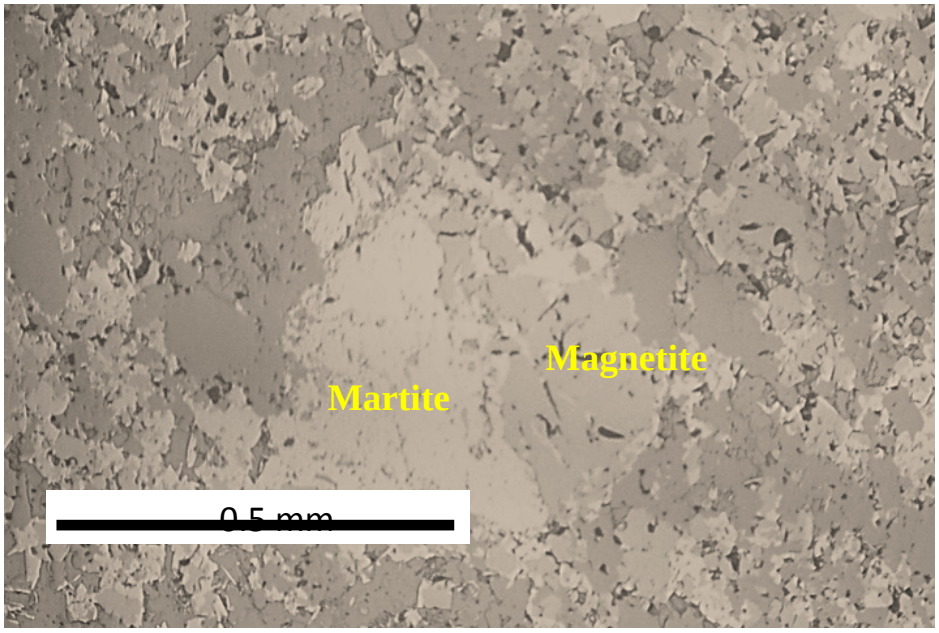

Plate 3.10: Photomicrographs of martite replacing magnetite in sample 26-075-1071. This is moderate replacement of magnetite (reflected light). Note the lack of specular hematite.

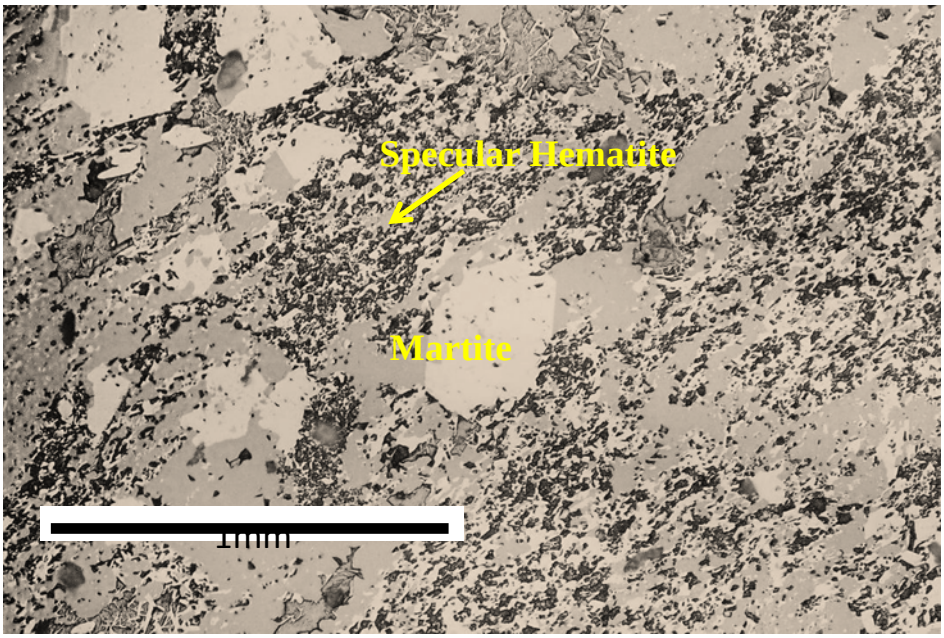

Plate 3.11: Photomicrograph of the near complete replacement of magnetite by martite and the abundant laths of specular hematite in sample 26-080-614 (reflected light). Note the hematite defines a weak foliation.

3.6 Upper Granular Iron Formation Facies

The Upper GIF Facies overlies the Medial BIF Facies and comprises the Martite Domain. As noted above granular-textured bands are common within the upper part of the Medial BIF Facies (Plate 3.4). The GIF Facies is up to 100 meters thick and tracts across the entire Tilden Pit. The Martite Domain has an iron recovery of ~50 weight% Fe and is considered a hematite flotation ore (Lukey et al., 2007).

The GIF Facies is dominantly grey to pink-grey in core and is massive to finely laminated (Plate 3.12). Individual laminations are comprised of ferri-hydrite granules, red jasper and rarely massive chert. In general this unit lacks cryptocrystalline chert bands (Plate 3.13). Other than banding, primary depositional features such as cross-beds and wave or current ripples were not observed.

Plate 3.12: Representative samples of the Upper GIF Facies in drill core. Note the lack of chert bands and laminations.

Plate 3.13: The Upper GIF Facies in drill hole 26-143-(721-741). Note the bleached areas of chert replaced granules and the occasional chert bands.

Granules rinded by ferri-hydrite are the dominant texture (Plate 3.14). These granules display varying degrees of replacement by blocky magnetite. Granules range from 0.5 to 2 mm in diameter and are generally elliptical indicating deformation. Delicate multiple concentric growth layers of ooids are occasionally preserved hence the granules are considered a primary sedimentary feature. Chert, commonly the dominant mineral (up to 60%) of the GIF Facies, can be observed both replacing and cementing granules. Chert is recrystallized, forming <0.1 mm cryptocrystalline mosaics. Detrital quartz laminae are extremely rare. Chert laminae with ferri-hydrite or hematite impurities form reddish jasper bands.

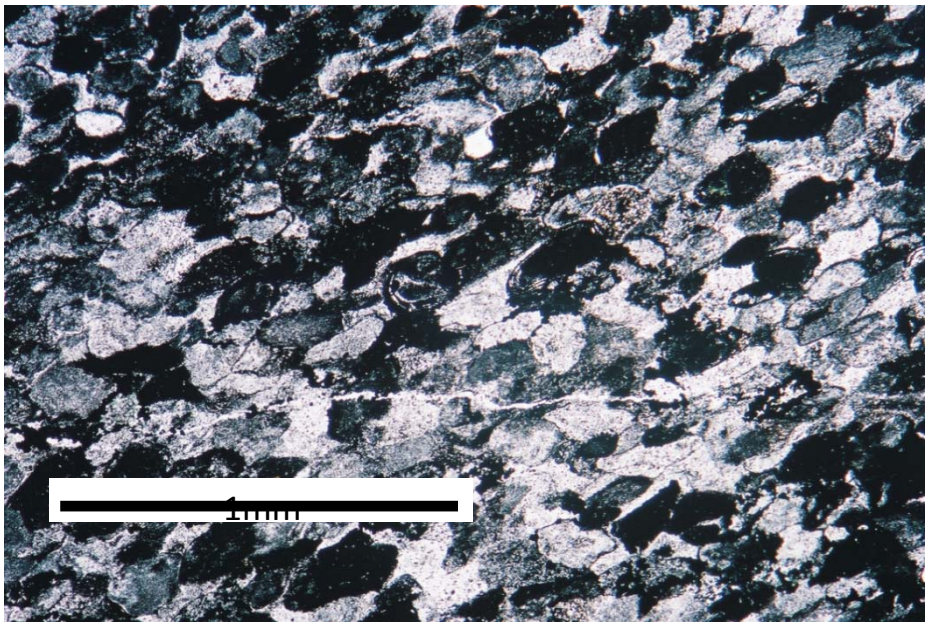

Plate 3.14: Photomicrograph of the granular texture in sample 26-075-1089 (plane polarized light). Most grains are granules however there are minor occurrences of ooids.

There are multiple generations of iron oxides within GIF. Primary or diagenetic ferri-hydrite rind granules and represent the first generation. There is no evidence that carbonate originally rinded the granules. Metamorphic blocky magnetite overgrows the ferri-hydrite representing the second generation (Plate 3.9). This magnetite may be a result of the reduction of the ferri-hydrite, or hematite during diagenesis (Ohmoto, 2003). Late martite replacement of magnetite results in very little magnetite (<15%) being preserved. Martite replacement represents a period of oxidation and clearly is post

magnetite growth. Platy hematite grows between martite grains, indicating these post-date oxidation of magnetite. Where platy specularite forms wavy bands it defines metamorphic foliation related to ductile shearing (Cannon, 1976). Specularite schists are most common in drill holes transecting the steepest south limb of the Main Pit Anticline, suggesting specularite growth accompanied high strain bordering the Southern Shear Zone. The platy hematite is therefore late metamorphic in origin.

Minor (< 5%) chlorite occurs as <0.2 mm feathery aggregates or isolated laths dispersed in chert. Early chlorite dispersed throughout the chert occasionally occupies the cores of granules. These chlorites are light green in colour and are likely metamorphic replacement of a trace clay component.

The Upper GIF Facies is capped by the metadiabase Pillar. About 15 meters of the GIF below the Pillar is overprinted by a hydrothermal aureole. Within the aureole, GIF is comprised essentially of recrystallized chert with only trace iron oxides. The primary granular textures are obliterated.

3.7 Metadiabase Pillar

A metadiabase Pillar caps the Martite Domain, forming a thin 18 to 30 meter unit that best delineates the west plunging nose of the Main Pit Anticline. It is an offshoot from the much thicker Summit Mountain greenstone sill to the north. To the south the Pillar is sheared out by the Southern Shear and may form the Palmer Gneiss within the Southern Shear Zone (Webster, 1999). A hydrothermal halo of 15-30 meters thick has been observed on both sides of the pillar in several exploration drill holes (Scott, personal communication, 2010). That the pillar is conformable and has a well developed hydrothermal aureole on both sides indicates sill emplacement.

The Pillar is green to grey green colour in core, is fine to medium grained, massive and dominantly comprised of chlorite. The margin is schistose but a relict gabbroic texture is preserved within its interior. Late brittle brecciation and fractures are noticeably absent. The chlorite (up to 80%) is coarse grained and lath shaped. Minor phases in the hydrothermal altered margin include carbonate, quartz, potassium feldspar, apatite and monazite.

The Pillar and underlying feeder dykes were emplaced pre-metamorphism. Most of these metadiabase dykes display weak foliation indicating ductile shearing was post-emplacement. Dykes are typically narrow and range from 2 cm up to 0.5 meters thick. Contacts are almost completely chlorite in composition and generally schistose (Plate 3.15). In thin section, relict primary igneous textures are locally preserved, however primary minerals have been completely replaced by chlorite (Plate 3.16). The replaced minerals retain euhedral plagioclase and pyroxene shapes (Plate 3.16). The occurrence of ilmenite in several dykes signifies a magmatic origin (Deer et al., 1966).

Plate 3.15: A chloritized dyke intruding the Upper GIF Facies in drill hole 26-076 (782-818).

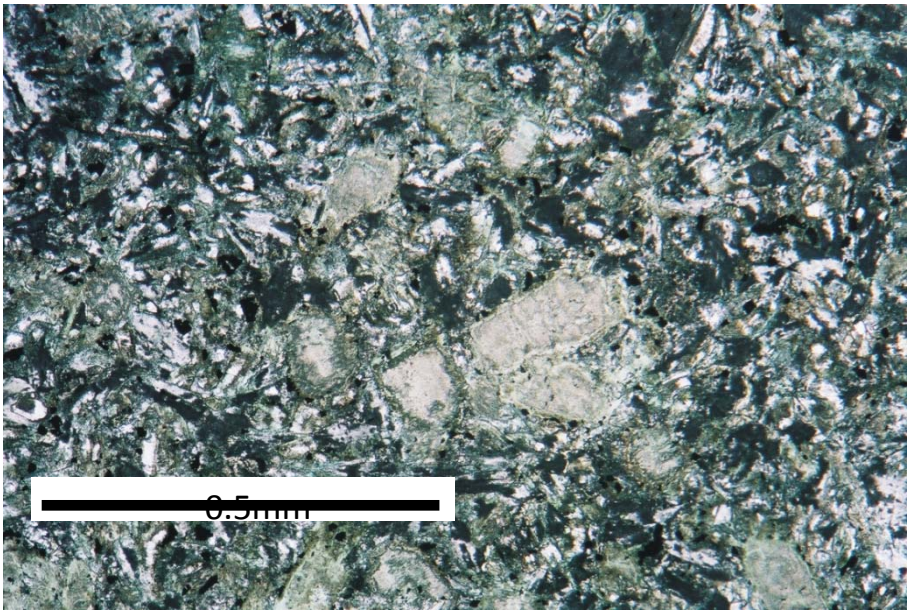

Plate 3.16: Photomicrograph of a metadiabase dyke for sample 26-198-1058 containing magmatic textures that are replaced by chlorite (plane polarized light).

3.8 Late Brittle Hydrothermal Overprint

Following deposition, diagenesis and metamorphism, the basal Negaunee exposed in the Tilden Pit was subjected to a late brittle hydrothermal overprint. Brittle fracturing is most intense in the Basal Clastics proximal to the Palmer Gneiss and decreases up section. Intense fracturing and brecciation within the Basal Clastics was observed in drill core, indicating late movement proximal to the Southern Shear Zone and Tower Hill fault. The Medial BIF Facies is strongly fractured but does not show the same degree of brecciation as the Basal Clastics. In general, the Upper GIF is the least fractured of the three lithofacies.

Late hydrothermal mineral assemblages are restricted to brittle structures (Plate 3.17). The hydrothermal mineral assemblage is defined by abundant chlorite, carbonate, and trace Cu-Fe sulphide, apatite and monazite. Chlorite dominates fracture walls and veinlets. Intergrowths of late chlorite away from fractures in the Basal Clastic suggest greater degrees of chlorite overgrowth exterior to fracture walls. The late chlorite is relatively coarser grained and exhibits dark green to yellow green pleochroism.

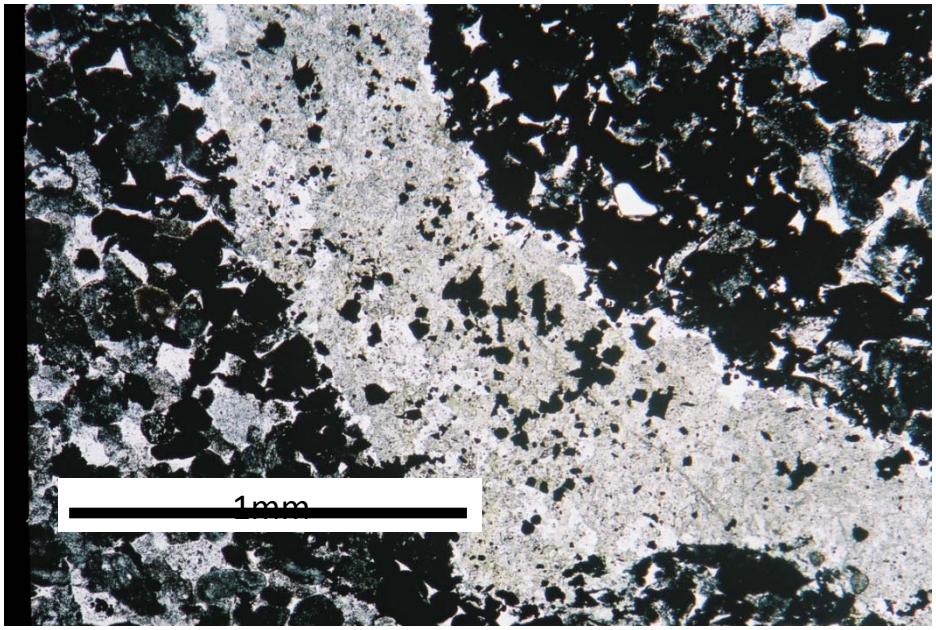

Plate 3.17: A photomicrograph of sample 26-075-1021 showing a late fracture within the Upper GIF Facies that is in filled with hydrothermal chlorite and carbonate (plane polarized light).

Carbonate is the second most abundant late hydrothermal mineral. The late carbonate is patchy and occupies veinlets and fracture infill in all three facies. Within the Basal Clastics high Fe and Mn-carbonate varieties are common. However, in the Medial BIF and Upper GIF Facies, Fe-dolomite/ankerite is dominant. Locally, hydrothermal carbonate is domainal containing zones of siderite, ankerite and rhodochrosite.

Late hydrothermal carbonate is occasionally accompanied by trace chalcopyrite and tennantite. Although minor to rare (<1%), the presence of these Cu-Fe sulphides suggest high temperature fluid ingress (Klein and Hurlbut, 1993). These sulphides are fracture controlled and are commonly associated with high-Fe or zoned carbonate and high-Fe chlorite adjacent to the Palmer Gneiss. Chalcopyrite is most concentrated (up to 2-4%) in fault breccia (Plate 3.18). Chalcopyrite and tennantite occur in trace amounts (<1%) on fractures crosscutting the Medial BIF Facies. Sulphides are not associated with the carbonate-chlorite veinlets crosscutting the Upper GIF Facies.

Rare apatite and monazite form isolated laths within or proximal to fractures transecting the Upper GIF Facies. The grains are typically <1 mm and most commonly intergrown with hydrothermal chlorite. Trace monazite locally accompanies late apatite.

Both apatite and monazite are absent in the Basal Clastic Facies and therefore are a result of hydrothermal remobilization from within the Upper GIF Facies

Fe-dolomite/ankerite can be associated with late vein quartz hosting coarse specular hematite. Late quartz veins cross-cut all brittle fractures and these locally contain very coarse specular hematite (Plate 3.19).

Plate 3.18: Sample 26-77-1157 depicting late sulphides infilling fractures within the Basal Clastics.

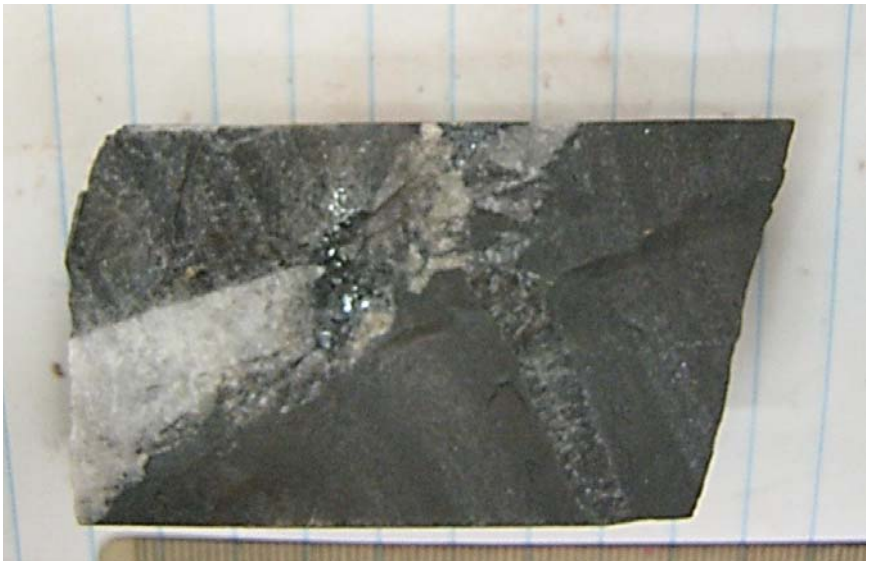

Plate 3.19: Sample 26-75-1066 showing coarse specular hematite within a late quartz vein.

Chapter 4: Mineral Chemistry

4.1 Introduction

The mineral assemblages of the flotation ores from the Tilden Mine can be separated into primary/diagenetic, metamorphic and hydrothermal stages of mineral growth. In addition to primary quartz/chert, ore assemblages include various species of iron oxide, chlorite and carbonate. Trace minerals include apatite, monazite and sulphide. The majority of the chlorite and carbonate species are closely linked to a late retrograde hydrothermal overprint, however, specific species relate to diagenetic/metamorphic growth. Chlorite, carbonate and iron oxide speciation is discussed for each lithofacies below, including Basal Clastic Facies, Medial BIF Facies and Upper GIF Facies as well as for the metadiabase Pillar and feeder dykes. This is followed by discussing mineral speciation related to the late hydrothermal overprint, including trace apatite, monazite and sulphide. Mineral species identification is based on microprobe analytical results.

4.2 Methods

Samples of core were cut and made into polished thin sections. Thin sections were carbon coated and examined in transmitted and reflected light with a Zeiss petrographic microscope. Regions of interest and specific grains were photographed and circled using diamond scribe to enable relocation of the selected areas when in the microprobe. Backscatter electron detector images of relevant mineralogical and textural relationships were collected digitally. All minerals were analyzed using a JEOL 733 microprobe equipped with a Tracor Northern Energy Dispersive System (EDS) and five wavelength spectrometers. Mineral chemical results are presented in weight percent oxides.

It was hypothesized prior to analyses that martite would represent an oxidized form of magnetite and have a composition approaching hematite. Martite is therefore chemically indistinguishable from hematite based on microprobe analyses. In an attempt to tie microprobe analyses of martite to its crystallography, XRD spot analysis (~300

microns) was employed on a few selected samples. However, only crystal structure patterns of hematite and magnetite were recognized (Figure 4.0). There are three possibilities for this including: 1) the fine grain size of the martite rimming magnetite grains did not give a conclusive XRD pattern to indicate martite; 2) martite does not have a crystal structural pattern significantly different from magnetite; or 3) it is only hematite rimming the magnetite. Ferri-hydrite identified via microprobe analyses were too fine grained to be recognized by XRD patterns.

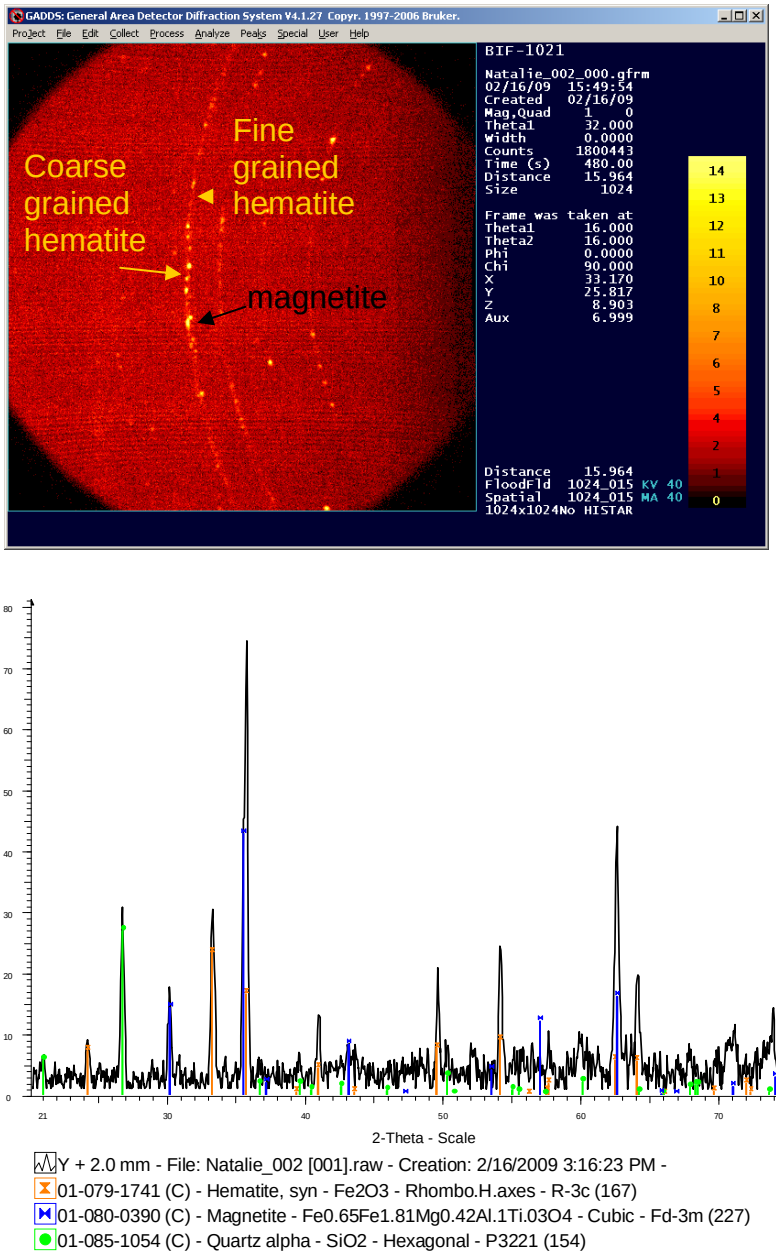

Figure 4.0: X-ray diffraction data demonstrating the presence of chert, magnetite and hematite.

4.2.1 Method of Recalculating Fe^{2+} and Fe^{3+}

Iron oxides including magnetite, hematite and ferri-hydrite (goethite or limonite) were identified and analyzed. Magnetite has the formula $Fe_2^{3+}Fe^{2+}O_4$ containing the ratio of 2 ferric iron to 1 ferrous iron. Hematite has the formula $Fe^{3+}{}_2O_3$ where all the iron is in the ferric state. Martite is formed by oxidation of magnetite to hematite with all the iron again in the ferric state.

Electron microprobe analyses presents iron as a total in the form of Fe^{2+} (i.e. FeO). In an attempt to identify specific iron oxide minerals the variations in total wt% FeO signifies different iron oxide species. Electron microprobe analyses of magnetite results in totals of approximately 92-93 wt% FeO. Analysis of hematite and martite result in totals of near 90 wt% FeO. The ferri-hydrite reported totals of < 90 wt% FeO. The iron oxide analyses were run through the Fe^{2+}/Fe^{3+} recalculation program "Valmag" which recalculates the total iron content. On recalculation, the totals of magnetite and hematite approach 100 % respectively. The ferri-hydrite totals still did not exceed 90% indicating up to 10% water. Ferri-hydrite minerals such as goethite, lepidocrosite or limonite cannot be separated by mineral chemical analysis. Therefore the generic term ferri-hydrite is applied to iron minerals with ~ 10% water.

4.3 Basal Clastic Facies

As described in the petrographic chapter, the Basal Clastic Facies can be subdivided into coarse-grained and fine-grained variants. The mineral assemblage of the coarse grained clastics consists of quartz-chlorite-magnetite-carbonate. The fine-grained clastics are dominated by quartz, carbonate, chlorite and magnetite with trace occurrence of illite/sericite.

4.3.1 Chlorite

Chlorite typically comprises up to 25% of the coarse clastic rocks and occurs interstitial to and grows around detrital quartz grains. Chlorite in the Basal Clastics has the widest range of compositions with Fe-dominant and Mg-dominant end-members. When plotted

on a discriminant plot of Zane et al., (1998) these species include pycnochlorite, lesser ripidolite, brunsvigite and minor diabantite (Figure 4.1). In the Basal Clastics chlorite iron contents range from 21 to 39 wt% FeO and aluminum contents from 19 to 24 wt% Al_2O_3. Magnesium contents are inverse to iron and range from 8 to 24 wt% MgO. Chlorites commonly exhibit domainal growth patterns that suggest changing fluid chemistry accompanied chlorite growth. The pycnochlorite and ripidolite compositions reflect metamorphism of a pelitic sediment and therefore have primary compositional control.

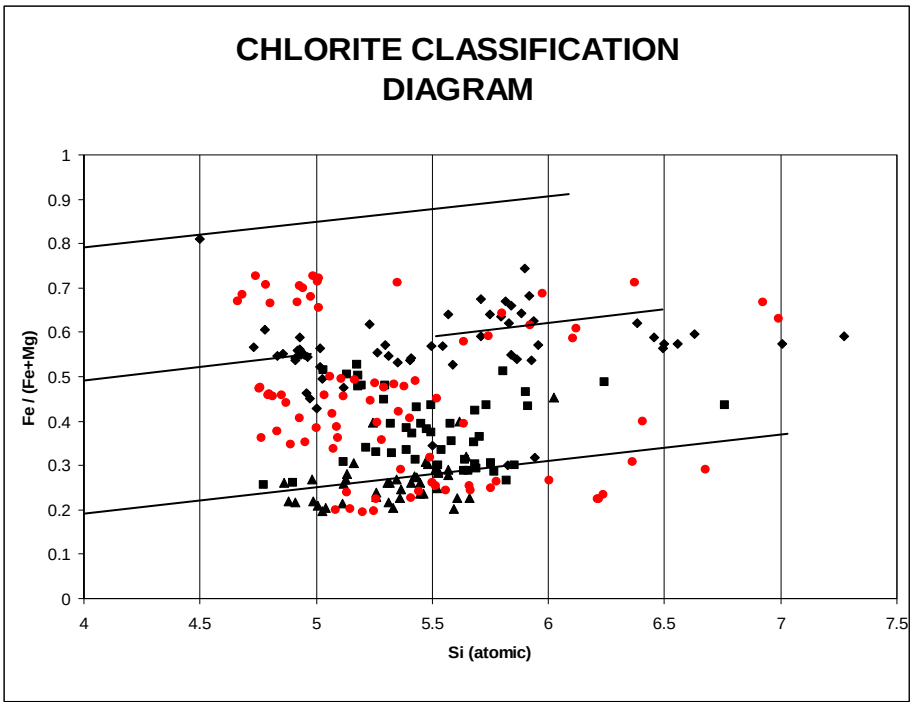

Figure 4.1: Classification diagram after Zane et al., (1998) depicting the chlorite species of the Basal Clastic Facies (red dots). Note that other symbols on the chlorite classification diagrams are: squares represent Medial BIF, triangles represent Upper GIF and diamonds represent hydrothermal chlorite.

4.3.2 Carbonate

Due to recrystallization, carbonates in the Basal Clastics vary both in grain size and composition. In the coarse grained clastics, carbonate is blocky and occurs interstitial to quartz, chlorite and iron oxides. This coarse carbonate plots in the siderite-magnesite solid solution series (Figure 4.2). Occasionally, the coarse carbonate grains exhibit

domains with varying amounts of Fe, Mg and Mn, again suggesting changing fluids conditions accompanied mineral growth. Dolomite-ankerite species are absent with Ca contents below 1% for all analyzed grains. In the fine grained clastics, carbonate occurs in the matrix along with chlorite and illite/sericite. The composition is dominantly siderite and grain size is less than 0.1 mm.

Fe-dominant siderite species in the clastics may stem from diagenetic processes in reducing conditions. Magnesite and siderite commonly forms as diagenetic cement as basinal fluids circulated during burial and compaction (Beukes and Gutzmer, 2008). In samples from drill hole 26-77 near the Tower Hill Fault, the Basal Clastics contain carbonate species with elevated Mn and lower Mg that plot on the siderite-rhodochrosite solid solution series (Figure 4.3). This elevated Mn is may be due to the late hydrothermal overprint proximal to the Southern Shear Zone.

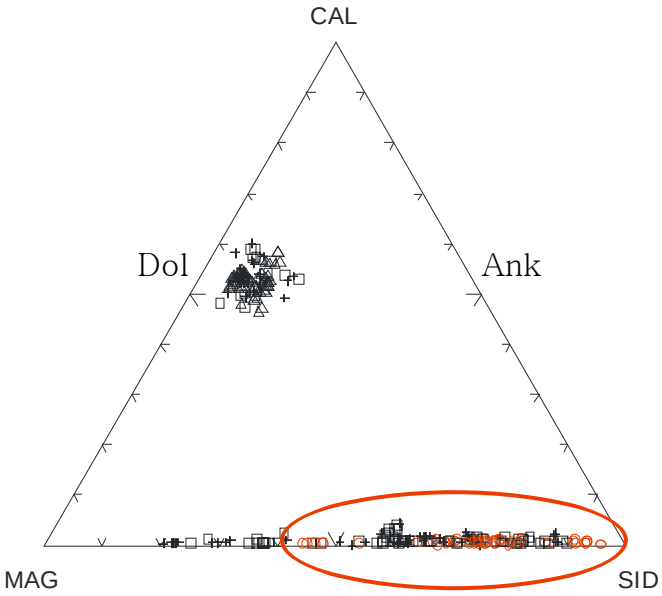

Figure 4.2: Ternary diagram after Chang et al., (1998) of the carbonate species within the Basal Clastic Facies (open red circles). Other symbols are: squares represent Medial BIF, triangles represent Upper GIF and crosses represent initially determined hydrothermal carbonates.

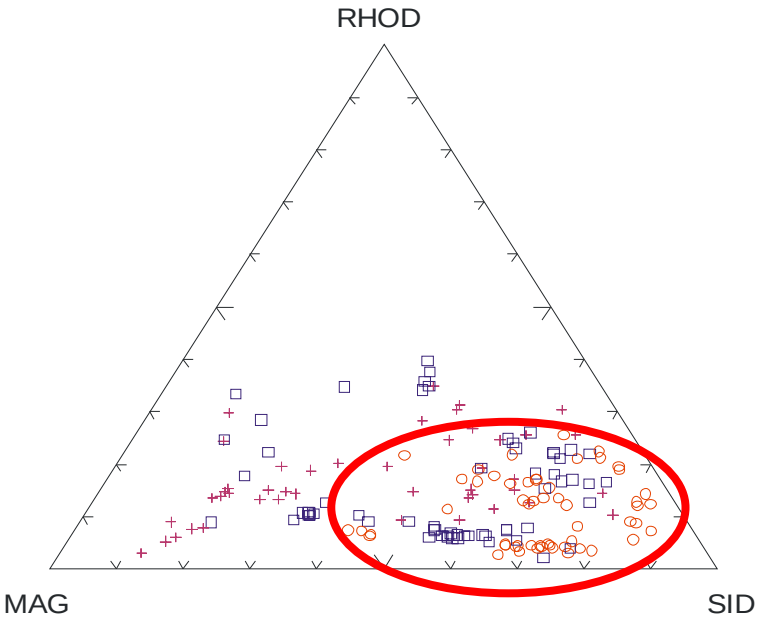

Figure 4.3: Ternary diagram after Chang et al., (1998) depicting the Mn-rich carbonates of the Basal Clastic Facies. Other symbols are: squares represent Medial BIF, triangles represent Upper GIF and crosses represent initially determined hydrothermal carbonates. The high Mn component is attributed to late hydrothermal carbonates.

4.3.3 Iron Oxide

The dominant Fe-oxide in the Basal Clastics is blocky magnetite. This magnetite is typically not zoned, is uniformly ~93 wt% FeO and does not contain any impurity. Proximal to the Tower Hill Fault some of the magnetite displays zoning. Zoned magnetite grains contain a lower Fe cores (<90 wt% FeO) and a higher Fe rims (~93 wt % FeO) (Plate 4.0). Core totals less than 90% FeO suggest ferri-hydrite compositions. Cores of ferri-hydrite may stem from primary or diagenetic precipitate while the pure magnetite rims indicate porphyroblastic growth (Konhauser et al., 2002; Lacelles, 2006).

Also proximal to the Tower Hill Fault, inclusions of silica occasionally form vermiform intergrowths within magnetite (Plate 4.1). The wormy textured domains contain trace amounts of silica (up to 2.5 wt% SiO), occasionally aluminum (up to 1.5 wt% Al_2O_3) and titanium (up to 0.5 wt% TiO_2). Such impurities suggest magnetite grains reacted with bordering silicates.

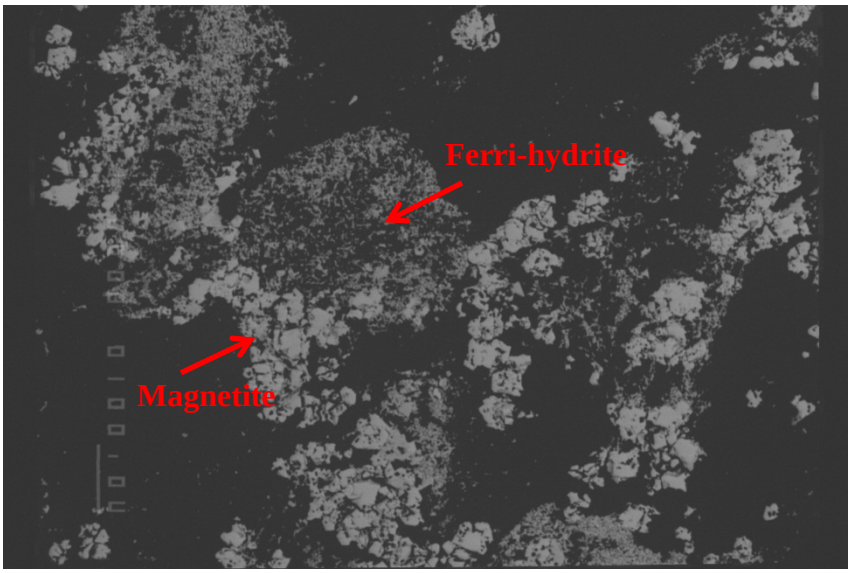

Plate 4.0: A backscatter image depicting magnetite overgrowing ferri-hydrite in sample 26-080-716.

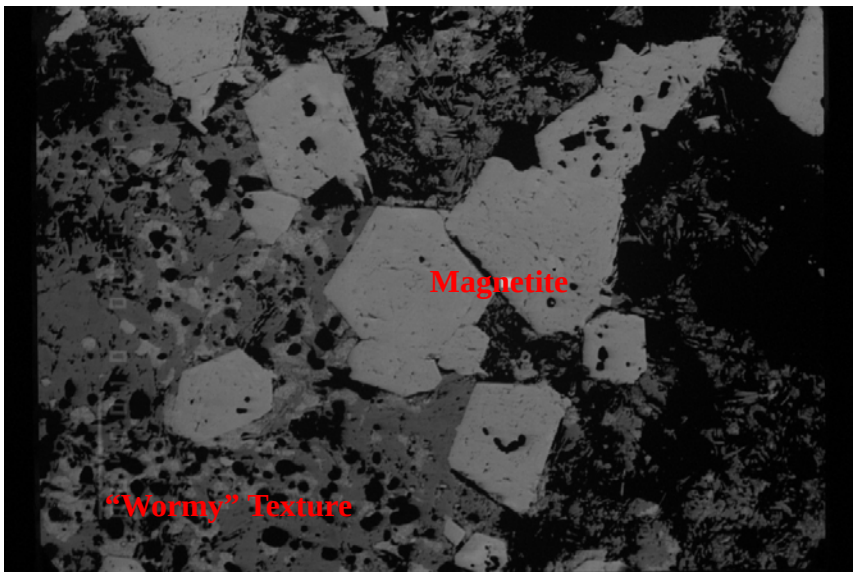

Plate 4.1: A backscatter image of magnetite grains that display "wormy" texture in sample 26-080-163.

4.4 Medial Banded Iron Formation Facies

The Medial BIF Facies is laminated to thinly bedded, displaying alternating dark grey oxides, white to grey chert, pink-red jasper, cream carbonate and pinkish to reddish- grey

granular-textured layers. The mineral assemblages are unique for each band type. Chlorite, carbonate and iron oxides are found in most band types except the cryptocrystalline chert bands.

4.4.1 Chlorite

Chlorite is a minor constituent in this subdomain. Fine-grained feathery to lath shaped chlorite occurs within oxide, carbonate and granular-textured bands. These exhibit a range from 14 to 37 wt% FeO, 7 to 26 wt% MgO and 16 to 24 wt% Al_2O_3. These compositions are similar to, but are more restricted in composition compared to those found in the Basal Clastics (Figure 4.4). Detrital mineral chemistry therefore reflects host lithology. The chlorites hosted by clastic bands displayed a broader range in iron and magnesium compositions with both Mg- and Fe-rich end members. Trace Mg-rich chlorites occur within the granular layers. This textural control suggests that primary sedimentary bulk rock composition controls the metamorphic mineral chemistry. Chlorite is absent in the cryptocrystalline chert and jasper layers.

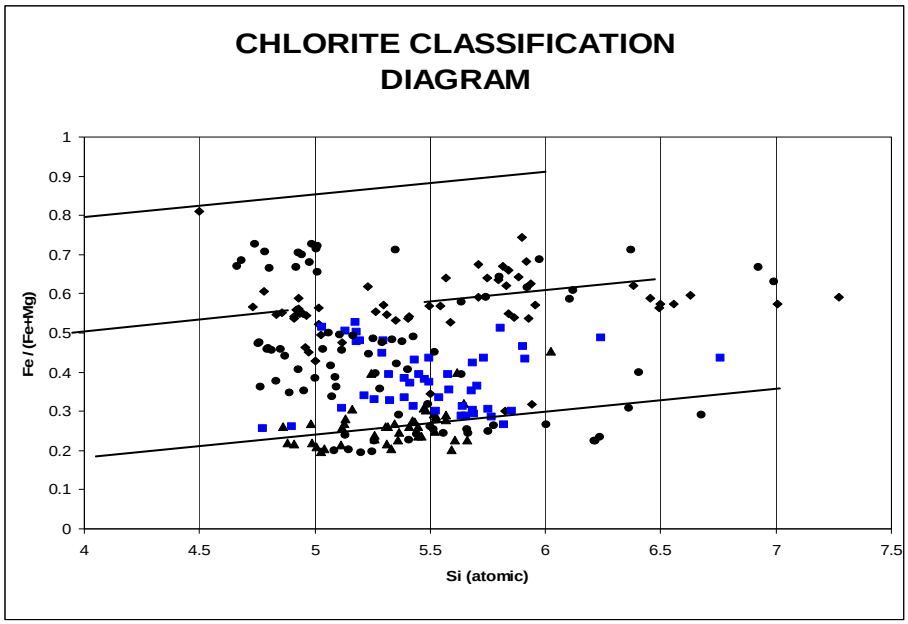

Figure 4.4: A classification diagram of the chlorite species in the Medial BIF Facies (blue squares). Diagram is after Zane et al., (1998). Note that other symbols on the chlorite classification diagrams are: circles represent Basal Clastics, triangles represent Upper GIF and diamonds represent hydrothermal chlorite.

4.4.2 Carbonate

In the Medial BIF Facies primary or diagenetic carbonate occurs within the clastic and oxide layers. It is absent in the cryptocrystalline chert and jasper bands. Only trace amounts occur in the granular-textured layers. The Medial BIF Facies show two distinct compositional groups representing dolomite-ankerite and magnesite-siderite solid solution series (Figure 4.5). The Mg-siderite ranges from 8 up to 42 wt% FeO and from 2 to 19 wt% MgO. Similar to the chlorites, the carbonate compositions are influenced by host lithology. Carbonates within clastic, oxide and granular-textured bands are dominantly Mg-siderite suggesting primary or diagenetic origin. The Fe-dolomite/ankerite carbonates are late hydrothermal species.

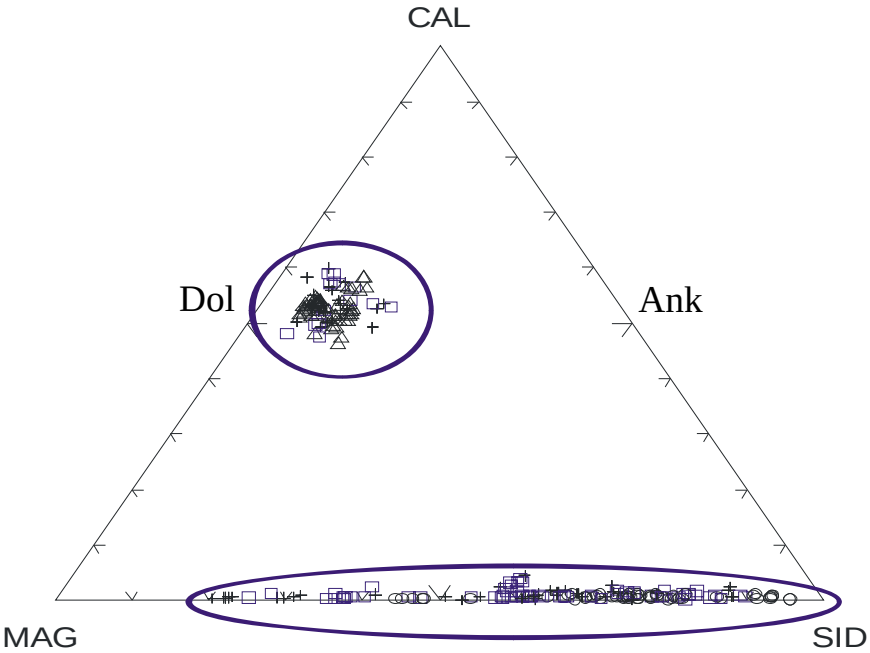

Figure 4.5: A ternary diagram after Chang et al., (1998) of the two different carbonate groups (magnesite-siderite and Fe-dolomite-ankerite) within the Medial BIF Facies. Other symbols are: circles represent Basal Clastics, triangles represent Upper GIF and crosses represent initially determined hydrothermal carbonates. The high Mn component is attributed to late hydrothermal carbonates.

4.4.3 Iron Oxide

The Medial BIF Facies are dominated by blocky magnetite with thin martite rims (Plate 4.2). The martite rims increase in thickness up section (Plate 4.3). Martite is most

abundant when Mg-siderite species of carbonate is absent. Magnetite cores contain ~93 wt% FeO. Martite rims contain ~90 wt% FeO. These rims also contain trace amounts of aluminum, silica, titanium and occasionally chrome. Martite rinds indicate a late metamorphic overprint (Ohmoto, 2003) that involved the interaction of magnetite grains with oxidizing fluids enriched in aluminum (up to 1.5 wt% Al_2O_3), silica (up to 0.8 wt% SiO_2), titanium (up to 0.5 wt% TiO_2) and chrome (up to 0.1 wt% Cr_2O_3). Trace ferri-hydrite "dust" is occasionally encased within Mg-siderite. These ultra fine iron grains are lath-shaped and contain <90 wt% FeO with no impurities. The ferri-hydrite is likely a primary precipitate that was subsequently dehydrated and replaced by diagenetic Mg-siderite.

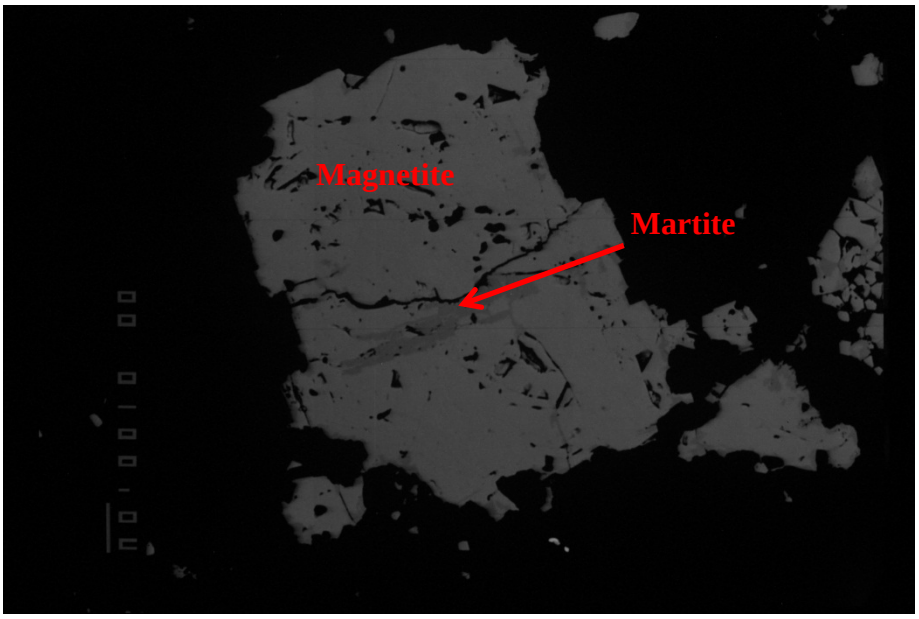

Plate 4.2: Backscatter image of blocky magnetite grains with minor martite replacement in sample 26-075-1089.

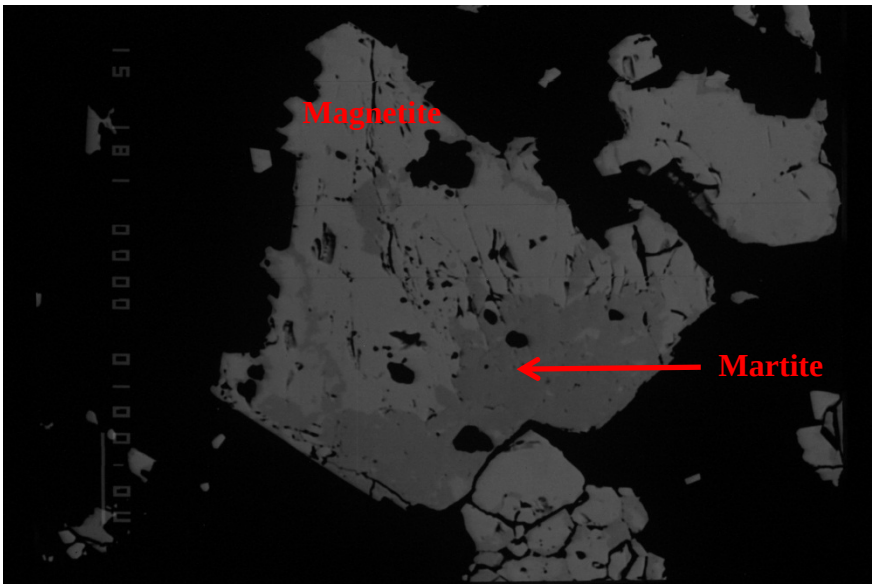

Plate 4.3: Backscatter image of blocky magnetite grains with major martite replacement in sample 26-143-715.

4.5 Upper Granular Iron Formation Facies

The Upper GIF Facies dominates the top of the Main Pit Carbonate Domain and comprises the entire Martite Domain. It is the most texturally and mineralogically uniform of the three lithofacies. The dominant minerals are quartz and iron oxide. The top of this facies is capped by the sheared and chloritized base of the metadiabase Pillar. Chlorite occurs as trace feathery laths within the Upper GIF Facies and late hydrothermal chlorite occurs in fractures. Primary or diagenetic carbonate is absent, however late hydrothermal carbonate occurs in fractures.

4.5.1 Chlorite

Chlorite is a minor to trace constituent in this rock type. It occurs as rare isolated laths interstitial to granules. These chlorites have a lower Fe-component compared to those in the Basal Clastics and Medial BIF Facies. On a discriminant plot by Zane et al., (1998) chlorite compositions include sheridanite, clinochlore with some ripidolite and pycnochlorite (Figure 4.6). The chlorites associated with granular- textured lithology are

Mg-dominant, ranging from 12 to 18 wt% FeO, 20 to 24 wt% MgO and 20 to 24 wt% Al_2O_3. Chlorite grains occasionally display domains with varying FeO and MgO but are not zoned. High-Fe chlorite (25 wt% FeO) was observed adjacent to fractures in association with hydrothermal carbonate.

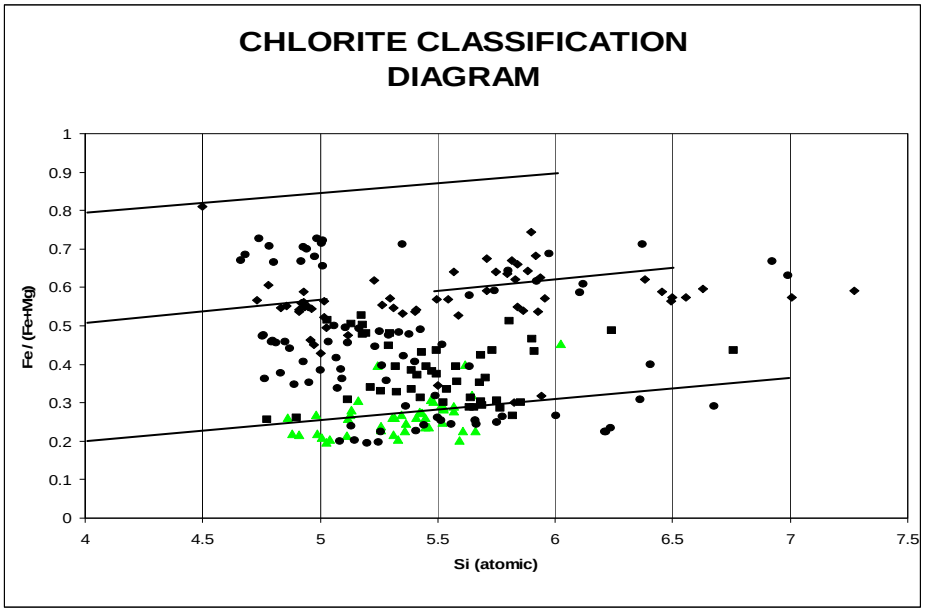

Figure 4.6: Classification diagram after Zane et al., (1998) depicting the chlorite species within the Upper Granular-Chert Facies (green triangles). Note that other symbols on the chlorite classification diagrams are: circles represent Basal Clastics, squares represent Medial BIF and diamonds represent hydrothermal chlorite.

4.5.2 Carbonate

Fe-dolomite/ankerite form late hydrothermal species restricted to fractures.

4.5.3 Iron Oxide

Fine ferri-hydrite laths with <90 wt% FeO, and hematite with ~91 wt% FeO rinding granules, indicate primary iron precipitate with silica (Simonson, 1987). The ferri-hydrite and hematite that rind granules is overgrown by blocky magnetite (Plate 4.4). The magnetites within the Upper GIF Facies are wholly replaced by martite (Plate 4.5). Blocky martite grains that retain their original magnetite shape may contain trace cores of

magnetite with ~94 wt% FeO but thick martite rims have ~90 wt% FeO. The martite rinds contain trace amounts of aluminum, silica, titanium and chrome.

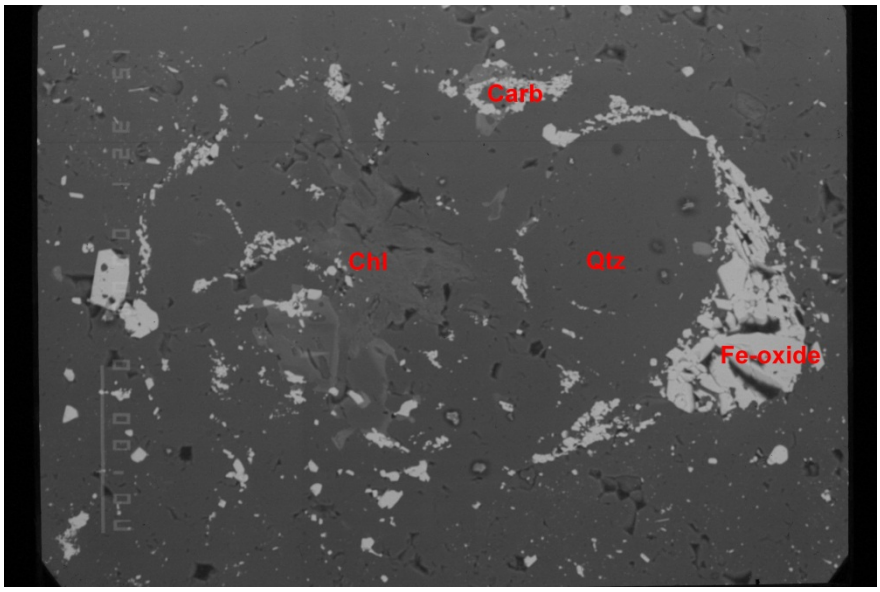

Plate 4.4: A backscatter image of ferri-hydrite laths rinding a granule in the Upper GIF Facies in sample 23-035-1000. Note the metamorphic magnetite overgrowing the ferri-hydrite grains.

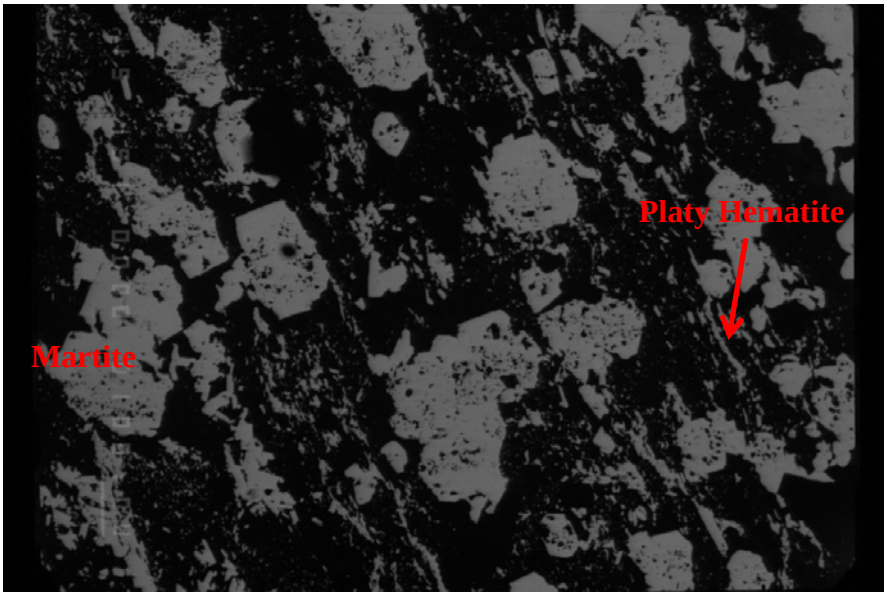

Plate 4.5: A backscatter image of abundant intergrowths of specular hematite laths growing between martite grains in sample 26-203-354.

Abundant platy specular hematite grows between the blocky martite grains (Plate 4.5). These platy laths first appear in the Medial BIF Facies but become more abundant

upsection in the Upper GIF Facies (up to 25 modal %). Specularite has 91 wt% FeO and contains trace amounts of silica and aluminum (up to 1.5 wt% Al_2O_3), but does not contain titanium or chrome. The lack of titanium and chrome in the hematite plates as compared to martite suggests an evolution of the late oxidizing fluids. Martite and specularite are abundant in the Upper GIF Facies where Mg-siderite is absent; carbonate was not present to act as a buffer to magnetite oxidation.

4.6 Chloritized Metadiabase Pillar and Dykes

Chlorite dominates the Pillar-iron formation contact and cross-cutting metadiabase dykes, and represents hydrothermal retrogression of primary diabasic textures. Pillar chlorite ranges between 22 and 26 wt% FeO. Chloritized dykes cross-cut stratigraphy and possibly acted as feeder dykes to the overlying Pillar. Chlorites of the metadiabase dykes are Mg-dominant with significantly lower iron contents (12-16 wt% FeO) than chlorites found in the surrounding iron formation. A mineral chemical profile of chlorite compositions across a dyke contact with the Medial BIF iron formation shows a marked decrease in Fe-chlorite in the iron formation and increase in Mg-chlorite approaching the dyke margin (Figure 4.7). Iron formation chlorites at dyke margins therefore display the more Mg-rich chemistry of the dyke.

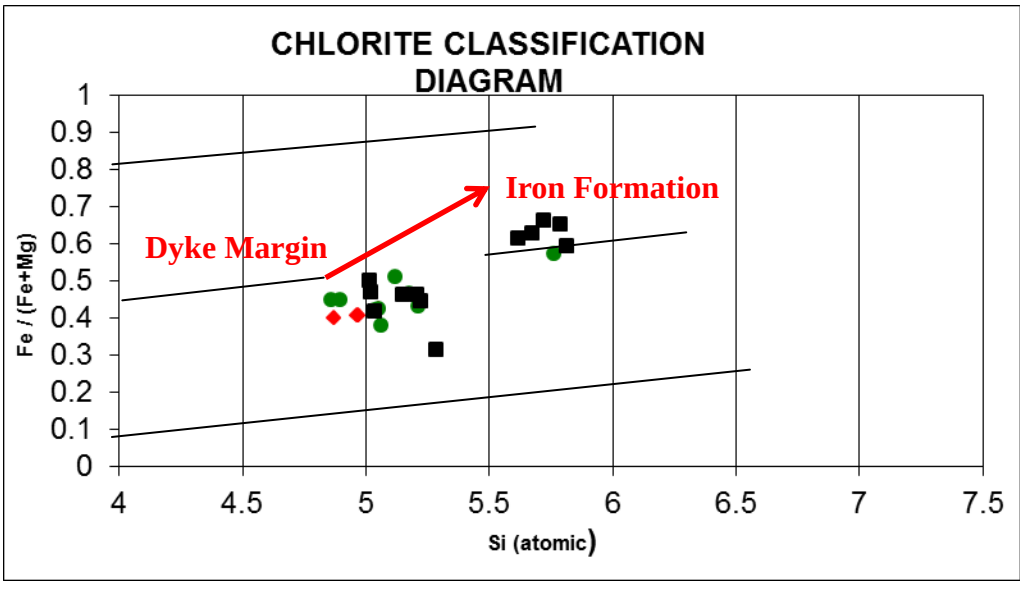

Figure 4.7: Classification Diagram after Zane et al., (1998) profiling the chlorites from the dyke and across the dyke margin from dyke to iron formation. Samples include red diamonds (26-198-709), green circles (26-198-710) and black squares (26-198-713).

Carbonate is relatively minor in the Pillar (up to 5 modal %). The majority is calcite and occurs in cavities or veinlets. Rare dolomite/ankerite was identified. Carbonate is absent in the metadiabase dykes.

Trace minerals identified within the hydrothermal margin of the Pillar margin include apatite and monazite dispersed within chlorite and carbonate. These minerals were not analyzed; however EDS spectrum from the electron microprobe identified an REE component to the monazites. Trace titanite, magnetite, rutile and chalcopyrite were identified within metadiabase dykes.

4.7 Late Hydrothermal Overprint

Late brecciation and fracturing was accompanied by hydrothermal ingress, resulting in high Fe-chlorite, carbonate, and trace apatite, monazite and sulphide coating fracture surfaces. Fracturing decreases upsection and away from the Signal Hill Fault with brecciation of the Basal Clastics, fracture offsets in the Medial BIF and stockwork veinlets within the Upper GIF Facies.

4.7.1 Chlorite and Carbonate

Late hydrothermal chlorite overprinting the Basal Clastics Facies and Medial BIF Facies include high iron ripidolite, brunsvigite and diabantite species (Figure 4.8). Iron ranges between 25 to 37 wt% FeO. Conversely late chlorite overprinting the Upper GIF Facies is dominantly Mg-rich. Chlorite within the feeder dykes is also Mg-dominant.

Late carbonate is typically associated with high iron chlorites (i.e. 37 wt% Fe). In the Basal Clastics fracture controlled carbonate varies in composition from high Mn (up to 27%) to high Fe (up to 42%). Zoned carbonates contain high iron and manganese contents (ie. 42 wt% FeO and 19 wt% MnO) with high Mn cores to high Fe rims. Occasional Mg-Fe zoned grains were observed (Figure 4.9). Carbonate with low-Fe magnesite cores to Fe-rich siderite rims indicates an evolution of fluids to increasingly Fe-rich (Plate 4.6). Late carbonate within the Medial BIF and Upper GIF Facies are dominantly Fe-dolomite/ankerite. Some grains display domains that reflect variable Fe

and Mg contents. Iron contents are typically low and do not exceed 10 wt% FeO where as calcium contents are between 16 and 31 wt% CaO.

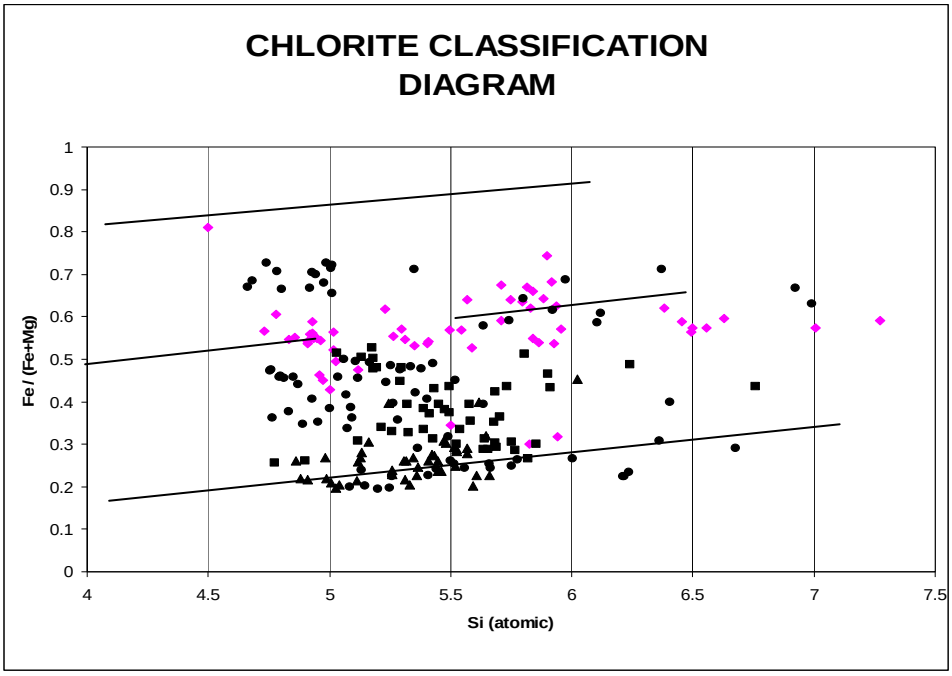

Figure 4.8: A classification diagram after Zane et al., (1998) depicting the late hydrothermal chlorite species (pink triangles). Note that other symbols on the chlorite classification diagrams are: circles represent Basal Clastics, triangles represent Upper GIF and squared represent Medial BIF chlorite.

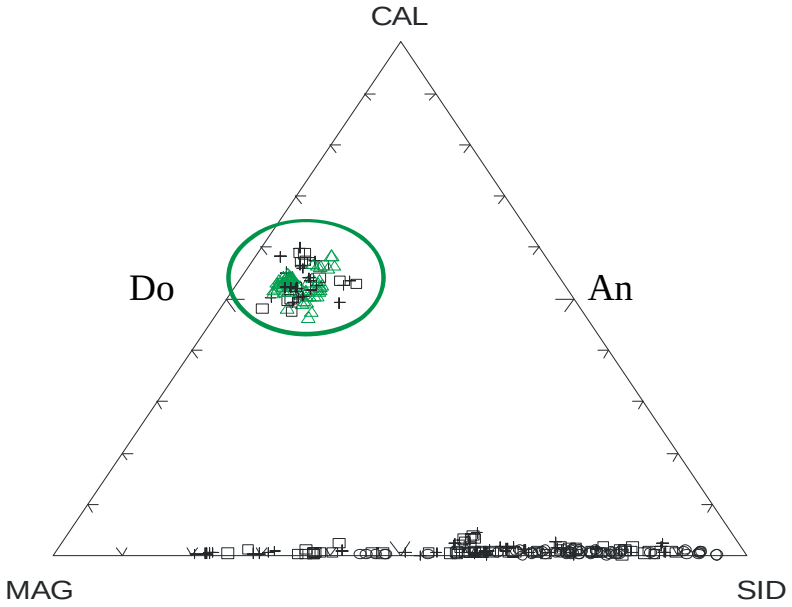

Figure 4.9: A ternary diagram after Chang et al., (1998) depicting the Fe-dolomite-ankerite carbonates of the Upper Granular-Chert Facies (green open triangles). Other symbols are: circles represent Basal Clastics, squares represent Medial BIF and crosses represent initially determined hydrothermal carbonates.

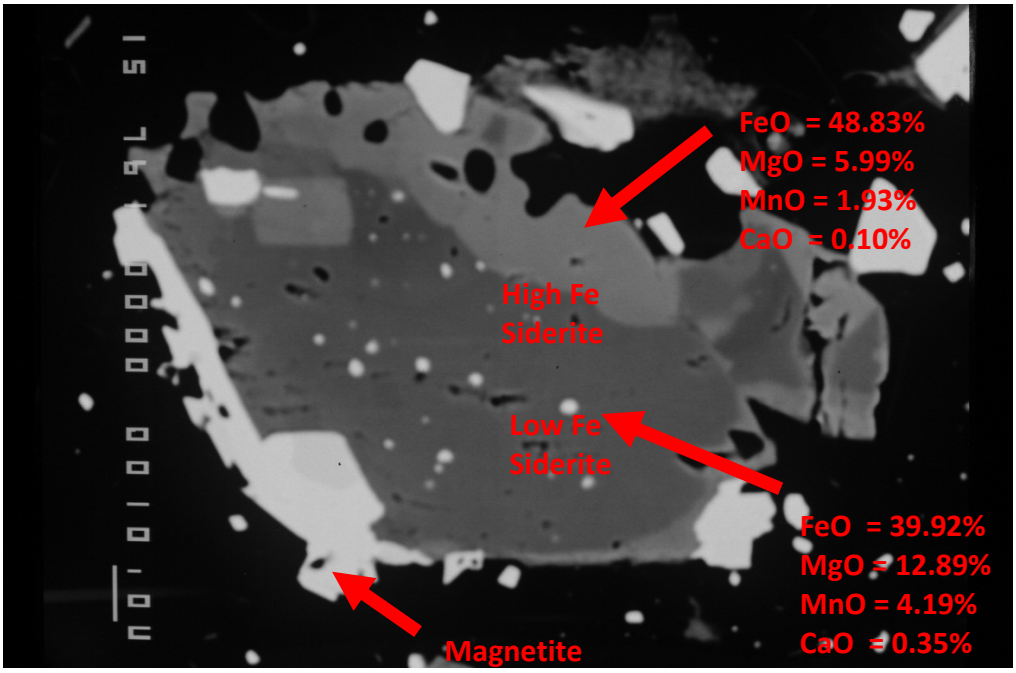

Plate 4.6: A backscatter image of late hydrothermal zoned carbonate in sample 26-075-1103. Note the lower Fe cores and higher Fe rims.

4.7.2 Apatite

Trace apatite, monazite and sulphide are associated with late hydrothermal chlorite and carbonate. Apatite (<5%) is dominantly found in veinlets crosscutting the Upper GIF Facies and granular-textured bands in the Medial BIF Facies. These grains are typically dispersed proximal to fractures. Apatite is absent in cryptocrystalline chert and jasper bands and has not been observed in the Basal Clastic Facies. Isolated grains are very fine grained (< 1 mm) and typically have a prismatic habit. These grains are fluro-apatites with an approximate composition of $Ca_5(PO_4)_3F$, with trace manganese and iron. No growth zoning was observed and there is very little variation in mineral chemistry. Apatite associated with chlorite and carbonate in fractures occasionally occurs with trace monazite and sulphide (Plate 4.7).

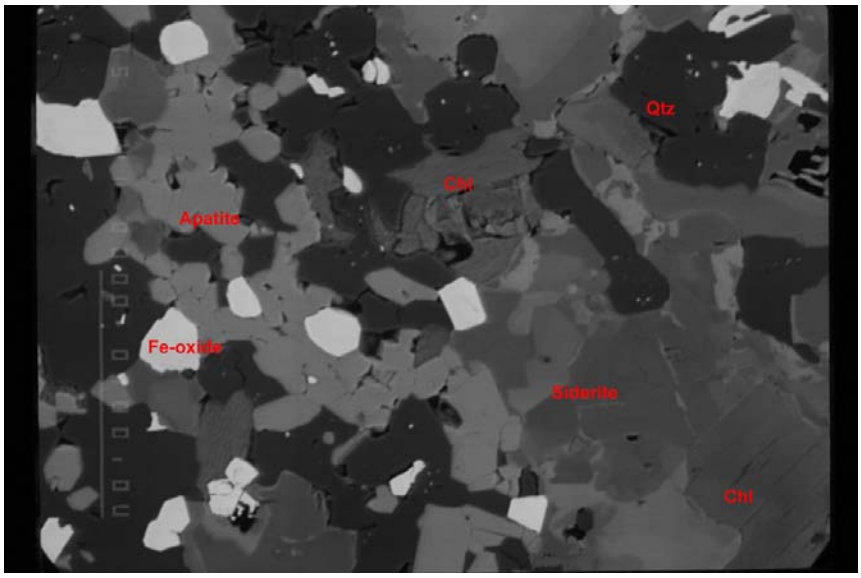

Plate 4.7: A backscatter image of apatite associated with late hydrothermal chlorite and carbonate in sample 23-018-725.

4.7.3 Monazite

Monazite is extremely fine grained (~60 um) and prismatic. This mineral occurs only within the Upper GIF Facies and granular-textured bands of the Medial BIF Facies. It is absent in the Basal Clastic Facies. The rare (< 1 modal %) monazite is associated with fracture controlled apatite, chlorite and carbonate (Plate 4.8). The monazite contains an REE component linked to secondary redistribution during the late hydrothermal overprint.

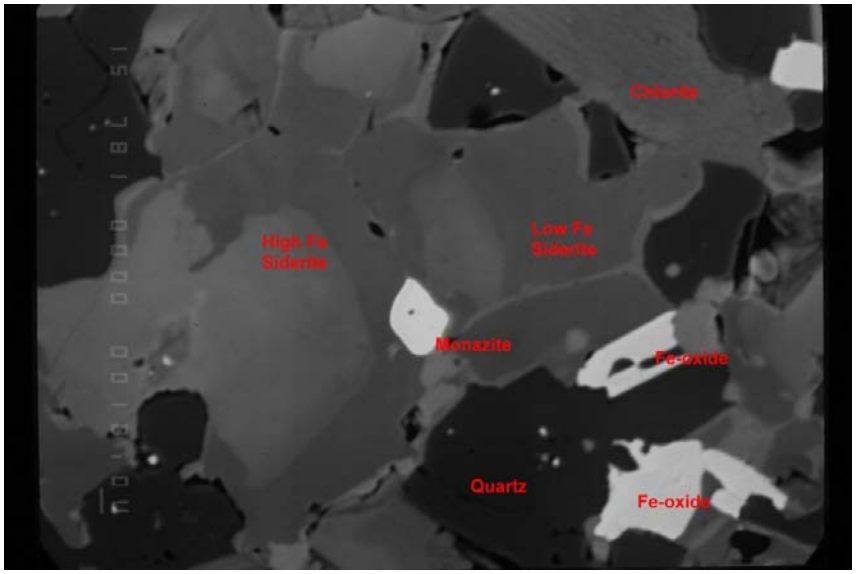

Plate 4.8: Monazite with late hydrothermal chlorite and carbonate in sample 23-018-725.

4.7.4 Sulphide

Trace sulphide (<2 modal %) serves as an important identifier of the late hydrothermal overprint. The dominant sulphide mineral is chalcopyrite (Plate 4.9). It is most abundant within the Basal Clastics Facies where it occurs as coarse grained fracture fill. In the Medial BIF Facies it is less abundant and is occasionally associated with other trace sulphides such as tennantite, cuperite and a CuSb mineral accompanied by Fe-dolomite/ankerite or Mn-zoned siderite. Cu-bearing sulphide species are most commonly associated with high Fe-chlorite in the Basal Clastics, are rare in the Medial BIF Facies, and are absent in the Upper GIF Facies.

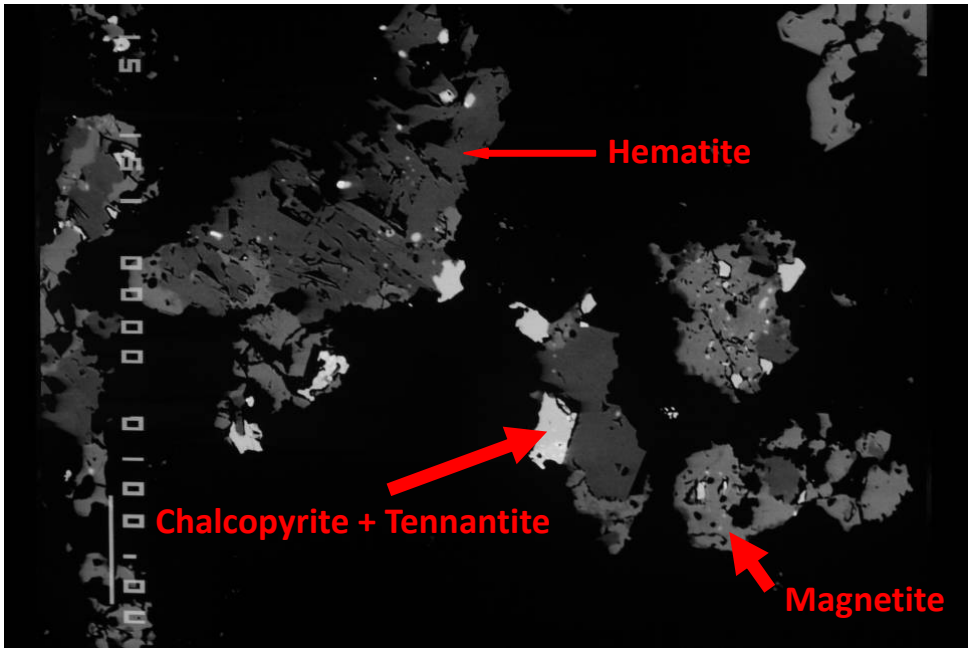

Plate 4.9: The sulphide minerals including chalcopyrite and tennantite in sample 26-075-1071.

Chapter 5: Discussion

5.1 Introduction

At the Tilden Main Mine the basal Negaunee Iron Formation has complex mineral paragenesis and chemical speciation that stems from primary mixed clastic and chemical sediments that have been subsequently overprinted by diagenetic, metamorphic and hydrothermal processes. Interpretations based on core-logging, petrography and microprobe analyses can be made concerning: 1) the paleoenvironment for deposition of Basal Clastics, Medial BIF and Upper GIF; and 2) the paragenetic sequence for growth of chlorite, carbonate, chert, iron oxides and trace minerals.

5.2 Paleoenvironment of the Basal Negaunee Lithofacies

At Tilden, the Negaunee Iron Formation is in fault contact against the Archean-aged Southern Gneiss Complex. The Basal Clastic Facies comprises the stratigraphic base of the Negaunee Iron Formation within the Tilden Pit. Coarse polycrystalline and strained detrital quartz indicate limited clastic transport of wacke-type sediments infilling a fault bounded trough. The poorly sorted texture and abundant chlorite matrix suggests a large primary detrital clay component that further attests to the textural and compositional immaturity of the clastic input. This early transgressive phase of sedimentation resulted in clastics being shed off the south margin into a subsiding rift basin (Larue and Sloss, 1980; Barovich et al., 1989). Increased thickness of the Basal Clastics proximal to the Southern Gneiss Complex and Tower faults suggests that initial clastic deposition was growth fault controlled. Interfingering of the clastics with overlying iron formation indicates periodic growth fault reactivation. On a regional scale, the Southern Shear system, separating the Negaunee Iron Formation and the Southern Gneiss Complex, demonstrates that early normal fault reactivation along the Great Lakes Tectonic Zone played a key role in controlling the paleoenvironment within the Marquette Range

Supergroup. The relatively low iron content in the Basal Clastic Facies indicates that ongoing clastic sedimentation prohibited iron formation deposition.

The overlying Medial BIF Facies is comprised of multiple band types. Diminishing and upward fining of clastics into the thinly banded iron formation sequence indicates evolution towards a starved shallow marine environment. Waning of clastic sedimentation indicate the basin became increasingly restricted. Alternating chemical and clastic deposition suggests fluctuating water depth and water chemistry controlled the sediment supply (Harris, 1990). The cyclic silica-iron chemical precipitation competed with slow rates of subsidence over a considerable time period to give rise to the tremendous 1300 meter thickness of the Negaunee Iron Formation.

The first appearance of banded iron formation suggests a significant change in the depositional setting to one that favoured chemical sedimentation. Recrystallization during diagenesis and subsequent metamorphism, has overprinted primary textures, accordingly, any interpretation of specific band origin remains somewhat speculative. There are two plausible processes for the chert bands, primary precipitation or carbonate replacement, however, the former is favoured.

The millimeter to centimeter thick monomineralic chert bands suggest periodic deposition of silica from oversaturated waters in an evaporitic setting. Evaporitic pans that emerged during regressive stands could facilitate chert precipitation (Trendall and Blockey, 2004). Silica-rich waters precipitate primary siliceous ooze in such restricted environments (Hinman and Lindstrom, 1996). The source of abundant silica is problematic and it is possible that higher geothermal gradients related to overlapping mafic magmatism could play a role in dewatering and promote discharge of warm silica and iron enriched formational water.

Mixing of formational brine with cooler surface seawater would certainly enhance silica precipitation. Simonson (1987) cites temperature gradients of 300^{o}C to 100^{o}C at seafloor volcanic centers as a modern environment for considerable silica precipitation. Alternatively, Hinman and Lindstrom (1996) describe silica precipitation from geysers at Yellowstone National Park, Wyoming. In this case, colder air temperatures in the winter promote precipitation of silica due to the decreased silica solubility in colder water. Chert bands might therefore indicate seasonal deposition. In addition, Blatt (1992)

suggests that microbial activity could affect water chemistry and that lowering water pH would promote silica precipitation. Potentially, microbial blooms could alter water chemistry sufficiently to facilitate silica precipitation.

Primary precipitation is suggested by jasper bands that contain micro-millimeter disseminated ferri-hydrite. In this case, primary ferri-oxyhydroxide precipitates were occasionally trapped within the precipitating silica ooze and recrystallized to ferri-hydrite during diagenesis. In jasper bands containing abundant ferri-hydrite this iron species is readily transformed to goethite or hematite during diagenesis and subsequent metamorphism, thus obliterating the primary textures of the original precipitates (Beukes and Gutzmer, 2008).

The alternative explanation for chert bands is by way of replacement. Primary ferri-oxyhydroxide precipitates are highly reactive with dissolved silica (Konhauser et al., 2007). Slack et al., (2007) and Fischer and Knoll (2009) propose that the silica is initially scavenged by iron precipitation at the sediment-water interface. During diagenesis when ferri-oxyhydroxides are converted to more stable compounds, silica is released into the pore waters and available for replacement. This is a plausible mechanism for forming the jasper bands but is difficult to explain how selective chert replacement can give rise to alternate chert-carbonate bands.

Kimberly (1974) and Krapez et al., (2003) suggest that chert bands in iron formations are not primary but form diagenetically by replacing initially precipitated carbonate. Acidic silica-rich pore water could dissolve carbonate and promote chert replacement. The abundance of siderite within the Basal Clastic Facies and within the Negaunee Iron Formation north of Tilden supports cyclic primary iron carbonate and chert deposition. Silica replacement of siderite not only raises the problem for the source of abundant silica but is also not supported by the complete absence of carbonate in most chert bands. Simonson (1987) suggests that hydrothermal waters circulating through basin sediments could promote carbonate dissolution and silica replacement. The source of silica could then be from hydrothermally evolved formational brine fluxed from the underlying clastic sediments. Discharged hydrothermal brine could carry both iron and silica and give rise to jasper bands. The syn-sedimentary mafic magmatism indicated by the autohydrated metadiabase units interfingering with the Negaunee Iron Formation

could supply heat and drive hydrothermal fluid expulsion for diagenetic replacement. Why alternate carbonate bands are replaced by chert remains problematic. Regardless of the specific origin of the chert bands, subsequent diagenesis and metamorphism results in recrystallized chert (Grenne and Slack, 2005; Klein, 1974).

Siderite bands within iron formations are commonly attributed to microbial activity in reduced conditions during burial and diagenesis (Miyano, 1987). The occurrence of unique Mg-siderite species within individual bands supports primary or diagenetic carbonate precipitation. Many siderite bands contain disseminated detrital quartz grains suggesting subtle transgression, and rapid capping by chert could play a role in siderite preservation. However, carbonate is very amenable to grain coarsening during metamorphism, thus all primary depositional characteristics have been obliterated.

Interruption of cyclic precipitation by wave action resulted in deposition of non-banded granular iron formation upward in the sequence. Periodic flooding due to storm waves initiated reworking of unconsolidated silica-iron precipitates and re-working of these granule rip-ups constitutes the granular-textured bands. Rapid burial by granular bands during transgressive pulses could also play a role in rapid burial of carbonate bands. In modern environments interbedding of such diverse lithologies is characteristic of carbonate ramps at or near storm wave base (Beukes and Gutzmer, 2008).

The transition from the Medial BIF Facies with granular-textured interbeds into the Upper GIF Facies is quite dramatic, occurring over a few meters. The disappearance of the banded lithologies and subsequent dominance of granular texture indicates basin evolution into a wave dominated environment. This transition marks a change in depositional environment from banded iron formation to a granular iron formation. This contact therefore marks a major transgression where cyclically precipitated banded iron formation is flooded by an encroaching sea (Simonson and Hassler, 1996). Continuous wave action causes ongoing disruption of silica-iron precipitation (Simonson, 1987). Individual ferri-hydrite rinded granules reflect wave-induced erosion of semi-lithified silica-iron gels (Dimroth, 1976; Simonson, 1987; Maliva et al., 2005). The extensive thickness of the Upper GIF Facies of ~ 100 meters indicates that silica-iron precipitation was ongoing during prolonged wave action. Examples from modern granular environments are dominated by the formation of carbonate ooids in agitated water

(Boggs, 1995). However, the lack of primary or relict carbonate within the granules and the occurrence of ferri-hydrite within the Negaunee do not support the formation of granules in a carbonate-mud environment as suggested by Maliva and Siever (1989). However, the granular textures do indicate an open-shelf ramp dominated by wave processes that precipitated primary ferri-oxyhydroxides on granule surfaces (Harris et al., 1985; Sellwood, 1986).

The start of the Great Oxygenation Event at ~2.4 Ga predates the Nipissing silling event recorded in the Huronian (Holland, 2006). Evidence for early oxygenating microbes has been observed in the Upper Huronian and correlative Kona Dolomite of the Chocolay Group (Hoffman, 1980). This unit occurs well below the Negaunee Iron Formation and suggests that the atmosphere was oxygenated prior to Negaunee deposition. Although the atmosphere was oxygenated, it may have been of low oxidizing potential and still contain abundant CH_4 and CO_2 so that the oceans remained buffered by ferrous iron (Kump and Seyfried, 2005; Bekker and Kaufman, 2007). Holland (2006) suggests that the shallow oceans were oxygenated, however deep oceans remained anoxic. The conditions of an oxic atmosphere and anoxic seas containing abundant ferrous iron could facilitate ferri-oxyhydroxide during oxidative regressive cycles and siderite precipitation during reduced transgressive cycles. Primary precipitation of ferri-oxyhydroxides requires either abiotic free oxygen interaction or microbial metabolic activity. Free oxygen produced by cyanobacteria could create oxygen oases or an oxic-anoxic stratified ocean water column to cause abiotic ferri-oxyhydroxide precipitation (Klein and Beukes, 1989).

Many authors suggest metabolic ferrous iron oxidation is responsible for iron formation precipitation. Two mechanics have been proposed. Fe (II) oxidizers utilize Fe (II) and free oxygen to precipitate Fe (III) in low atmospheric oxidizing conditions (Sogaard et al., 2000). Alternatively Fe (II) is used as a reductant for carbon dioxide fixation and no free oxygen is required (Widdel et al., 1993; Heising et al., 1999; Straub et al., 1999). A model utilizing Fe (II) as a carbon dioxide fixer is attractive since experiments have shown that this primary oxidation of iron could account for the abundance of ferri-oxyhydroxide and siderite in the Negaunee (Konhauser et al., 2005). Carbon dioxide fixation can occur at hundreds of meters of water depth, thus any

upwelling Fe (II) could be completely oxidized before iron rich waters come into contact with an oxygenated water column or atmosphere (Kappler et al., 2005). Although oxygenation of the atmosphere occurred pre-Negaunee deposition however, the seawater was sufficiently anoxic to facilitate iron formation precipitation.

Bekker et al., (2010) propose a temporal link between iron formation deposition and large igneous provinces (LIPs) (Figure 5.0). The igneous events would contribute large amounts of SO_2 and CO_2 to the atmosphere and enhance weathering under greenhouse conditions. Such weathering would contribute bicarbonate and nutrients such as phosphorous and to lesser extent nitrogen to the oceans, increasing the bioavailabity of these nutrients and thus triggering the Great Oxygenation Event. Extensive mafic magmatism would also provide abundant Fe^{2+} and reductants such as H_2 and H_2S to buffer the global oceans from an oxygenated atmosphere. The simultaneous construction of large continental shelves created a depository for granular iron formation deposition in the suboxic shallow waters. The concentration of greenstone units within the Negaunee Iron Formation could signify such a triggering mechanism.

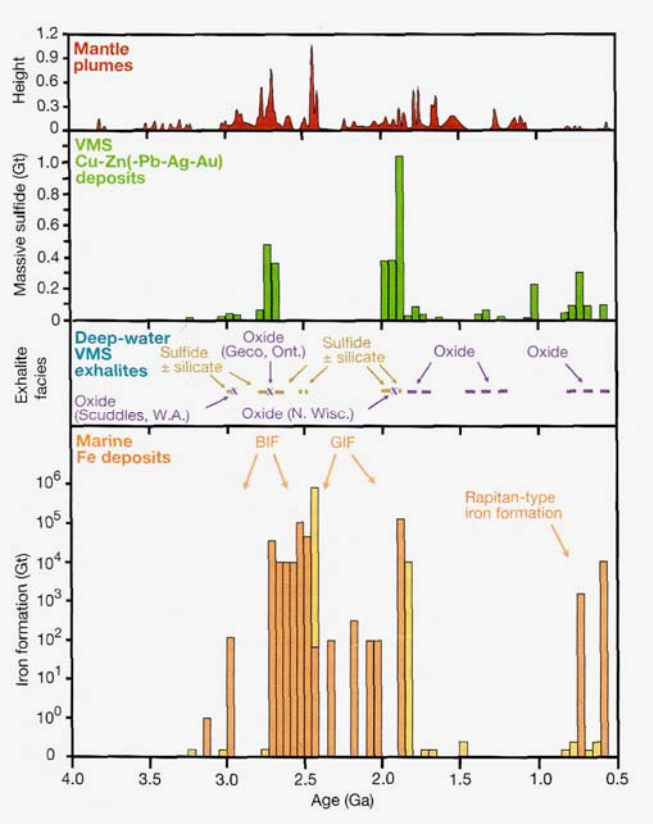

Figure 5.0: A graph depicting the temporal relationship between iron formations and mantle plume events (Bekker et al., 2010)

According to Slack and Cannon (2009) depositions of most iron formations ended abruptly at 1.85 Ga, coincident with impact of the Sudbury extraterrestrial bolide. These authors propose a model in which the impact caused global mixing of shallow oxic and deep anoxic waters to create a suboxic redox state in deep seawater. Limited concentrations of dissolved O_2 prevented the transport of hydrothermally derived Fe^{2+} from the deep ocean to the continental margin settings, ending the iron formation deposition. However, in the Marquette Range Supergroup, iron formation deposition terminated with the Bijiki Iron Formation significantly above the Sudbury impactite.

5.3 Paragenetic Sequence

The Tilden iron ores record a complex paragenetic sequence that can be subdivided into: 1) primary clastic and chemical sedimentary deposition and prelithification diagenetic processes including dewatering and cementation; 2) low grade greenschist metamorphism; and 3) a late hydrothermal overprint. These stages are demonstrated by the texture and mineral chemistry of the iron oxides, chlorites, carbonates and trace minerals.

5.3.1 Primary Deposition and Diagenesis

Given the subsequent metamorphic as well as late hydrothermal overprints, relict primary depositional and diagenetic textures are surprising well preserved. Silica cement rinding detrital quartz in the Basal Clastics reflects early cementation. Cryptocrystalline chert bands and jasper bands in the Medial BIF Facies suggest primary silica precipitation and diagenetic cementation. The Upper GIF Facies indicates wave re-worked silica-iron precipitation. All chert lithologies were lithified by dehydration and silica cementation. The presence of ferri-hydrite both rinding granules and occurring a micromillimeter “dust particles” is evidence for encapsulating primary ferri-oxyhydroxide precipitate in silica gels (LaBerge et al., 1987). Konhauser et al., (2002) advocate that the iron within iron formations is concentrated by way of precipitating ferri-oxyhydroxide that dehydrates during diagenesis to form ferri-hydrite. These authors suggest that the presence of iron oxidizers can precipitate iron by the process:

(1) $6Fe^{2+} + 0.5O_2 + CO_2 + 16H_2O \rightarrow CH_2O + 6Fe(OH)_3 + 12H^+$

Posth et al., (2008) demonstrates that changes in seawater temperatures above or below 20-25^{o}C can cause the slowing of iron oxidizing microbes. The retardation of microbial processes could subsequently promote the precipitation of abiotic silica. Precipitation of siliceous ooze or amorphous chert could modify the seawater to sufficiently anoxic and acidic conditions to promote microbially-mediated ferri-oxyhydroxide co-precipitation (Robbins et al., 1987). Fluctuating pH and water temperatures could therefore account for bands of jasper with abundant ferri-hydrite rather than the typical cryptocrystalline chert bands that lack iron minerals. Primary precipitated ferri-oxyhydroxide is metastable but diagenetic processes accompanying burial, with possibly overlapping microbial activity, results in dehydrating ferri-oxyhydroxide to form either goethite or hematite, again depending on temperature and pH. Acidic formational waters with pH levels of 2-5 in the jasper and granular-textured lithologies would favour goethite whereas, higher temperatures and pH would favour the formation of hematite (Cudennac and Lacerf, 2006).

Although no primary siderite survived the metamorphic overprint, it is likely that iron carbonate occurred as both a primary and diagenetic product. James (1955) noted that siderite is abundant in the Negaunee Iron Formation north of the iron mines. Therefore, primary carbonate was likely abundant within the Basal Clastics and Medial BIF prior to metamorphism. However iron carbonate is absent in the Upper GIF Facies. Silica cements the granules in GIF Facies and any primary carbonate was dissolved. The Mg-siderite species in the Basal Clastics and Medial BIF bands reflect the elevated Mg contents within the Basal Clastic detritus and subsequent carbonate replacement by magnetite. It is likely that siderite formed as a microbial precipitate within the reduced clastic sedimentary substrate. Subsequent grain coarsening accompanying metamorphism formed idioblastic textures that modify but did not destroy the diagenetic carbonate chemical signatures.

Within the Medial BIF Facies siderite is likely a primary or diagenetic precipitate. However, there is also textural evidence for diagenetic reduction of primary ferri-

oxyhydroxide to siderite (Beukes and Gutzmer, 2008). In a reduced environment siderite precipitates form by the reaction:

(2) $Fe^{2+} + CO_2 + H_2O \rightarrow FeCO_3 + 2H^+$ (Stumm and Morgan, 1996)

The siderite occurring in both the Basal Clastics and Medial BIF, occasionally preserves ferri-hydrite cores, suggesting the dehydration reduction of ferri-hydrite to form siderite. Beukes and Gutzmer (2008) proposed that microbial respiration during diagenesis released CO_2 and aided in conversion of primary ferri-oxyhydroxide to diagenetic siderite under suboxic conditions. Breakdown of ferri-oxyhydroxide can lead to siderite if conditions are more alkaline and sediments contain abundant organic matter and followed by rapid burial. However, as no organic matter was identified it is unlikely that microbial matter played a significant role.

Both the Basal Clastics and Medial BIF report relatively low phosphorous contents and lack phosphorous minerals (Lukey et al., 2007). Notably the low levels of phosphorous in the Basal Clastics and within bands of the Medial BIF Facies coincide with abundant siderite. Zachara et al., (1998) propose that the presence of phosphorous can have effect on iron precipitation. During reduction experiments, siderite was the only crystalline reduction product of goethite in the absence of a phosphorous component. Significantly, the higher phosphorous content in the Upper GIF Facies, accounted for by ubiquitous trace apatite and monazite, coincides with the absence of siderite.

5.3.2 Effects of Low Grade Metamorphism

The Marquette Range Supergroup was folded during the Penokean orogeny. Open folds to the north tighten toward the Southern Shear Zone giving rise to the Main Pit Anticline on the hanging wall of the Southern Gneiss Complex (Lukey et al., 2007). No biotite was observed, indicating low grade metamorphic conditions. Carbonate and chlorite grain coarsening, and the growth of magnetite, martite and specular hematite can be linked to metamorphic recrystallization. Magnetite is abundant within the Basal Clastics and Medial BIF Facies but has been completely oxidized to martite in the Upper GIF Facies. In the Basal Clastics and Medial BIF Facies, magnetite forms coarse, euhedral grains that

overgrew early ferri-hydrite, hematite and siderite. The magnetite in iron formations has been commonly attributed to reactions between hematite and siderite:

(3) $Fe_2O_{3(hm)} + FeCO_{3(sid)} \rightarrow Fe_3O_{4(mt)} + CO_2$ (Burt, 1972)

This reaction is favoured at higher temperatures and pressures and therefore occurs when an iron formation is buried and subjected to regional metamorphic conditions (Ohmoto, 2003). Siderite is lacking in the Upper GIF Facies and therefore reaction (3) may not proceed. The Upper GIF Facies represents a more open-shelf environment lacking the suboxic conditions necessary for siderite precipitation.

Beukes and Gutzmer (2008) propose that fine grained magnetite growth can be initiated during diagenesis when conditions do not favour the formation of siderite. Instead of siderite precipitating, magnetite can form by reduction of primary ferri-oxyhydroxide:

(4) $Fe(OH)_3 + Fe^{2+} \rightarrow Fe_3O_4 + 2H_2O + 2H^+$ (Beukes and Gutzmer, 2008)

Reduced diagenetic fluids may also have caused magnetite replacement of early hematite by the addition of Fe^{2+}:

(5) $Fe_2O_{3(hm)} + Fe^{2+} + H_2O = Fe_3O_{4(mag)} + 2H^+$ (Ohmoto, 2003).

Although magnetite growth in the Upper GIF Facies may have been initiated during diagenesis, subsequent metamorphic overprint of all three lithofacies caused grain coarsening of magnetite through porphyroblastic growth and annealing. The annealed glomeroporphyroblastic magnetite occurring within the Basal Clastic Facies and magnetite-rich bands of the Medial BIF Facies is typical of metamorphic recrystallization (Lascelles, 2006).

The degree of coarse idioblastic magnetite replacement by martite is variable, and band specific through the Medial BIF lithology and martite dominates in the Upper GIF Facies. Specular hematite is most abundant within the Upper GIF Facies, where platy

hematite replaces martite. Ohmoto (2003) and Lascelles (2006) suggest that martite and specular hematite form at high temperatures related to metamorphism. Metamorphic fluids oxidized the magnetite grains to form variably thick martite rims on magnetite. Cannon (1976) and Ohmoto (2003) evoked a model whereby oxidized metamorphic fluids leached Fe^{2+} from magnetite to form platy hematite. The magnetite-chert ores at the Tom Price deposit, Australia were transformed into hematite-chert ores by such a process.

(6) $Fe_3O_{4(mt)} + 2H^+ \rightarrow Fe_2O_{3(hm)} + Fe^{2+} + H_2O$ (Ohmoto, 2003)

Precipitation and growth of specular hematite from oxidizing fluids has also been documented at the Carajas Deposit, Brazil (Lobato et al., 2005). Impurities in martite rinds including Al, Si, Ti and occasionally Cr suggest martite replacement was facilitated by hydrous and oxidized metamorphic fluids as these elements are only mobile under highly oxidizing conditions (Velilla and Jimenez-Millan, 2003). Impurities such as trace Al and Si in the specularite laths indicate hematite replacement of martite.

The leaching of Fe^{2+} from magnetite via oxidation to form martite precedes the growth of texturally mature specularite. In the Upper GIF Facies specular hematite laths locally define tectonic foliations that are proximal to the limbs of the Main Pit Anticline, indicating specularite schists formed during metamorphic-related ductile shearing. Martite replacement of magnetite is minimal in the Basal Clastics and in specific bands of the Medial BIF Facies where siderite is present. This clearly demonstrates that siderite buffered the oxidation of magnetite to martite. In the Upper GIF Facies where siderite is lacking, metamorphic oxidation is not buffered by siderite and magnetite is completely oxidized to martite showing variable transformation to texturally mature platy specularite.

Metamorphic chlorites also reflect primary compositional control by bulk chemistry. Fe-dominant chlorites in the Basal Clastics and Medial BIF Facies occur interstitial to detrital quartz and represent the recrystallized clay component of the detritus. According to Zane et al., (1998) chlorites of metapelites that crystallize under greenschist facies are Fe-dominant. Haase (1979) demonstrated that the Tilden Pit occurs

just outboard of the biotite isograd bounding the Republic Metamorphic Node. A low greenschist overprint is therefore responsible for the Fe-dominant species in the Basal Clastics.

The metadiabase Pillar and underlying feeder dykes have undergone complete autohydration during emplacement into semi-wet sediments, supporting syn-depositional magmatism. Remnant diabasic textures are completely retrograded to chlorite during emplacement, obliterating the primary magmatic mineral species. These units display chlorite grain coarsening and alignment indicating effects of the post emplacement metamorphic overprint. The metamorphic chlorite in metadiabase is Mg-dominant, reflecting the bulk chemistry of the original greenstone. A detailed transect across a dyke boundary into the surrounding iron formation clearly demonstrates the change from Mg-dominant to Fe-dominant chlorite away from the dyke contact.

5.3.3 Late Hydrothermal Overprint

The Tilden Pit is sited on the hanging wall of the Southern Gneiss Complex and late brittle deformation increases towards the shear zone. This shear forms the north boundary to the Republic Metamorphic Node, related to thermal doming at 1750 Ma. Brittle deformation decreases upwards through stratigraphy from intense brecciation of the Basal Clastics, to fracture sets in the Medial BIF Facies, to stockwork veinlets in the Upper GIF Facies. A late hydrothermal overprint accompanied brittle deformation and gives rise to ubiquitous chlorite, carbonate and sulphide coating fracture walls, with trace associated apatite and monazite increasing upsection.

The hydrothermal chlorite is generally coarser than metamorphic chlorite and has diagnostic composition. Hydrothermal chlorite ranges from very high iron pseudothuringite, ripidolite, brunsvigite and diabantite species, as opposed to the lower iron metamorphic ripidolite and pycnochlorite species abundant in the Medial BIF and Basal Clastics.

Late hydrothermal carbonate includes zoned siderite-rhodochrosite and Fe-dolomite/ankerite species. Mn-zoned siderite and rhodochrosite coat fractures in the Basal Clastics and Medial BIF Facies. Mn-zoned siderite displays increasing iron towards grain rims, indicating increased Fe^{2+} in the hydrothermal fluids. Very high-Fe

and Mn-zoned siderites dominate the Basal Clastic fractures and occur less commonly through the Medial BIF Facies. Hydrothermal Fe-dolomite and ankerite are more abundant in the Medial BIF Facies and are the only hydrothermal carbonate species observed in the Upper GIF Facies. Calcite and dolomite are rare and are restricted to late fractures on the sheared margin of the metadiabase Pillar capping the Upper GIF Facies. Beukes and Guztmer (2008) noted that hydrothermal dolomite and calcite are common in high-grade iron ore deposits of the Carajas and Hamersley ranges.

Sulphides are most abundant in the Basal Clastics and are markedly less abundant in the Medial BIF Facies. Pyrite, chalcopyrite and tennantite are most concentrated in the chlorite-carbonate cemented breccias in the Basal Clastics. Fractures coated with chlorite and carbonate has rarely associated dispersed chalcopyrite and tennantite in the Medial BIF Facies. Fracture controlled sulphide indicate the high Fe-Mn hydrothermal fluid carried minor ubiquitous copper. Similar sulphide species have been documented in the Champion mine in association with late Mn-silicates (Babcock, 1966).

The trace apatite and monazite linked to the late hydrothermal overprint are remobilized out of the iron formation. Late apatite and monazite commonly intergrow with coarse Fe-dolomite, ankerite and chlorite within the granular iron formation. This stratigraphic control clearly indicates the increase in P-species with hydrothermal chlorite and carbonate is due to primary phosphorous in granular iron formation being remobilized during late hydrothermal conditions (Deer et al., 1966; Spry et al., 2000). Both monazite and apatite contain trace amounts of REEs as shown by microprobe EDS spectrum and the apatites prove to be a fluro-apatite species.

Chapter 6: Conclusions

6.1 Introduction

As a result of the interpretive discussions regarding the paleoenvironment and paragenetic sequence, conclusions can be made with respect to the metallogenic framework. This metallogenic history is followed by geometallurgical characterization of the complex iron ores making up the Main Pit Carbonate and Martite ore domains. A final summary lists the relevant conclusions from this thesis.

6.2 Metallogenic Model

The complex paragenesis of the Tilden ores can be tied to the regional tectonic framework. Detailed textures and mineral compositions of the three lithofacies suggest that the basal Negaunee Iron Formation at Tilden represents a rift basin setting that evolved to a more restricted evaporitic environment. Deposition of the basal Negaunee represents evolution from a clastic filled trough to an evaporitic pan to an off shelf ramp. Most of the lower Negaunee Iron Formation can be classified as a Superior-type, wave dominated granular iron formation. Regional folding between 1870 and 1830 Ma overprinted the original mineral assemblages and caused iron oxide enrichment. Late brittle deformation continued well after 1750 Ma and this was accompanied by a post thermal peak retrograde hydrothermal overprint proximal to the Southern Shear Zone.

Initial clastic sedimentation resulted in deposition of wacke sandstone containing quartz and abundant clay. Clastic sedimentation overlapping with banded iron formation marks periods of normal fault reactivation along the Southern Shear Zone. During the following regressive phase, evaporitic pan chemical sedimentation of ferri-oxyhydroxide, silica and siderite gave rise to the Medial BIF Facies. Subsequent transgression flooded the evaporitic pan and silica-iron precipitation reworked by wave-action produced ferri-oxyhydroxide granules comprising the Upper Granular Iron Formation. Diagenetic

processes included silica gel dehydration to chert and siderite cementing the Basal Clastics and Medial BIF Facies. Primary ferri-oxyhydroxides dehydrated to ferri-hydrite and lesser hematite.

The Negaunee Iron Formation has an unusual concentration of interlayered metadiabase. Complete autohydration of the Pillar and feeder dykes indicates syn-sedimentary mafic magmatism. Autohydration reflects emplacement into still semi-lithified wet sediments prior to regional deformation. Based on the evidence for syn-depositional emplacement, it is likely that the metadiabase units approximates the 2.1 Ga date suggested by Hans and Runnegar (1992) for the Negaunee Iron Formation. A 2.1 Ga age of the metadiabase units suggests rift related magmatism on the outer shelf of the trailing margin well before Penokean arc-craton collision. The absence of chloritized metadiabases above the Goodrich Quartzite unconformity strongly suggests that Negaunee mafic magmatism terminated iron formation deposition on the outer shelf.

Trendall and Blockey (2004) point out that most granular iron formations form discrete, well defined units that are commonly interstratified with associated volcanics. Intimate association of granular textured iron formation and volcanics has been documented in the Carajas Deposit, Brazil (Beukes and Gutzmer, 2008). The associated mafic magmatism suggests a close link between granular iron formation deposition and active rift environments. Bekker et al., (2010) point out that mafic magmatism associated with LIP development can be temporally linked to iron formation deposition.

The erosional unconformity between the Negaunee Iron Formation and the overlying Goodrich Quartzite at the base of the Baraga Group represents the onset of Penokean collision and marks a reversal in sediment provenance (Young, 1983). Arc-continent collision between 1870 and 1830 Ma gave rise to the Penokean fold and thrust belt and to the development of a foreland basin. Regional deformation resulted in the formation of the Main Pit Anticline within the Tilden Pit, and clearly involves folding of the interlayered metadiabase. At Tilden, greenschist regional metamorphism promoted glomeroporphyroblastic growth of magnetite, recrystallization of chlorite in the Basal Clastics and grain coarsening of the primary/diagenetic carbonates. Oxidized

metamorphic fluids unbuffered by siderite, resulted in replacement of magnetite by martite in the Medial BIF and Upper Granular Iron Formation. Martite is replaced by recrystallization to platy hematite.

The magnetite replacement of iron carbonate and martite replacement of magnetite is centered along the axis of the Main Pit Anticline (Lukey et al., 2007). This suggests a structural control for iron enrichment. The Main Pit Anticline may have acted as a focus for metamorphic fluids. Dalstra and Rosiere (2008) observed that hematite ores in the Hamersley, Kapvaal and Quadrilatero Ferrifero are also structurally controlled, indicating synclines and anticlines are important in concentrating fluids for iron ore enrichment. Magnetite and hematite flotation ores only occur proximal to the Southern Gneiss Complex and do not occur in the northern, less deformed part of the Negaunee (Lukey et al, 2007).

The late 1750 Ma Republic Metamorphic Node imposed greenschist facies thermal metamorphic conditions at the Tilden Pit. Temperatures between 200 and 300^{o}C and pressures of no greater than 1.2 kbar (Klein, 2005) are consistent with producing abundant chlorite in the absence of biotite, stilpnomelane and minnesotaite in the Tilden Pit (Hasse, 1979). Retrograde shearing post-dates peak thermal metamorphism and is accompanied by a late hydrothermal chlorite-carbonate-sulphide overprint proximal to the Southern Gneiss Complex. Brittle deformation decreases upsection and away from the Southern Gneiss Complex causing brecciation in the Basal Clastics, fractures in the Medial BIF and veinlets in the Upper Granular Iron Formation. The late hydrothermal overprint proximal to the Southern Gneiss Complex is characterized by zoned siderite-rhodocrosite, Fe-dolomite, ankerite, high-Fe chlorite, and Cu-Fe sulphide accompanied by trace fluro-apatite and monazite. Co-existing chalcopyrite and tennantite can suggest fluid temperatures between 260 and 370^{o}C (Valencia et al., 2008). Rare cross-cutting undeformed quartz veins containing minor specular hematite are linked to this late stage overprint.

A similar overprint is recorded at the Champion Mine, occurring at higher metamorphic grades along the same northern boundary of the Republic Metamorphic Node. The late hydrothermal minerals at the Champion Mine include molybdenite,

native gold, boron and bismuth (Cannon, 1976; Waggoner, 2010). Recent Os-Re dating of molybdenite and Mn-bearing magnetites at the Champion Mine places the late hydrothermal overprint between 1672 and 1570 Ma (Waggoner, 2010). The late hydrothermal overprint may be related to waning stages of the 1720 to 1680 Ma development of the Republic Metamorphic Node.

Hydrothermal fluids enriched in Mn-Fe-Cu-Au-Mo-Bi with trace REEs, suggests an iron-oxide-copper-gold (IOCG) signature at both the Champion and Tilden mines. At Olympic Dam, Australia the IOCG mineralization, expressed by complex, magnetite-chalcopyrite, hematite-bornite, Au, and U-REE apatite ores are broadly similar in geochemical signature to the trace hydrothermal minerals observed at Tilden (Bastrakov et al., 2007).

6.3 Geometallurgical Response of Carbonate and Martite Domain Iron Ores

For mine planning purposes the Tilden pit has been partitioned into ore domains based on bulk geochemistry and metallurgical response. The Carbonate and Martite domain characteristics are summarized in Table 2.0. Inconsistent metallurgical response of the Main Pit Carbonate Domain led to speculation that variations in ore textures and mineral compositions not identified by bulk chemical analyses were affecting ore treatments. Subsequent core-logging, petrographic investigations and microprobe analyses have identified three lithofacies that comprise the Main Pit Carbonate and Martite Domains. These account for textural variability. Determination of the paragenetic sequence and associated mineral compositions presented herein, aid in metallurgical trouble-shooting.

6.3.1 The Main Pit Carbonate Domain

The Carbonate Domain is dominantly comprised of the Medial BIF Facies and several meters of the upper Basal Clastics. Bulk chemistry is characterized by higher Mg, Mn, Ca, Al and slightly lower Fe compared to the Martite Domain. Petrographic investigations define the mineral assemblage to be quartz + magnetite + [martite/hematite

+ chlorite + siderite/magnesite]. Fracture controlled, hydrothermal minerals include Fe-dolomite or ankerite +/- chlorite +/- chalcopyrite +/- tennantite +/- apatite +/- monazite. Considering bulk geochemistry in the context of the complex mineral paragenesis, several metallurgical issues can be identified. The bulk head iron content is misleading since Fe is tied up in multiple mineral species. The recoverable iron is dominantly in magnetite, and minor martite/hematite, however, iron is also a major element in the abundant chlorite and carbonate minerals. Diagenetic Mg-siderite, Fe-dominant chlorites and the very high-Fe hydrothermal chlorites will add to the total Fe budget and therefore over-represent the total Fe available for liberation.

Bulk rock magnesium, manganese and calcium can be accounted for by clastic detritus and different species of diagenetic and hydrothermal carbonate. The bulk magnesium is largely contained in siderite/magnesite and lesser in chlorite. However, Mg-dominant chlorite in the chloritized metadiabase would add to the magnesium budget. Minor magnesium is tied up in the late hydrothermal Fe-dolomite/ankerite species. Manganese is a minor component in chlorite but a major element in late Mn-zoned siderite. The low phosphorous content of the Carbonate Domain reflects minor hydrothermal apatite and monazites associated with interlayered granular textured bands. The occurrence of trace hydrothermal sulphide is unlikely to affect ore treatment.

Textures not expressed by bulk chemistry can have an impact on metallurgical treatment. The Main Pit Carbonate Domain is largely comprised of the Medial BIF Facies and minor components of the Basal Clastics and Upper Granular Iron Formation. These texturally distinct lithologies will respond differently to treatment. Silica comprises three morphological varieties including primary detrital quartz grains, primary or diagenetic cryptocrystalline chert or jasper and granular-chert. Grain size and degree of iron oxide encapsulation in chert will affect Fe liberation during grinding. The dominant iron oxide is coarse magnetite, forms disseminations in the Basal Clastics, replaces discreet bands, and overgrow granules in the Medial BIF and Granular Iron Formation. Degrees of martite replacement are tied to the presence of siderite. Where siderite is absent, magnetite oxidation is unbuffered and is replaced by martite.

6.3.2 Martite Domain

The Martite Domain contains lower bulk rock Al, Mg, Mn, and Ca and slightly higher Fe and P compared to the Carbonate Domain, reflecting the significant decrease in abundance of chlorite and carbonate. The mineral assemblage that defines the Martite Domain is quartz + martite/hematite. Trace hydrothermal minerals include chlorite +/- Fe-dolomite/ankerite +/- apatite +/- monazite. Metallurgical response of this Domain has been relatively consistent and therefore ore definition on the basis of bulk chemistry is more effective.

Martite and hematite are the dominant iron phases present and therefore define head iron content. Trace Fe-chlorite and Fe-dolomite/ankerite will have little impact on iron content. Mg-mineral species in chloritized diabases will contribute to the Mg and Al bulk chemistry. The trace hydrothermal carbonate is solely Fe-dolomite/ankerite contributing negligible Mg, Ca and Mn to the bulk rock chemistry. However, phosphorous content in the Martite Domain is accounted for by both primary and hydrothermal apatite and monazite.

Texturally, this domain is also relatively uniform with recrystallized primary and diagenetic silica dominating. The primary iron oxide phase is martite, replacing coarse metamorphic magnetite and overgrown by platy hematite. Magnetite is absent. The consistency in both silica and iron oxide textures leads to the much more predictable ore treatment response of the Martite Domain compared to the more variable Main Pit Carbonate Domain.

6.3.3 Geometallurgical Statement

Metallurgical interpretations based on bulk rock chemistry irrespective of the pit geology and mineralogy has and will continue to lead to unpredictable ore treatment response in the Main Pit Carbonate Domain. The development of a metallogenic model accounting for the multistage paragenetic sequence has shown that textures and mineral chemistries reflect a complex evolution. Bulk chemical analyses do not reliably predict concentrate chemistries. Textural variations and mineral speciation of the different lithofacies can affect grinding and liberation and must be taken into account. Therefore, ore treatment

processes are more effective when the genesis of the ore deposit is fully understood. Metamorphic overprinting has significantly upgraded primary iron formation via oxidation and grain coarsening. The primary ferri-hydrite reacted with siderite to form magnetite, and magnetite was further oxidized to martite and platy hematite. The metamorphic enrichment produced the economic ores. Intense brittle deformation accompanied by strong hydrothermal alteration complicates the Carbonate Domain metallurgical response proximal to the Southern Gneiss Complex.

This thesis has proven that bulk rock chemistry established at the blast hole scale can mask multiple facets of iron ores that ultimately influence metallurgical processing. In order to successfully predict metallurgical response, mineral speciation within paragenetic stages must be considered in characterizing the geometallurgical response of ores.

6.4 Summary

Variable mineral chemistry and textures of basal Negaunee iron ores mined in the Main Tilden Pit have led to metallurgical difficulties. Core-logging, detailed petrography and microprobe investigations were carried out to characterize the iron ores of the Main Pit Carbonate Domain and Martite Domain. As a result of these investigations the following conclusions can be made regarding: 1) the paleoenvironment of the basal Negaunee lithofacies; 2) the detailed paragenesis of the Main Pit Carbonate and Martite iron ores; 3) a metallogenic model; and 4) the predictive geometallurgical response of ores to treatment.

1) Three lithofacies were identified comprising the Main Pit Carbonate and Martite domains including Basal Clastics, Medial BIF and Upper Granular Iron Formation.

2) The paleoenvironment of the basal Negaunee evolves from clastic infilling a fault bounded trough to a starved evaporitic pan on a stable shelf, to wave reworked off shelf ramp.

3) The paragenetic sequence of the basal iron ores entail: a) primary/diagenetic silica, ferri-hydrite and carbonate; b) metamorphic chlorite, carbonate and magnetite plus martite and platy specular hematite; and c) late hydrothermal chlorite, carbonate, Cu-Fe sulphide and remobilized apatite and monazite.

4) The paragenetic sequence can be linked to the Penokean cycle such that: a) primary/diagenetic sediments and mafic magmatism are related to a trailing margin setting; b) regional metamorphism is related to the Penokean arc/craton collision; and c) the late hydrothermal overprint reflects an IOCG signature that may be linked to the 1750 to 1680 Ma development of the Republic Metamorphic Node.

5) The geometallurgical response of the Main Pit Carbonate and Martite domains can be linked to: a) silica textures; b) bulk iron content expressed in numerous minerals; and c) the metamorphic and hydrothermal overprinting.

References

Babcock, L.L., 1966. The Manganese-Bearing Minerals of Champion Mine, Champion, Michigan. Institute of Lake Superior Geology, 12th Annual Meeting.

Barovich, K., Patchett, J., Peterman, Z. and Sims, P., 1989. Origin of 1.9-1.7 Ga Penokean Continental Crust of the Lake Superior Region. *Geological Society of America Bulletin* (101): 333-338

Bastrakov, E.N., Skirrow, R.G., and Davidson, G.J., 2007. Fluid Evolution and Origins of the Iron Oxide Cu-Au Prospects in the Olympic Dam Disctrict, Gawler Craton, South Australia. *Economic Geology and the Bulletin of the Society of Economic Geologists* (102) 8: 1415-1440

Bekker, A., and Kaufman, A.J., 2007. Oxidative Forcing of Global Climate Change: A Biogeochemical Record Across the Oldest Paleoproterozoic Ice Age in North America. *Earth and Planetary Science Letters* (258): 486-499

Bekker, A., Slack, J.F., Planavsky, N., Krapez, B., Hofman, A., Konhauser, K.O. and Rouxel, O.J., 2010. Iron Formation: The Sedimentary Product of a Complex Interplay among Mantle Tectonic, Oceanic, and Biospheric Processes. Economic Geology, Bulletin of the Society of Economic Geologists (105) 3: 467-508

Beukes, N. and Gutzmer, J., 2008. Origin and Paleoenvironment Significance of Major Iron Formations at the Archean-Paleoproterozoic Bounary. *In*: Banded Iron Formation-Related High-Grade Iron Ore. Edited by Hagemann, S., Rosiere, C., Gutsmer, J. and Beukes, N. *Economic Geology Reviews* (15): 5-47

Blatt, H., 1992. *In*: Sedimentary Petrology. Edited by: W.H. Freeman and Company.

Boggs, S., Jr., 1969. Relationship of Size and Composition in Pebble Counts. *Journal of Sedimentary Petrology* (39): 1326-1339

Boggs, S., Jr., 1995. In: Principles of Sedimentology and Startigraphy. Edited R. A. McConnin, Simon and Schuster Company:

Boyum, B., 1975. The Marquette Mineral District of Michigan. *Unpublished Report to Cleveland-Cliffs Iron Company: Ishpeming*

Burt, D., 1972. The System Fe-Si-C-O-H: A model for metamorphosed Iron Formations. *Carnegie Institutes Washington Year Book*: 1971-1972

Cambray, F.W., 2002. The Evolution of a Paleoproterozoic Plate Margin, Northern Michigan. *Field Trip Guide for the Great Lakes Section, SEPM 32nd Annual Fall Field Conference.*

Cannon, W., 1975. Stratigraphic Relationships within the Baraga Group of Precambrian Age, Central Upper Peninsula Michigan. *Journal of Research USGS* (3): 47-51

Cannon, W., 1976. Hard iron ore of the Marquette Range, Michigan. *Economic Geology* (71): 1012-1028

Cannon, W.F., 1986. Bedrock Geologic Map of the Iron River 1^{o} x 2^{o} Quadrangle, Michigan and Wisconsin. *United States Geological Survey, Miscellaneous Investigation Series Map I-1360-B*, scale 1:250,000.

Cannon, W.F. and Gair, J.E., 1970. A Revision of the Stratigraphic Nomenclature for Middle Precambrian Rocks in Northern Michigan. *Geological Society of America Bulletin* (81): 2843-2846

Cannon, W.F., Schultz, K.J., Horton, Jr., J.W., and Kring, D.A., 2010. The Sudbury Impact Layer in the Paleoproterozoic Iron Ranges of Northern Michigan, USA. *Bulletin of the Geological Society of America* (122) no.1-2: 50-75

Chang, L.L.Y., Howie, R.A., and Zussman, J., 1998. *In*: Rock Forming Minerals, Vol. 5B Non-Silicates: Sulphates, Carbonates, Phosphates, Halides. The Geological Society, London (2^{nd} edition)

Corfu, F., and Andrews, A.J., 1986. A U-Pb for Mineralized Nipissing Diabase, Gowganda, Ontario. *Canadian Journal of Earth Sciences* (23): 107-109

Cudennec, Y. and Lecerf, A., 2006. The Transformation of Ferrihydrite into Goethite of Hematite, Revisted. *Journal of Solid State Chemistry* (179): 716-722

Dalstra, H. and Rosiere, C., 2008. Structural Controls on High-Grade Iron Ores Hosted by Banded Iron Formation: A Global Perspective. In: Banded Iron Formation-Related High-Grade Iron Ore. Edited by Hagemann, S., Rosiere, C., Gutzmer, J. and Beukes, N. *Society of Economic Geologists Reviews* (15): 73-106

Deer, W.A., Howie, R.A., and Zussman, J., 1966. *In*: An Introduction to The Rock Forming Minerals 2^{nd} edition. Edited by Pearson Education Ltd and British Library Cataloguing in Publication Data

Dimroth, E., 1976. Aspects of Sedimentary Petrology of Cherty Iron-Formations. In: Handbook of Stratabound and Stratiform Ore Deposits. Edited by: K.H. Wolfe, Elsevier, Amsterdam (7): 203-254

Exploring the North, 2011. http://www.exploringthenorth.com/cvillage/marqishmp.html (2011) (Marquette Map)

Fischer, W.W., and Knoll, A.H., 2009. An Iron Shuttle for Deep-Water Silica in Late Archean and Early Paleoproterozoic Iron Formation. Geological Society of America Bulletin (121): 222-235

Gair, J.E., 1970. Marquette Range Field Guidebook. *(1970) Geological Society of America Annual Meetings* in Milwaukee, Wisconsin: 28

Gair, J.E., 1975. Bedrock Geology and Ore Deposits of the Palmer Quadrangle, Marquette County, Michigan. *United States Geological Survey Professional Paper* 769: 159

Gair, J.E., and Weir, K.L., 1956. Geology of the Kiernan Quad., Iron County, Michigan, USA. *Geological Survey Bulletin 1044*

Grenne, T., and Slack, J.F., 2005. Geochemistry of Jasper Beds from the Ordovician Lokken Ophiolite, Norway: Origin of Proximal and Distal Siliceous Exhalites. *Economic Geology and the Bulletin of the Society of Economic Geologists* (100) 8: 1511-1527

Hans, T.M., and Runnegar, B., 1992. Megascopic Eukaryotic Algae from the 2.1-Billion-Year-Old Negaunee Iron-Formation, Michigan. *Science* (257): 232-235

Harris, M.T., 1990. Modeling Carbonate Progradation Geometry and Sediment Accumulation Rates; a Comparison of MARGIN Results with Outcrop Data. *AAPG annual convention with DPA/EMD divisions and SEPM, an associated society; technical program with abstracts*

Harris, P.M., Moore, C.H., and Wilson, J.L., 1985. Carbonate Depositional Environments, Modern and Ancient. *Pt 2: Carbonate Platforms: Colorado School of Mines Quarterly* (80): 1-60

Haase, 1979. Metamorphic Petrology of the Negaunee Iron-Formation, Marquette District, Northern Michigan. Doctor of Philosophy Thesis, Indiana University: 19

Heising, S., Richter, L., Ludwig, W., and Schink, B., 1999. Chlorobium Ferrooxidans Sp. Nov., A Phototrophic Green Sulfur Bacterium that Oxidizes Ferrous Iron in Coculture with a "Geospirllum" Sp. Strain. *Archives of Microbiology* (172): 116-124

Hinman, N. and Lindstrom, R., 1996. Seasonal Changes in Silica Deposition in Hot Spring Systems. *Chemical Geology* (132): 237-246

Hoffman, P., 1980. Stromatolites and Fenestral Fabric in Early Proterozoic Huronian Supergroup, Ontario. *Canadian Journal of Canadian Earth Sciences* (17) no.10: 1351- 1357

Hoffman, P., 1987. Early Proterozoic Foredeeps, Foredeep Magmastism and Superior-type Iron Formations of the Canadian Shield. In: Proterozoic Lithospheric Evolution. Edited by A. Kroner. *American Geophysical Union Geodynamics Series* (17): 85-98

Hoffman, P.F., 1988. United Plates of America, the Birth of a Craton: Early Proterozoic Assembly and Growth of Laurentia. *Annual Review of Earth and Planetary Science* (16): 543-603

Holland, H.D., 2006. The Oxygenation of the Atmosphere and Oceans. *Philisophical Transactions of the Royal Society, Biological Sciences* (361) no. 1470: 903-915

James, H.L., 1954. Sedimentary Facies of Iron Formation. *Economic Geology* (49): 235-293

James, H.L., 1955. Zones of Regional Metamorphism in the Precambrian of Northern Michigan. *Bulletin of the Geological Society of America* (66): 1455-1487

James, H.L., Dutton, C.E., Pettojohn, F.J. and Weir, K.L., 1968. Geology and Ore Deposits of the Iron River-Crystal Falls District, Iron County Michigan. *United States Geological Survey Professional Paper* 570: 134

Kalstrom, K.E., Ahall, K.I., Harlan, S.S., Williams, M.L., McLelland, J., and Geissman, J.W., 2001. Long-Lived (1.8-1.0 Ga) Convergent Orogen in Southern Laurentia, Its Extensions to Australia and Baltica, and Implications for Refining Rodinia. *Precambrian Research* (111): 5-30

Kappler, A., Pasquero, C., Konhauser, K.O., and Newman, D.K., 2005. Deposition of Banded Iron Formations by Anoxygenic Phototrophic Fe(II)-oxidizing bacteria. *Geology* (33): 865-868.

Kimberly, M.M., 1974. Origin of Iron Ore by Diagenetic Replacement of Calcareous Oolite. *Nature* (250): 199-217

Klein, C., 1974. Greenalite, Stilpnomelane, Minnesotaite, Crocidolite and Carbonates in A Very Low-Grade Metamorphic Precambrian Iron-Formation. *Canadian Mineralogist* (12): 474-498

Klein, C., 2005. Some Precambrian Banded Iron Formations (BIFs) from Around the World: Their Age, Geologic Setting, Mineralogy, Metamorphism, Geochemistry, and Origin. *American Mineralogist* (90): 1473-1499

Klein, C., and Beukes, N.J., 1989. Geochemistry and Sedimentology of a Facies Transition from Limestone to Iron-Formation Deposition in the Early Proterozoic Transvaal Supergroup, South Africa. *Economic Geology* (84): 1733-1774

Klein, C. and Hurlbut, C.S.Jr., 1993. Manual of Mineralogy 20st edition. Edited by John Wiley and Sons Inc.

Konhauser, K.O. Hamade, T., Raiswell, R., Morris, R.C., Ferris, F.G., Southam, G., and Canfield, D.E., 2002. *Geology* (30): 1079-1082

Konhauser, K.O., Newman, D.K., and Kappler, A., 2005. Fe(III) Reduction in BIFs: The Potential Significance of Microbial Fe(III) Reduction During Deposition of Precambrian Banded Iron Formations. *Geobiology* (3): 167-177

Konhauser, K.O., Amskold, L., Lalonde, S.V., Posth, N.R., Kappler, A., and Anbar, A., 2007. Decoupling Photochemical Fe(II) Oxidation from Shallow-Water BIF Deposition. *Earth and Planetary Science Letters* (258): 87-100

Krapez, B., Barley, M.E. and Pickard, A.L., 2003. Hydrothermal and Resedimented Origins of the Precursor Sediments to Banded Iron Formations: Sedimentological Evidence from the Early Proterozoic Brockman Supersequence of Western Australia. *Sedimentology* (50): 979-1011

Kuenen, Ph., H., 1958. Experiments in Geology. *Geological Society of Glasgow Transactions* (23): 1-28

Kump, L.R., and Seyfried, W.E., 2005. Hydrothermal Fe Fluxes During the Precambrian: Effect of Low Oceanic Sulfate Concentrations and Low hydrostatic Pressure on the Composition of Black Smokers. Earth and Planetary Sciences Letters (235): 654-662

LaBerge, G.L., Robbins, E.I., and Han, T.H., 1987. A Model For the Biological Precipitation of Precambrian Iron-Formations –A: Geological Evidence. *In*: Precambrian Iron-Formations edited by Appel and LaBerge. Theoprastus Publications, S.A.: 69-96

Larue, D. and Sloss, L., 1980. Early Proterozoic Sedimentary Basins of the Lake Superior Region. *Geological Society of America Bulletin* (91) Part I: 450-452

Lascelles, D.F., 2006. The Genesis of the Hope Downs Iron Ore Deposit, Hamersley Province, Western Australia. *Economic Geology* (101): 1359-1376

Lobato, L., Figueiredo e Silva, R. Rosiere, C., Zucchetti, M. Baars, F., Pimentel, M., Rios F., Seoane, J, and Monteiro, A., 2005. Hydrothermal Origin for the Iron Mineralization, carajas Province, Para State, Brazil. *Australasian Institute of Mining and Metallurgy Publication Series* (8): 99-110

Lukey, H.M., Johnson, R.C., and Scott, G.W., 2007. Mineral Zonation and Stratigraphy of the Tilden Haematite Deposit, Marquette Range, Michigan, USA. *Iron Ore Conference*

Maliva, R.G., and Siever, R., 1989. Nodular Chert Formation in Carbonate Rocks. *Journal of Geology* (97): 421-433

Maliva, R., Knoll, A. and Simonson, B., 2005. Secular Changes in the Precambrian Silica Cycle: Insights from Chert Petrology. *Geological Society of America Bulletin* (117): 835-845

Miyano, T., 1987. Diagenetic to Low Grade Metamorphic Conditions of Precambrian Iron Formations. *In*: Precambrian Iron Formations edited by P.W.U. Appel and G.L. LaBerge, Theophrastus Publications S.A. Greece: 155-186

Mongabay, 2011. http://www.mongabay.com (2011) (iron ore prices)

North, J., 1993. Iron ores of the pre-Penokean, Superior-Type Riverton Iron Formation, Michigan: Keweenawan Supergene oxidation, iron enrichment, and paucity of other metals. *Phd Thesis. University of Western Ontario.*

Ohmoto, H., 2003. Nonredox Transformations of Magnetite-Hematite in Hydrothermal Systems. *Economic Geology* (98): 157-161

Posth, N., Hegler, F., Konhauser, K. and Kappler, A., 2008. Alternating Si and Fe Deposition Caused by Temperature Fluctutations in Precambrian Oceans. *Nature Geoscience* (1): 703-708

Reuters, T., 2010. Iron Ore Demand to Continue Strongly in 2011. Mineweb

http://www.mineweb.com/mineweb/view/mineweb/en/page504?oid=114739&sn=Detail

Robbins, E.I., LaBerge, G.L. and Schmidt, R.G., 1987. A Model For the Biological Precipitation of Precambrian Iron Formations –B: Morphological Evidence and Modern Analogs. *In*: Precambrian Iron-Formations edited by Appel and LaBerge. Theoprastus Publications, S.A.: 97-125

Sellwood, B.W., 1986. Shallow-Marine Carbonate Environments. *In:* Sedimentary Environments and Facies. Edited by H.G. Reading, Blackwell Oxford (2nd edition): 283-342

Schulz, K.J., 1990. Tectonic Evolution of the Early Proterozoic Penokean Orogen. *In*: Precambrian Geology of the Southern Canadian Shield and the Eastern Baltic Shield, USA, USSR and Canada Joint Seminar, Duluth, Minnesota. Edited by: R.W. Ojakangas: 29-32

Schulz, K.J., and Cannon, W., 2007. The Penokean Orogeny in the Lake Superior Region. *Precambrian Research* (157): 4-25

Schneider, D.A., Holm, D.K., and Lux, D., 1996. On the Origin of Early Proterozoic Gneiss Domes and Metamorphic Nodes, Northern Michigan. *Canadian Journal of Earth Sciences* (33): 1053-1063

Schneider, D.A., Bickford, M.E., Cannon, W.F., Schulz, K.J. and Hamilton, M.A., 2002. Age of volcanic rocks and syndepositional iron formations, Marquette Range Supergroup: Implications for the tectonic setting of Paleoproterozoic iron formations of the Lake Superior region. *Canadian Journal of Earth Sciences* (39): 999-1012

Scott, G.W., and Lukey, H.M., 1999. Geologic Field Trip to the Tilden Mine. *Institute on Lake Superior Geology 45th Annual Meeting, Abstracts and Proceedings* (45) Part II: 114-128

Sims, P. and Peterman, Z., 1983. Evolution of the Penokean Foldbelt, Lake Superior Region, and its Tectonic Environment. *Geological Society of America Memoir* (160): 2-14

Sims, P.K., Card, K.D., Morey, G.B., and Peterman, Z.E., 1980. The Great Lakes Tectonic Zone – A Major Crustal Structure in Central North America. *Geological Society of America Bulletin Part 1* (91): 690-698

Simonson, B., 1987. Early Silica Cementation and Subsequent Diagenesis in Arenites from Four Early Proterozoic Iron Formations of North America. *Journal of Sedimentary Petrology* (57): 494-511

Simonson, B. and Hassler, S., 1996. Was the Deposition of Large Precambrian Iron Formations Linked to Major Marine Transgressions? *The Journal of Geology* (104): 665-676

Slack, J.F., and Cannon, W.F., 2009. Extraterrestrial Demise of Banded Iron Formations 1.85 Billion Years Ago. *Geology* (37): 1011-1014

Slack, J.F., Grenne, T., Bekker, A., Rouxel, O.J., and Lindberg, P.A., 2007. Suboxic Deep Sea Water in the Late Paleoproterozoic: Evidence From Hematitic Chert and Iron Formation Related to Seafloor-hydrothermal Sulfide Deposits, Central Arizona, USA. *Earth and Planetary Science Letters* (255): 243-256

Sogaard, E.G., Nedenwaldt, R., and Abraham-Peskir, J.V., 2000. Conditions and Rates of Biotic and Abiotic Iron Precipitation in Selected Danish Fresh Water Plants and Microscopic Analysis of Precipitate Morphology. *Water Research* (34): 2675-2682

Spry, P.G., Peter, J.M. and Slack, J.F., 2000. Geochemistry and Genesis of the Banded Iron Formations of the Caue Formation, Quadrilatero Ferrifero, Minas Gerais, Brazil. *Precambrian Research* (152): 170-206

Straub, K.L., Rainey, F.A., and Widdel, F., 1999. Rhodovulum Iodosum Sp. Nov. and Rhodovulum Robiginosum Sp. Nov., two New Marine Phototrophic Ferrous-Iron-Oxidizing Purple Bacteria. *International Journal of Systematic Bacteriology* (49): 729-735

Stumm, W. and Morgan, J., 1996. *In*: Aquatic Chemistry. Edited by New York, John Wiley and Sons: 1022

Tinkham, D.K, and Marshak, S., 2004. Precambrian Dome-and-Keel Structure in the Penokean Orogenic Belt of Northern Michigan, USA. *In*: Gneiss Domes in Orogeny. Edited by Whitney, D., Teyssier, C and Siddoway, C. *Geological Society of America Special Paper* 380: 321-338

Trendall, A.F., 1983. Introduction *In*: Iron Formation: Facts and Problems, Edited by A.F. Trendall and R.C. Morris, Elsevier Amsterdam: 1-11

Trendall, A.F., 2002. The significance of Iron-Formation in the Precambrian Stratigraphic Record. In: Precambrian Sedimentary Environments: A Modern Approach to Ancient Depositional Systems. Edited by W. Altermann and P. Corcoran. *Special Publication International Association of Sedimentologists* (33): 33-36

Trendall, A.F. and Blockley, J.G., 2004. Precambrian Iron Formations *In*: The Precambrian Earth: Tempos and Events. Developments in Precambrian Geology (12): 403-421

Vallini, D.A., Cannon, W.F., Schulz, K.J., and McNaughton, N.J., 2007. Thermal History of Low Metamorphic Grade Paleoproterozoic Sedimentary Rocks of the Penokean Orogen, Lake Superior Region: Evidence for a Widespread 1786 Ma Overprint Based on Xenotime Geochronology. *Precambrian Research* (157): 169-187

Van Schmus, W. and Hinze, W., 1985. The Midcontinent Rift System. *Annual Review of Earth and Planetary Sciences* (13): 345-384

Van Schmus, W., and Bickford, M.E., 1981. Proterozoic Chronology and Evolution of The Midcontinent Region, North America. *In*: Precambrian Plate Tectonics, Edited by A. Kroner, Elsevier, New York: 261-296

Van Schmus, W., Bickford, M. and Zeitz, I., 1987. Early and Middle Proterozoic Provinces in the Central United States. *American Geophysical Union Geodynamics Series* (17): 43-68

Valenica, V.A., Eastoe, C., Ruiz, J., Ochoa-Landin, L., Gehrels, G.E., Gonzalez-Leon, C., Barra, F., and Espinoza, E., 2008. Hydrothermal Evolution of the Porphyry Copper Deposit at La Caridad, Sonora, Mexico, and the Relationship with a Neighboring High-Sulfidation Epithermal Deposit. *Economic Geology and the Bulletin of the Society of Economic Geologists* (103) no. 3: 473-491

Velilla, N., and Jimenez-Millan, J., 2003. Origin and Metamorphic Evolution of Rocks with Braunite and Pyrophanite from the Iberian Massif, SW Spain. *Mineralogy and Petrology* (78) 1-2: 73-91

Waggoner, T., 2010. Post Penokean Age of Mineralization on Marquette Range, Michigan. Institute of Lake Superior Geology

Webster, C.L., 1999. Structural Analysis of Ductile Shear Zone within the Marquette Iron Range, Upper Peninsula, Michigan. *MSc. Thesis (unpublished), Michigan State University, East Lansing.*

Widdel, F., Schnell, S., Heising, S., Ehrenreich, A., Assmus, B., and Schink, B., 1993. Ferrous Iron Oxidation by Anoxygenic Phototrophic Bacteria. *Nature* (362): 834-836

Young, G., 1983. Tectono-Sedimentary History of the Early Proterozoic Rocks of the Northern Great Lakes Region. *In*: Early Proterozoic Geology of the Great Lakes Region. Edited by G. Medaris. *Geological Society of America Memoir* (160): 15-32

Zachara, J., Fredrickson, J., Li, S., Kennedy, D., Smith, S. and Gassman, P., 1998. Bacterial Reduction of Crystalline Fe^{3+} oxides in Single Phase Suspensions and Subsurface Materials. *American Mineralogist* (83): 1426-1443

Zane, A., Sassi, R. and Guidotti, C.V., 1998. New Data on Metamorphic Chlorite as a Petrogenetic Inidicator Mineral, with Special Regard to Greenschist-Facies Rocks. *The Canadian Mineralogist* (36): 713-726

Appendix A

Informal Use of terms

Bulk/Head chemistry: this refers to the assayed results of the drill core from exploration holes. Bulk chemistry was performed on the major elements including Si, Fe, Mg, Mn, Ca and P.

Carbonate: is a general term that can include the solid solution series end members of magnesite, siderite, ankerite, Fe-dolomite, calcite, rhodocrosite and kutnohorite.

Chert: term has been adopted from mine classifications and used by the company staff. Chert in this thesis refers to chert that has re-crystallized to quartz. Polycrystalline chert, also used synonomously with "barren" chert, refers to the near uniform composition of the chert bands that are now re-crystallized quartz.

(Jasper) Chert: refers to chert bands that have been re-crystallized to quartz and contain tiny particles or iron oxides such as hematite or ferri-hydrite.

Ferri-hydrite: is used as a general term to include goethite, limonite, lepidocrosite and the classically termed ferri-hydrite (indeterminate crystal structure and formula). Due to the lack of x-ray diffraction identification, this general term refers to the undetermined dehydrated product of the initially precipitated amorphous iron particles or gels.

Ferri-oxyhydroxides: this term refers to the initially precipitated amorphous or non-crystalline iron particles or gels. No genetic connotation is implied.

Lithofacies: is used to group rock types of similar textures and mineral assemblages. These mineral assemblages include primary, diagenetic and metamorphic minerals. This non-traditional classification is to facilitate mine planning and metallurgical classifications.

Satmagan: is a tool used by the company to test for magnetic iron content. The tool is scans the drill core surface and measures the magnetism of the rock. High satmagan response suggests the presence of magnetite versus low satmagan response that suggests the absence of magnetite.

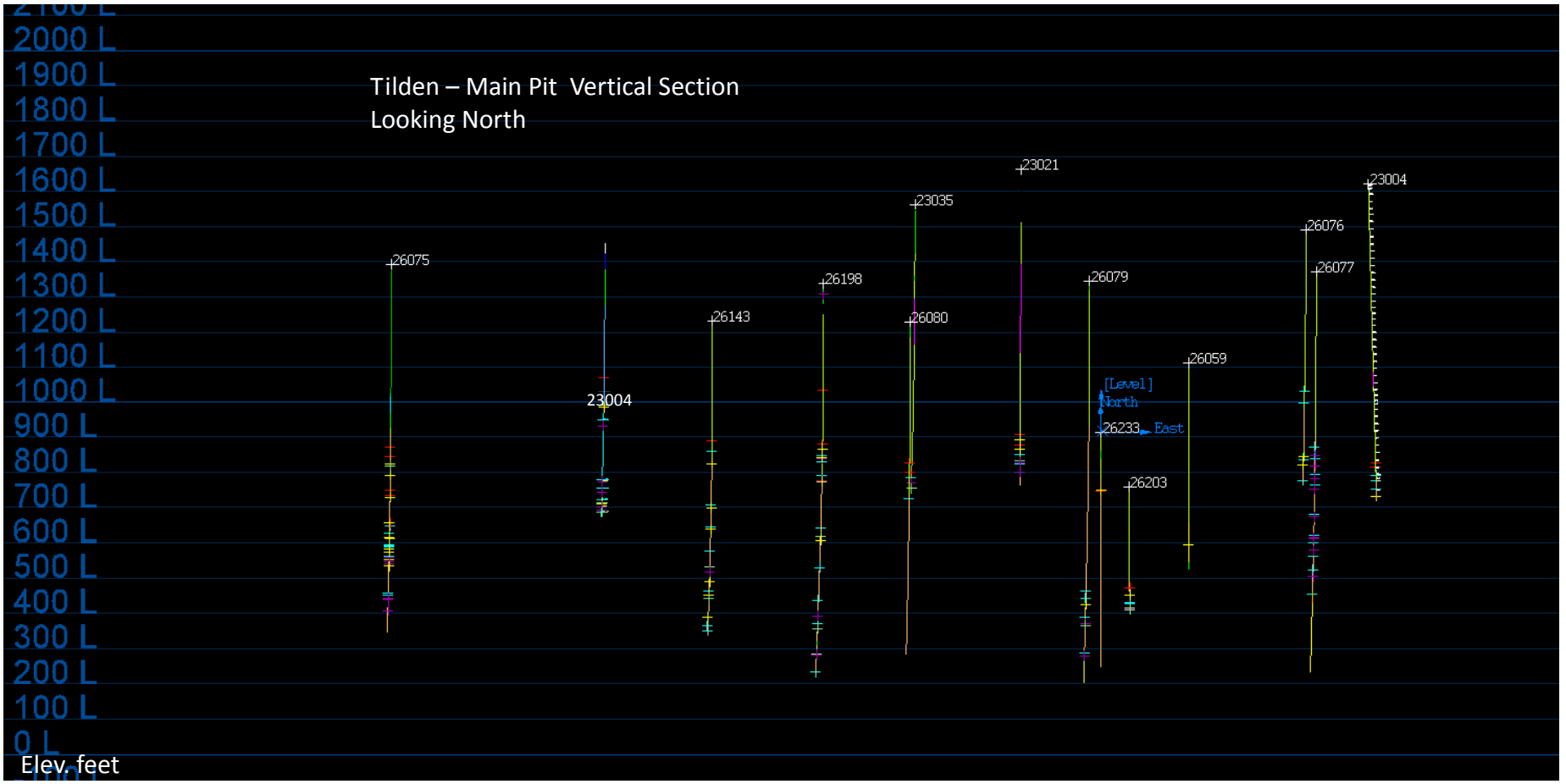

Appendix B2: Cross-section map. Sample Locations of the drill holes investigated in this these. Elevations relative To sea level are marked by the blue numbers on the left side of the diagram. The X,Y and Z co-ordinates are listed in the Sample List of Appendix B.

Drill Hole	Sample #	Location (X)	Location (Y)	Location (Z)	Domain	Lithofacies
23-004	1018	26086477.93	607553.335	1053.3	350	GIF (+ jasper)
23-004	1023	26086477.93	607535.835	1048.3	350	Medial BIF
23-004	1025	26086477.93	607538.335	1046.3	350	Medial BIF
23-004	1041	26086478.33	607520.358	1027.1	340	Medial BIF
23-004	1060	26086478.33	607515.358	1008.1	340	Lower Medial BIF
23-018	588	26083937.74	608191.664	1028.0	350	GIF
23-018	628	26083937.07	608171.221	983.3	340	Medial BIF
23-018	725	26083935.37	608164.903	879.3	340	GIF
23-018	894				340	GIF
23-018	902	26083930.92	608108.648	682.6	340	Medial BIF
23-018	950	26083929.96	608110.833	648.5	340	Medial BIF
23-018	987	26083928.86	608104.403	609.6	340	Medial BIF
23-021	1077	26085315.37	608361.1707	682.3	350	GIF
23-021	1096	26085315.11	608368.5313	642.4	350	Medial BIF
23-021	1136	26085314.92	608338.4394	612.4	340	Medial BIF
23-021	1190	26085314.7	608324.5083	577.5	340	Medial BIF
23-080	77	26084939.4	607526.7	1593.0	350	Pillar aureole
23-080	163	26084939.4	607526.7	1505.0	350	Pillar aureole
23-080	363	26084938.77	607517.651	1305.2	350	GIF
23-080	614	26084936.51	607485.299	1057.6	350	GIF
23-080	632	26084935.85	607475.965	1013.5	350	GIF
23-080	716	26084934.47	607456.214	930.9	350	GIF
26-075	612	26083230.37	608010.31	974.2	350	GIF
26-075	718	26083229.29	607994.783	867.8	350	GIF
26-075	768	26083228.88	607991.3227	832.8	350	GIF
26-075	775	26083228.85	608007.6309	828.3	350	GIF
26-075	909	26083227.38	607967.519	720.3	350	GIF
26-075	913	26083227.38	607990.019	720.3	350	Dyke
26-075	914	26083227.38	607972.519	720.3	350	Dyke
26-075	923	26083227.38	607990.019	710.0	350	GIF
26-075	932	26083227.38	607965.1506	710.7	350	GIF
26-075	1021	26083226.48	607949.6985	612.4	350	GIF
26-075	1046	26083224.62	607928.006	582.0	340	GIF
26-075	1064	26083223.71	607921.9381	544.1	340	Medial BIF
26-075	1066	26083223.71	607905.015	541.7	340	Medial BIF
26-075	1071	26083223.71	607901.515	532.1	340	Medial BIF
26-075	1089	26083222.88	607875.574	511.3	340	Medial BIF

26-075	1103	26083222.88	607872.1216	514.8	340	Medial BIF
26-075	1123	26083223.87	607912.678	551.7	340	Medial BIF
26-075	1136	26083222.88	607893.074	511.3	340	Medial BIF
26-075	1228	26083220.45	607856.8717	432.0	340	Medial BIF
26-075	1234	26083219.37	607827.3373	396.8	340	Medial BIF
26-075	1296	26083218.42	607828.1678	370.1	340	Clastics
26-076	454	26086251.62	607969.463	1289.7	350	GIF
26-076	628	26086248.35	607905.167	1116.0	350	GIF
26-076	666	26086248.35	607922.667	1116.0	340	Medial BIF
26-076	877	26086247.53	607903.501	1077.7	340	Medial BIF
26-076	884	26086243.36	607845.4903	898.7	340	Medial BIF
26-077	679	26086279.77	607633.835	1090.5	340	GIF
26-077	691	26086279.14	607624.859	1051.5	340	Medial BIF
26-077	704	26086278.59	607617.005	1017.4	340	Medial BIF
26-077	744	26086279.14	607653.7876	1051.5	340	Medial BIF
26-077	749	26086278.59	607633.6717	1017.4	340	Medial BIF
26-077	822	26086277.91	607586.8975	978.6	340	Medial BIF
26-077	837	26086277.19	607592.3811	940.0	340	Medial BIF
26-077	925	26086275.04	607572.8677	844.9	340	Medial BIF
26-077	1039	26086273.45	607530.035	784.0	340	Medial BIF
26-077	1048	26086272.54	607523.2811	751.5	340	Medial BIF
26-077	1119	26086272.31	607529.5377	744.6	340	Medial BIF
26-077	1136	26086270.03	607492.2886	669.0	340	Clastics
26-077	1162	26086267.59	607479.672	597.1	340	Clastics
26-079	1152	26085519.4	607502.2	603.6	340	GIF
26-079	1158	26085519.4	607496.2	603.6	340	Medial BIF
26-079	1183	26085518.6	607478.378	581.3	340	Medial BIF
26-079	1236	26085516.64	607432.3043	528.3	340	Medial BIF
26-079	1349	26085512.88	607382.3063	432.4	340	Clastics
26-143	40	26084287.5	607640.3	1563.5	350	Pillar aureole
26-143	100	26084287.5	607640.3	1536.0	350	Pillar aureole
26-143	300	26084287.05	607633.859	1306.1	350	Pillar aureole
26-143	525	26084285.93	607645.365	1106.8	350	GIF
26-143	555	26084285.41	607617.3272	1060.9	340	GIF
26-143	699	26084282.66	607571.136	902.4	340	GIF
26-143	715	26084282.66	607560.4217	902.4	340	GIF
26-143	801	26084280.76	607548.22	827.2	340	Medial BIF
26-143	933	26084277.36	607474.0386	725.1	340	Medial BIF
26-143	958	26084276.16	607478.067	695.5	340	Medial BIF

26-143	1018	26084273.79	607425.444	643.0	340	Medial BIF
26-143	1103	26084268.34	607382.6852	545.8	340	Medial BIF
26-198	16	26084660.8	608042.5714	1483.0	350	Pillar aureole
26-198	90	26084660.8	608021.5	1443.5	350	Pillar aureole
26-198	185	26084660.8	608024	1343.0	350	Pillar aureole
26-198	480	26084659.44	608022.042	1074.1	350	GIF
26-198	652	26084656.45	607979.29	889.2	350	GIF
26-198	669	26084655.54	607948.799	851.4	350	GIF
26-198	685	26084655.54	607941.299	861.4	350	GIF (+chert bands)
26-198	696	26084655.54	607967.3704	851.4	340	GIF
26-198	710	26084654.67	607950.787	822.0	340	Medial BIF
26-198	709	26084654.67	607950.787	821.0	340	Dyke
26-198	713	26084654.67	607936.287	818.7	340	Medial BIF
26-198	719	26084654.67	607963.787	818.7	340	Dyke
26-198	762	26084653.85	607929.344	791.1	340	GIF
26-198	956	26084648.7	607817.4693	638.1	340	Medial BIF
26-198	1058	26084644.02	607821.565	532.7	340	Dyke
26-198	1196	26084638.61	607722.8328	429.4	340	Dyke
26-198	1236	26084635.4	607679.3424	375.6	340	Medial BIF
26-198	1321	26084631.45	607604.303	313.6	340	Medial BIF
26-198	1358	26084629.67	607578.79	286.1	340	Medial BIF
23-333	220-230	26085577	607944.1	727.0	340	unknown
23-035	1000	26084952.74	608170.552	624.0	340	Medial BIF
26-059	674	26085845.96	606674.925	1267.4	350	GIF

Curriculum Vitae

Name: Natalie Pietrzak

Post-secondary Education and Degrees:

University of Western Ontario
London, Ontario, Canada
1997-2001 H.B.Sc.

The University of Western Ontario
London, Ontario, Canada
2001-2003 M.Sc.

The University of Western Ontario
London, Ontario, Canada
2006-2011 Ph.D.

Honours and Awards:

NSERC-IPS
2007-2009

Institute of Lake Superior Geology Best Student Paper Award
(2009)

W. Fyfe Graduate Award in Natural Resources (UWO)
(2009)

J.P. Bickell Foundation Graduate Scholarship (UWO)
(2008)

Related Work Experience

Renaud Geological Consulting Ltd.
Secretary and Assistant Microprobe Operator (2005-present)

Teaching Assistant
The University of Western Ontario
2006-2009

Publications:

2010 *Hydrothermal Overprint by Greenstone Sills within the Tilden Pit, Michigan*

Proceedings and Abstracts – Institute of Lake Superior Geology – in print
Pietrzak, N., Duke, N., Scott, G. and Lukey, H.

2009 *Ore Textures and Mineral Chemistry within the Oxide-Carbonate-Silicate Flotation Ores at the Cliffs Natural Resources' Tilden Mine, Michigan*
Programs with Abstracts – Institute of Lake Superior Geology Meeting
Vol. 55, Part 1, pp. 66
Pietrzak, N., Duke, N., Scott, G., and Lukey, H.

2008 *A Study of Paragenetic Stages of Mineral Growth in Complex Iron at the Tilden Mine, and Development of a Mine Scale Model of Application of Ore Treatment Methods*
Programs with Abstracts – Institute of Lake Superior Geology Meeting Vol. 54, Part 1, pp. 71
Pietrzak, N., Duke, N., Scott, G. and Lukey, H.